

PHASE 2 - 3D SEISMIC INVESTIGATION, SOUTH BRUCE

Data Interpretation and Inversion Report

APM-REP-01332-0455

December 2024

Geofirma Engineering Ltd.

nwmo

NUCLEAR WASTE
MANAGEMENT
ORGANIZATION

SOCIÉTÉ DE GESTION
DES DÉCHETS
NUCLÉAIRES



This report has been prepared under contract to NWMO. The report has been reviewed by NWMO, but the views and conclusions are those of the authors and do not necessarily represent those of the NWMO.

All copyright and intellectual property rights belong to NWMO.

Nuclear Waste Management Organization

22 St. Clair Avenue East, 4th Floor

Toronto, Ontario

M4T 2S3

Canada

Tel: 416-934-9814

Web: www.nwmo.ca

Phase 2 - 3D Seismic Investigation, South Bruce

Data Interpretation and Inversion Report

Geofirma Document ID:

SB_3DSeismic_Interpretation and Inversion Report_R0

NWMO Document ID: APM-REP-01332-0455

Revision: 0 (Final)

Prepared for:

Nuclear Waste Management Organization

22 St. Clair Avenue East, 4th Floor
Toronto, ON, M4T 2S3

Prepared by:



GEOFIRMA
ENGINEERING

1 Raymond St. Suite 200, Ottawa, Ontario K1R 1A2
📞 613.232.2525 📠 613.232.7149 🌐 geofirma.com

Project Number: 21-210-1

Document ID: SB_3DSeismic_Interpretation and Inversion Report_R0

December 19, 2024

| | | |
|-------------------------|--|-------------------------|
| Title: | Phase 2- 3D Seismic Investigation, South Bruce Data Interpretation and Inversion Report | |
| Client: | Nuclear Waste Management Organization | |
| Project Number: | 21-210-1 | |
| Document ID: | SB_3DSeismic_Interpretation and Inversion Report_R0 | |
| Revision Number: | 0 (Final) | Date: December 19, 2024 |
| Prepared by: | David Schieck (Seismic Solutions), Onur Cip (Schlumberger) [<i>AVO Inversion</i>] | |
| Reviewed by: | Sean Sterling | |
| Approved by: |  Sean Sterling (M.Sc., P.Eng., P.Geo.) – Project Manager - Principal | |

Revision Tracking Table

| Revision | Revision Release Date | Description of Modifications/Edits |
|----------|-----------------------|---|
| R0A | 26 Feb 2024 | Initial Draft Release |
| R0B | 11 Jul 2024 | Revised draft report addressing NWMO comments |
| R0C | 13 Nov 2024 | Revised draft report addressing NWMO comments |
| R0D | 28 Nov 2024 | Revised draft report addressing NWMO comments |
| R0 | 19-Dec-24 | Initial Final Release |

TABLE OF CONTENTS

| | | |
|----------|--|-----------|
| 1 | INTRODUCTION | 1 |
| 1.1 | 3D Seismic Project Purpose and Objectives | 1 |
| 1.2 | 3D Seismic Data Acquisition and Processing Summary | 2 |
| 1.3 | Geological Background | 4 |
| 2 | CORRELATION OF SEISMIC REFLECTION EVENTS WITH EXISTING DATA | 5 |
| 2.1 | Seismic Correlation Methodology | 5 |
| 2.1.1 | Geophysical Log Data | 5 |
| 2.1.2 | Synthetic Seismogram | 5 |
| 2.2 | Definition of Marker Horizons | 11 |
| 3 | SEISMIC DATA INTERPRETATION APPROACH | 13 |
| 3.1 | Seismic Interpretation Methodology | 13 |
| 3.1.1 | Overview of workflow | 13 |
| 3.1.2 | Method of horizon interpretation | 13 |
| 4 | INTERPRETATION OF HORIZONS IN TIME AND STRUCTURE MAPPING | 15 |
| 4.1 | Description of horizons | 15 |
| 4.1.1 | Upper Silurian Seismic Horizons | 15 |
| 4.1.2 | Lower Silurian Seismic Horizons | 16 |
| 4.1.3 | Upper Ordovician Seismic Horizons | 16 |
| 4.1.4 | Precambrian Seismic Horizon | 19 |
| 4.2 | Reef Interpretation | 21 |
| 4.3 | Seismic Anomaly near Reef | 22 |
| 5 | VELOCITY MODELING AND DEPTH CONVERSION | 24 |
| 6 | SEISMIC INVERSION | 32 |
| 6.1 | AVO Inversion | 32 |
| 6.2 | Initial Low Frequency Model | 39 |
| 6.3 | Simultaneous Inversion | 44 |
| 6.4 | AVO Inversion Results | 45 |
| 6.5 | AVO Inversion Data Quality | 48 |
| 6.6 | Lithology Prediction | 48 |
| 7 | CONCLUSIONS | 52 |
| 8 | REFERENCES | 53 |

LIST OF FIGURES

| | | |
|------------|--|----|
| Figure 1 | 3D seismic survey study area..... | 3 |
| Figure 2 | Synthetic seismogram from borehole geophysical data in SB_BH01 | 6 |
| Figure 3 | Synthetic seismogram from borehole geophysical data in SB_BH02 | 7 |
| Figure 4 | Synthetic model with density and sonic well logs displayed..... | 9 |
| Figure 5 | Cross section showing SB_BH01 and SB_BH02 with AVO-compliant seismic data, including the displays of the optimal phase and time shifts and their correlation factors. | 10 |
| Figure 6 | Well ties for boreholes SB_BH01 and SB_BH02 to the AVO-compliant dataset, annotated with geological formation tops. | 12 |
| Figure 7 | Guelph Formation (a) plan view of interpreted time structure; (b) seismic amplitude. (also shown as Figure A-4) in Appendix A. | 18 |
| Figure 8 | Cobourg Formation – Collingwood Member (a) Plan view of interpreted time structure; (b) Seismic amplitude. (also shown as Figure A-10) in Appendix A..... | 20 |
| Figure 9 | Guelph – Cabot Isochron depicting the reef outline. | 21 |
| Figure 10 | Cross-line 207 showing the mounded reflection pattern near the anomaly on the western flank of the Guelph Reef..... | 23 |
| Figure 11 | Zones (hierarchy) property showing the zones of the 3D gridded model..... | 25 |
| Figure 12 | Upscaled average velocity (left) and upscaled average velocity logs (right)..... | 26 |
| Figure 13 | Final velocity model incorporating seismic and borehole data | 27 |
| Figure 14 | Cross-section of (a) the time horizons and (b) the depth horizons for the time to depth conversion. | 31 |
| Figure 15 | Wavelet generated from full stack for SB_BH01 (left) and SB_BH02 (right) for synthetic seismograms. | 32 |
| Figure 16 | SB_BH01 - Borehole geophysical data (left) alongside actual and synthetic seismic data (right), with a cross-correlation of 99.7% between synthetic and actual seismic traces. | 34 |
| Figure 17 | SB_BH02 - Borehole geophysical data (left) alongside actual and synthetic seismic data (right), with a cross-correlation of 98.2% between synthetic and actual seismic traces. | 35 |
| Figure 18 | SB_BH01 and SB_BH02 well tops, alongside the time-domain horizons. | 35 |
| Figure 19. | Wavelets extracted from angle gathers (14–21 degrees) for SB_BH01 (left) and SB_BH02 (right), illustrating the wavelet shape, power spectrum, phase spectrum, and predictability ratios..... | 37 |
| Figure 20 | Wavelets extracted from SB_BH01 and SB_BH02 for the 14–21° angle gather, averaged to produce a single wavelet input for simultaneous inversion. | 38 |
| Figure 21 | Acoustic impedance LFM cross-section..... | 40 |
| Figure 22 | Vp/Vs LFM cross-section along SB_BH01 and SB_BH02..... | 41 |
| Figure 23 | Density LFM cross-section along SB_BH01 and SB_BH02..... | 42 |
| Figure 24 | Two of the four angle gathers utilized in the inversion study. (a) Angle gather 4-14; (b) Angle gather 14-21..... | 43 |
| Figure 25 | SB_BH01 Inversion Results | 46 |
| Figure 26 | SB_BH02 Inversion Results | 47 |
| Figure 27 | The lithology logs of SB_BH01 and SB_BH02 | 49 |
| Figure 28 | Lithology Prediction Intersection | 51 |

LIST OF TABLES

| | | |
|---------|--|----|
| Table 1 | Summary of Picked Horizons | 11 |
| Table 2 | Levels of confidence for picking horizons | 14 |
| Table 3 | Summary of horizon picking method and confidence of picks | 14 |
| Table 4 | Comparative analysis of depth-converted seismic horizons and their corresponding geological markers using the initial velocity | 29 |
| Table 5 | Comparative analysis of depth-converted seismic horizons and their corresponding geological markers using the updated velocity | 30 |

LIST OF APPENDICES

| | |
|------------|---|
| Appendix A | Time Structure and Seismic Amplitude Figures for Key Interpreted Horizons |
| Appendix B | Seismic Wavelets Extracted from Select Angle Gathers |

1 INTRODUCTION

Geofirma Engineering Ltd. (Geofirma) has been contracted by the Nuclear Waste Management Organization (NWMO) to perform seismic interpretation and inversion of a 3D seismic project pertaining to the NWMO Phase 2 Geoscientific Preliminary Field Investigations within the South Bruce area, near Teeswater, Ontario as part of the NWMO's Adaptive Phased Management (APM) Site Selection Phase.

As part of this work, Geofirma completed a study of a 3D seismic reflection survey to provide further understanding and interpretation of deep subsurface geological conditions in the South Bruce Site. The study area for this 3D seismic reflection study is approximately 13.5 km² as shown in Figure 1, comprised of land parcels northwest of the community of Teeswater, Ontario.

Geofirma's team included four subcontracting partners: Echo Seismic Ltd. (seismic data acquisition services), Absolute Imaging (data processing), Schlumberger Canada (AVO Inversion and petrophysical properties prediction), and Seismic Solutions (geophysical technical input/design, seismic interpretation, and reporting).

1.1 3D Seismic Project Purpose and Objectives

This work was primarily completed to better understand the subsurface geological conditions at the South Bruce Site, which involved optimizing the seismic survey design to target the depth range between 500 to 1,000 m below ground surface (mBGS) and to a maximum depth of 1,500 mBGS. This study intends to:

- Target and image key sedimentary rock formations (horizons).
- Image and characterize seismic-scale reflections. These reflections may represent the result of lithological contrasts within the subsurface or correspond to fractured or sheared zones.
- Characterize petrophysical properties of sedimentary formations through AVO (amplitude versus offset, also referred to as amplitude variation with offset) seismic inversion and geostatistical techniques using deep boreholes (SB_BH01 and SB_BH02) in the area. Physical properties such as velocity, density, and porosity, as well as dynamic Young's and Bulk's moduli are derived from the products of seismic inversion and borehole data.

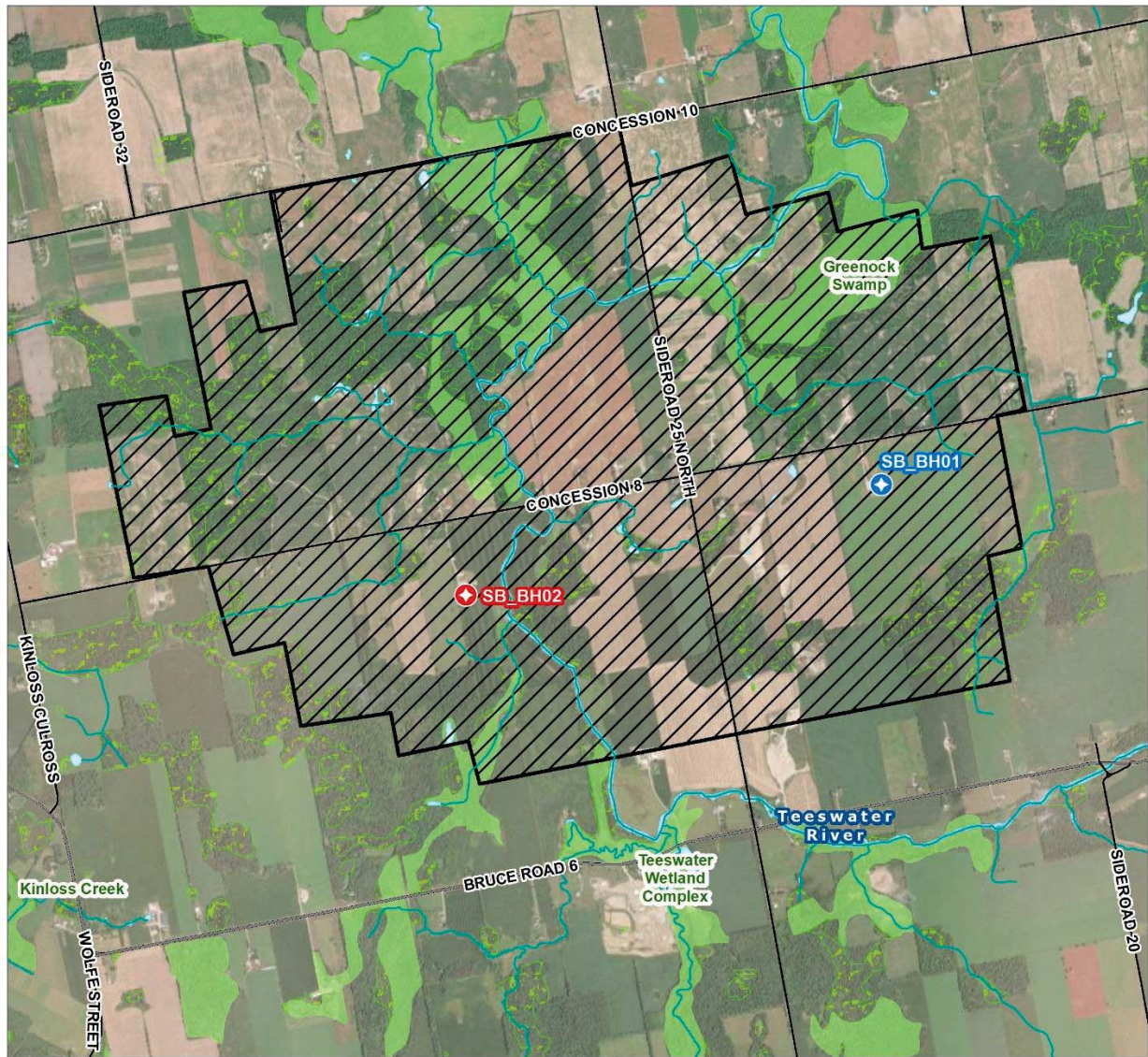
A broader objective of this work is to assist the NWMO in evaluating the South Bruce Site as a potential location where Canada's used nuclear fuel can be safely stored in a deep geological repository (DGR).

Note that this technical report exclusively covers activities associated with the data interpretation, seismic inversion, and petrophysical properties prediction derived from the 3D seismic survey. The data acquisition and data processing of the 3D seismic reflection survey are detailed in a separate report (Geofirma Engineering Ltd., 2024a). Geofirma also completed a 2D seismic reflection study focussing on a buried bedrock valley (paleochannel) within the 3D seismic study area. The data acquisition for this 2D seismic study was executed immediately after the recording operations of the 3D seismic survey. This 2D seismic study included three east-west oriented source lines along existing roads. Geofirma Engineering Ltd. (2024b) provides a detailed summary and interpretation of the 2D seismic paleochannel study.

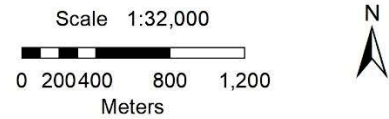
1.2 3D Seismic Data Acquisition and Processing Summary

Geofirma contracted with Echo Seismic Ltd, based in Calgary, to complete 3D seismic data acquisition during October - November 2021. Echo Seismic carried out Megabin and slip-sweep operations with 50m receiver intervals and 12.5 m source intervals along NS trending lines that were 100 m apart. The targeted 3D seismic survey area consisted of a substantial amount of wet ground conditions and treed/brush covered areas that could not be accessed by the Envirovibe sources. The areas without source points resulted in a seismic data volume with lower data density (lower fold), especially above 300 mBGS. Lower confidence was placed on the interpretation of horizons that are shallower than 300 m within these areas. Conversely, the areas with very high surface density of more randomly spaced source points resulted in exceptional data quality within an area of southwestern Ontario that historically has reported very poor seismic data results.

Geofirma subcontracted all 3D seismic data processing to Absolute Imaging, based in Calgary. Absolute Imaging completed two different processing sequences of these data. The initial reflection processing of the 3D seismic data was completed during early 2021. Initial seismic interpretation and AVO inversion analysis indicated that additional processing was required and therefore an AVO-compliant processing approach was taken and completed during early 2023. This was also guided by the final borehole geophysical data from SB_BH01 and SB_BH02 that were not available during the initial processing stage. Readers are referred to the Acquisition and Processing Report (Geofirma Engineering Ltd., 2024a) for detailed information.



-  3D Seismic Survey Area
-  Major Road
-  Local Street
-  Watercourse
-  Waterbody
-  Provincially Significant Wetland
-  Non-Provincially Significant Wetland
-  SB_BH01 Drill Site
-  SB_BH02 Drill Site



Coordinate System: NAD 1983 UTM Zone 17N
 Source: GeoHub Ontario, OGSRL, MECP,
 ESRI, NWMO

Figure 1 3D seismic survey study area

1.3 Geological Background

The Paleozoic bedrock near South Bruce is overlain by variable thicknesses of overburden (unconsolidated) sediments (including sand, gravel, boulders, till, etc.), ranging from tens of meters in average thickness and locally reaching a maximum thickness of approximately 250 m east of the Niagara Escarpment (Gao et al. 2006; Gao 2011). The Paleozoic-aged strata were deposited within the Michigan Basin northwest of the Algonquin Arch in southwestern Ontario. The Michigan Basin is a circular-shaped, carbonate dominated intracratonic basin that is composed primarily of shallow marine carbonates (limestone, dolostone), evaporites, and shales that were deposited while eastern North America was in tropical latitudes (Armstrong and Carter, 2010). West of the Algonquin Arch, the Paleozoic strata tend to gradually dip westward into the Michigan Basin. In the South Bruce area, this succession of Paleozoic strata rests unconformably on an erosional surface of the Precambrian crystalline basement (at approximately 900 m) of the Grenville Province, a tectonic subdivision of the Canadian Shield.

Boreholes SB_BH01 and SB_BH02 were drilled through the entire Paleozoic sequence to approximately 20 m and 14 m, respectively, into the Precambrian basement, which is composed of high-grade metamorphic rocks of the Grenville Province.

The thicknesses of the major stratigraphic packages in SB_BH01 and SB_BH02 were generally consistent with reported thicknesses for these packages in nearby oil and gas wells logs from the Oil, Gas, and Salt Resources Library (OGSRL) database, and regional descriptions of these units (Carter et al. 2022, Armstrong & Carter 2010). These major packages include approximately 80 -120 m thick Devonian aged dolostones as the upper bedrock units, underlain by approximately 290 to 320 m thick Silurian bedrock units, followed by a thick sequence of Ordovician-aged shales (~213 m) from the Queenston, Georgian Bay, and Blue Mountain formations that overlie ~225 m of dense Ordovician-aged limestones. The Ordovician-aged shales provide a low permeability caprock above the low permeability repository horizon within the upper Ordovician-aged limestones.

Geological and geophysical data collected by Geofirma as part of a drilling and testing program at SB_BH01 and SB_BH02 were used during the processing and interpretation of this seismic study. Geofirma (2024c) and Geofirma (2022) describe the geological and geotechnical core logging activities in SB_BH01 and SB_BH02, respectively, and include detailed assessment of the 34-35 bedrock formations intersected in each borehole. Similarly, Geofirma (2024d) and Geofirma (2024e) provide an overview and present the borehole geophysical logging data in the two boreholes.

One major difference between the two boreholes is that borehole SB_BH01 was drilled through a portion of a reefal structure which exhibited varying thicknesses of key Silurian bedrock formations / units compared to the regional average interpretation as exhibited in SB_BH02. This reef structure is referred to as the Guelph Reef throughout this report.

2 CORRELATION OF SEISMIC REFLECTION EVENTS WITH EXISTING DATA

2.1 Seismic Correlation Methodology

To identify the horizons of interest, we initiate by analyzing and correlating observable seismic reflection events with geophysical and stratigraphic well logs. This correlation is facilitated through the generation of synthetic seismograms, which compute the synthetic seismic response corresponding to the logged physical properties in boreholes. This synthetic seismic response is evaluated alongside the actual seismic data to identify interpretable horizons. Synthetic seismograms were created to help in the interpretation of horizons as depicted in Figure 2 and Figure 3.

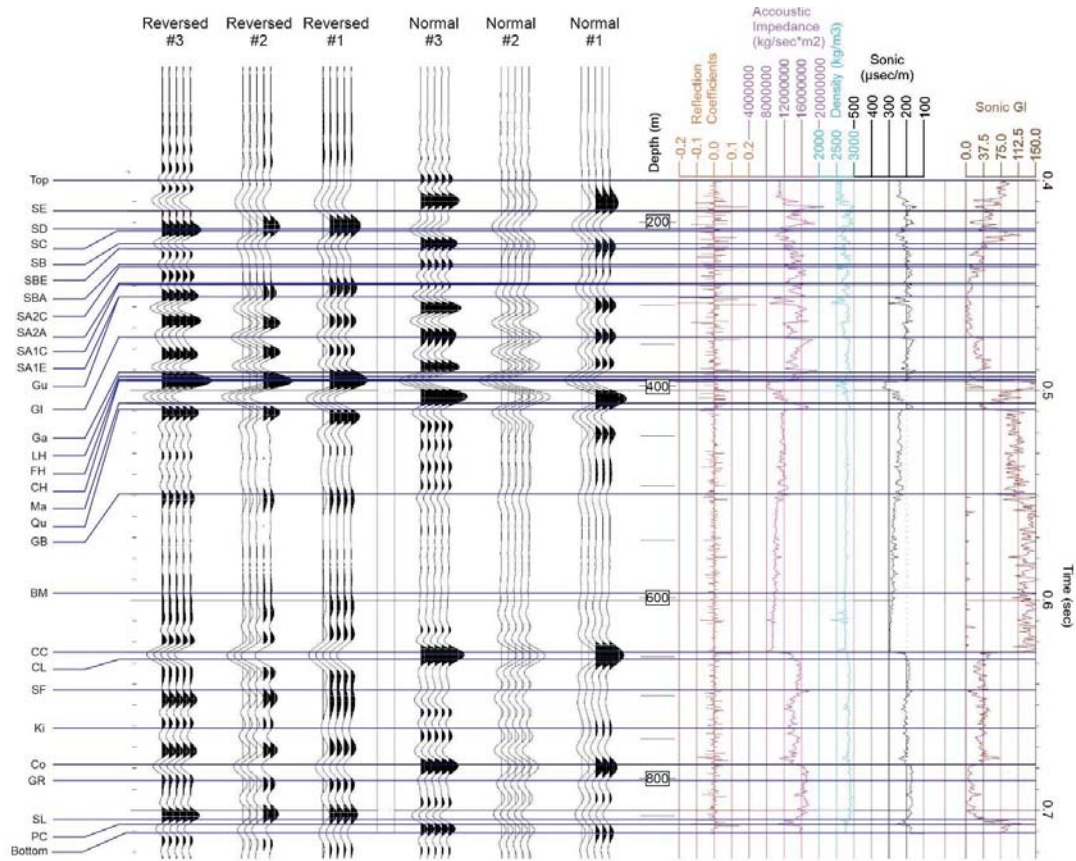
2.1.1 Geophysical Log Data

A comprehensive suite of borehole geophysical logs (including sonic, natural gamma, and compensated density logging) were completed in SB_BH01 and SB_BH02 as described in Geofirma (2024d and 2024e). These logs facilitate the identification of stratigraphic formation tops and are used to generate synthetic seismograms using the P-wave sonic and density logs from SB_BH01 and SB_BH02.

2.1.2 Synthetic Seismogram

Synthetic seismograms were created using Synth 1D software from Divestco with borehole geophysical data collected in SB_BH01 and SB_BH02 as input. Figure 2 (SB_BH01) and Figure 3 (SB_BH02) show the synthetic seismograms using the velocities (or inversely travel time) and densities from geophysical logs with a series of reflectivity coefficients (AI, acoustic impedance) shown on the right. Three Ormsby 0-phase wavelets with different frequency bandwidths 8-80, 8-100 and 8-120Hz were then convolved with the reflectivity to generate a synthetic reference trace that can be correlated with the processed seismic data at borehole location. These are shown as both normal and reversed phase traces labelled #1, #2 and #3, respectively, as shown in Figure 2 and Figure 3.

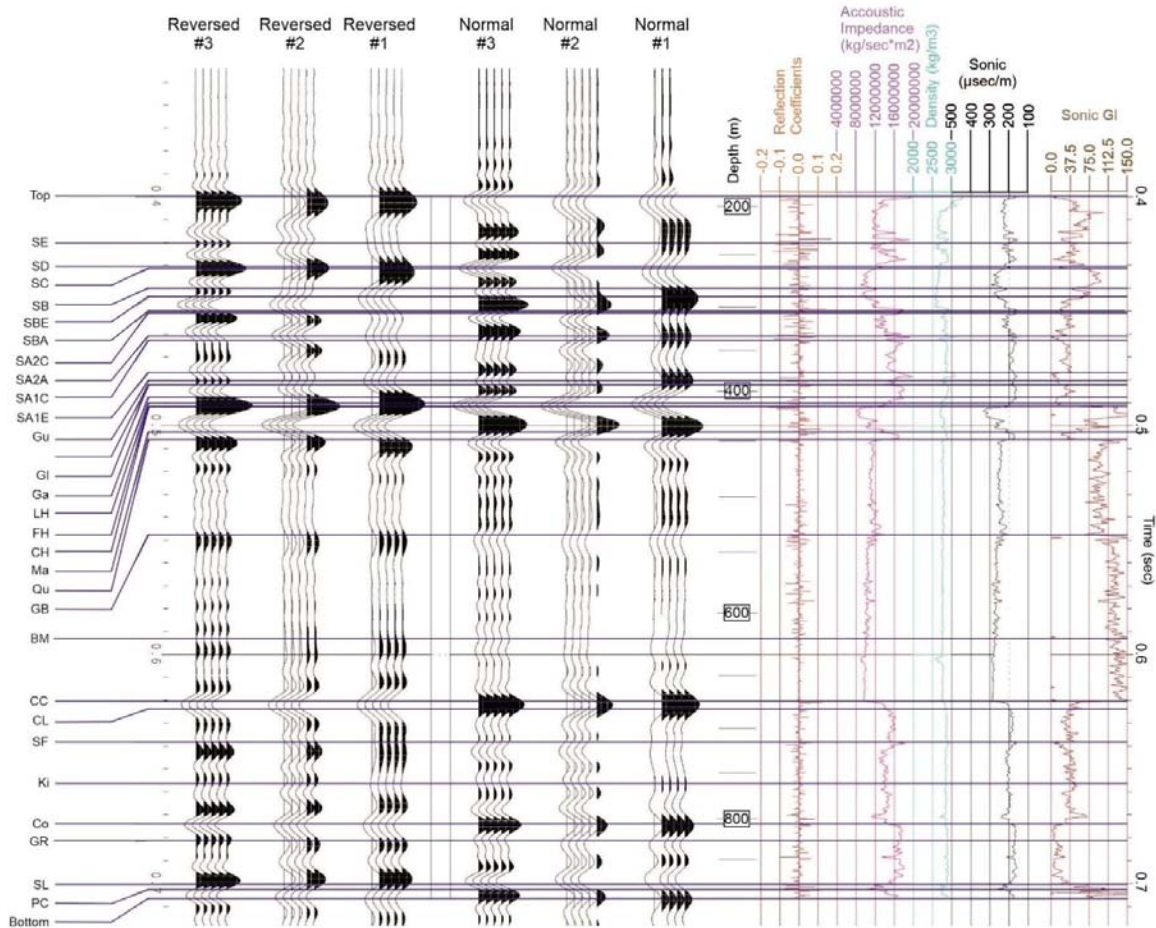
The stratigraphic formation tops were provided by Geofirma and interpreted based on borehole geophysical logs and geological core logs as mentioned above. These formation tops, originally identified in depth, were then marked on the resulting synthetic seismic in units of time (based on an estimated velocity relationship). This methodology facilitated the interpretation of horizons within the 3D seismic volume by aligning the formation tops with their corresponding responses in the actual seismic data at each borehole location.



LEGEND

| | | | |
|----------------------------|----------------------------|--------------------------|-------------------|
| SE - Salina_E | SA1C - Salina_A1_Carbonate | CH - Cabot Head | Ki - Kirkfield |
| SD - Salina_D | SA1E - Salina_A1_Evaporite | Ma - Manitoulin | Co - Coboconk |
| SC - Salina_C | Gu - Guelph | Qu - Queenston | GR - Gull River |
| SB - Salina_B | GI - Goat Island | GB - Georgian Bay | SL - Shadow Lake |
| SBE - Salina_B_Equivalent | Ga - Gasport | BM - Blue Mountain | PC - Pre-Cambrian |
| SBA - Salina_B_Anhydrite | LH - Lions Head | CC - Cobourg_Collingwood | |
| SA2C - Salina_A2_Carbonate | FH - Fossil Hill | CL - Cobourg_Lower | |
| SA2A - Salina_A2_Anhydrite | CH - Cabot Head | SF - Sherman Falls | |

Figure 2 Synthetic seismogram from borehole geophysical data in SB_BH01



LEGEND

- | | | | |
|----------------------------|----------------------------|--------------------------|-------------------|
| SE - Salina_E | SA1C - Salina_A1_Carbonate | CH - Cabot Head | Ki - Kirkfield |
| SD - Salina_D | SA1E - Salina_A1_Evaporite | Ma - Manitoulin | Co - Coboconk |
| SC - Salina_C | Gu - Guelph | Qu - Queenston | GR - Gull River |
| SB - Salina_B | Gi - Goat Island | GB - Georgian Bay | SL - Shadow Lake |
| SBE - Salina_B_Equivalent | Ga - Gasport | BM - Blue Mountain | PC - Pre-Cambrian |
| SBA - Salina_B_Anhydrite | LH - Lions Head | CC - Cobourg_Collingwood | |
| SA2C - Salina_A2_Carbonate | FH - Fossil Hill | CL - Cobourg_Lower | |
| SA2A - Salina_A2_Anhydrite | CH - Cabot Head | SF - Sherman Falls | |

Figure 3 Synthetic seismogram from borehole geophysical data in SB_BH02

A pseudo-2D synthetic model between boreholes SB_BH01 and SB_BH02 was generated using InterpaLog software from Divestco to help pick interpretable horizons. Figure 4 depicts a pseudo-2D synthetic seismic section, having approximately the same distance between the borehole locations (2,500 m) using a trace spacing of 50 m between each generated trace in the middle along with the stratigraphic logs for SB_BH01 and SB_BH02. This assists in the correlation of formation tops and their seismic response in between these two boreholes, as shown Figure 5. This figure represents a cross-section extracted along the line connecting the two boreholes.

Seismic-to-well tie analysis is performed at each borehole location using the initially processed 3D seismic volume as shown in Figure 4. Once an AVO-compliant version was provided, the tie analysis was repeated with no significant changes to the horizon interpretation. Figure 5 depicts the correlation results of each borehole with the AVO-compliant seismic data, including the phase and time shift needed to obtain the best match. For further information on the AVO-compliant version, refer to the Acquisition and Processing Report (Geofirma Engineering Ltd., 2024a).

The need for a 90-degree phase rotation was identified and applied to the data. The AVO-compliant data showed a slightly better correlation with the two boreholes (SB_BH01 and SB_BH02). For SB_BH01, the correlation with the initial seismic dataset was 61.4%, while the AVO-compliant data achieved an improved correlation of 65.6%. For SB_BH02, the initial seismic dataset showed a 53% correlation, which improved to 55.5% with the AVO-compliant data. Upon completion of the tie analysis, the formation tops and their corresponding seismic responses are aligned and prepared for interpretation across the entire seismic volume.

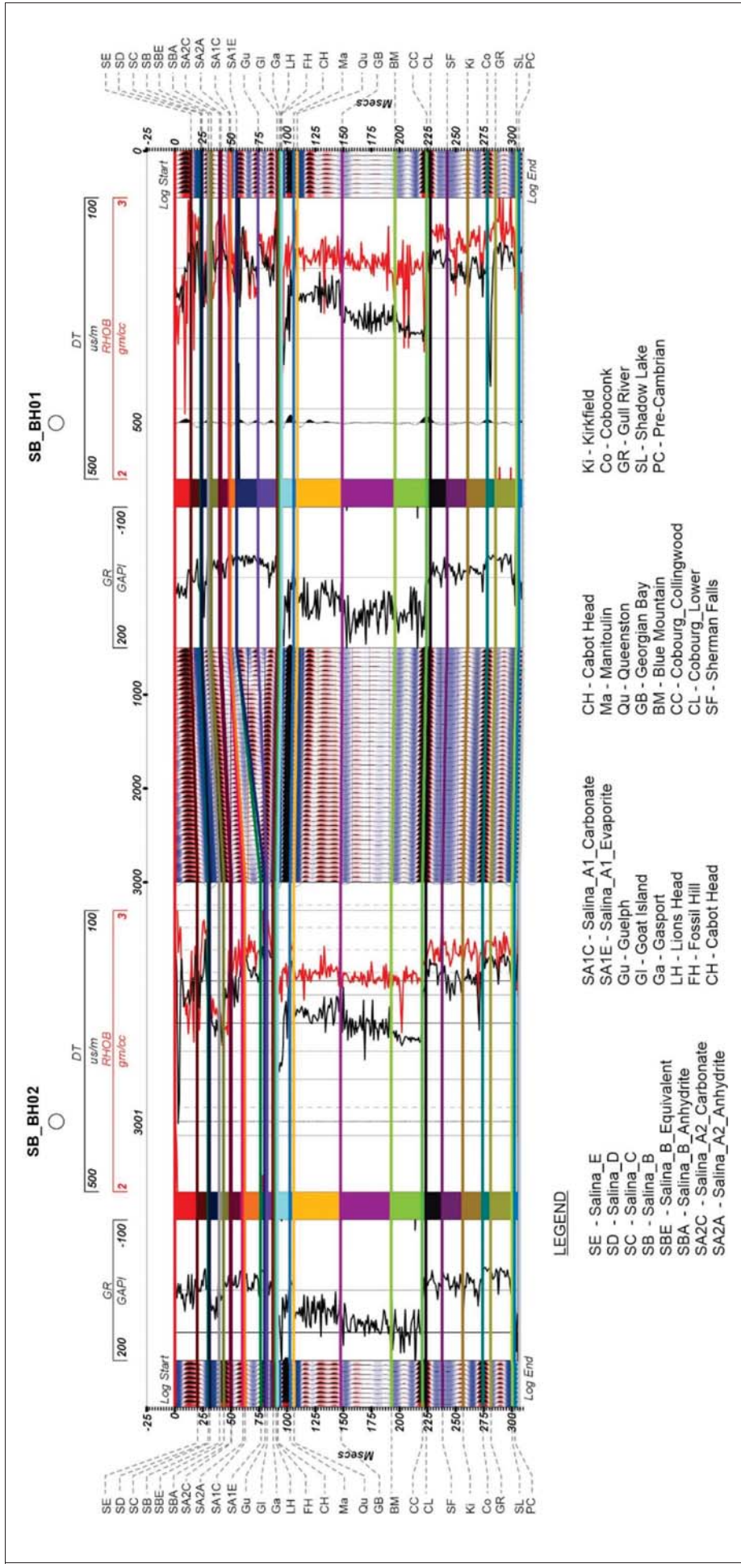


Figure 4 Synthetic model with density and sonic well logs displayed

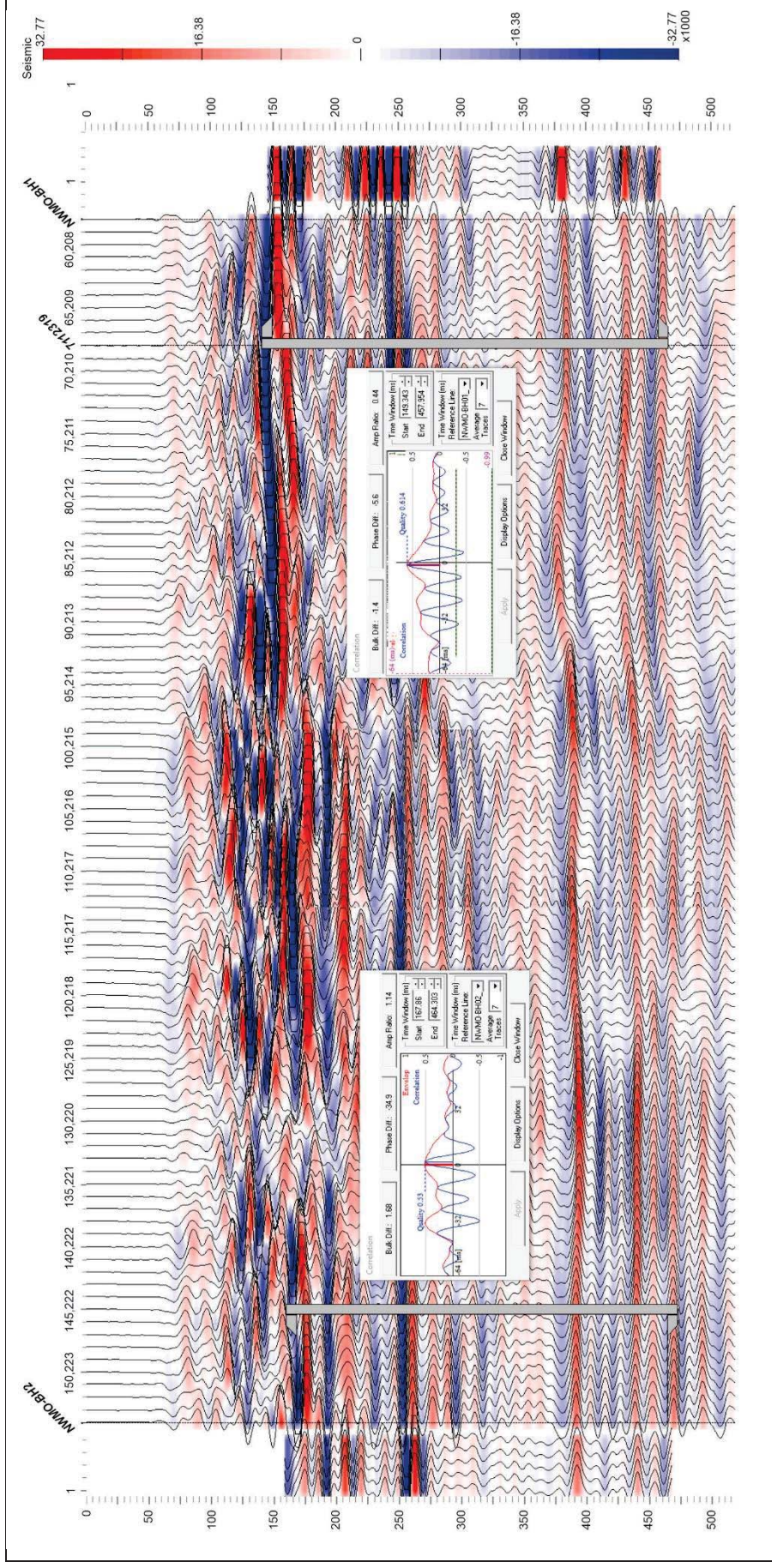


Figure 5 Cross section showing SB_BH01 and SB_BH02 with AVO-compliant seismic data, including the displays of the optimal phase and time shifts and their correlation factors.

2.2 Definition of Marker Horizons

The horizon markers were chosen based on tie points and potential lateral picking ability, as indicated in Table 1. Other formation tops identified in borehole logging were not observed in seismic data due to the limited thickness of some formations. Figure 6 presents the same seismic cross-section as Figure 5, now annotated with seismic horizons (geologic formation tops) from Table 1, labeled along each borehole track.

The horizons were assigned a positive acoustic impedance "Peak" if there was an increase in velocity/density across the top of the horizon boundary. Conversely, a horizon was assigned a negative acoustic impedance "Trough" if there was a decrease in velocity/density. Here, "Peak" corresponds to the maximum positive amplitude of the wavelet, while "Trough" represents the maximum negative amplitude. The horizons chosen for interpretation from deepest to shallowest are as follows:

Table 1 Summary of Picked Horizons

| Horizon Name | Peak / Trough |
|---------------------------------|---------------|
| Precambrian | Peak |
| Gull River Fm | Trough |
| Coboconk Fm | Peak |
| Kirkfield Fm | Trough |
| Sherman Falls Fm | Trough |
| Cobourg Fm – Collingwood Member | Peak |
| Georgian Bay Fm | Trough |
| Queenston Fm | Trough |
| Manitoulin Fm | Peak |
| Cabot Head Fm | Trough |
| Goat Island Fm | Peak |
| Guelph Fm | Zero Crossing |
| Salina Fm – A2 Unit carbonate | Peak |
| Salina Fm – D Unit shale | Trough |
| Salina Fm – F Unit shale | Trough |

3 SEISMIC DATA INTERPRETATION APPROACH

3.1 Seismic Interpretation Methodology

3.1.1 Overview of workflow

Seismic horizon interpretation was first carried out on the initially processed seismic volume and further refined using the AVO-compliant volume, which was particularly useful for shallow horizons as most of the “noise” or irregularity in the shallow horizon picks were minimized. A cosine of instantaneous phase attribute volume was produced to help guide horizon picking. This seismic attribute computes the phase at each sample point, maintaining a consistently smooth data display, facilitating a more consistent interpretation of seismic events.

3.1.2 Method of horizon interpretation

Horizons were interpreted using a combination of methods, including line-by-line picking with the WinPICS flood picker tool and grid-based picking with larger spacing. A “pick” refers to a specific time assigned to a horizon on an individual seismic trace. Flood picking involves automatically filling in horizon picks along waveform peaks or troughs within the seismic volume, guided by manually placed “seed” picks, typically selected along a sparse grid of lines. Manual picking, on the other hand, requires the interpreter to individually select peaks or troughs on each trace throughout the data volume.

To rank the reliability of the interpretations, a confidence level ranging from 1 to 3 was assigned to each horizon pick: a rating of 3 indicates the easiest horizons to interpret, while a rating of 1 reflects the most challenging horizons within the 3D seismic volume, as summarized in Table 2.

Table 3 provides a summary of the 15 geological horizons interpreted in this study, detailing the confidence levels, picking methods employed for each horizon, the rationale behind the chosen methods, and the smoothing/gridding techniques applied to the final displays. Of these, nine seismic horizons were classified as easy to interpret with high confidence, two horizons (Georgian Bay Formation and Kirkfield Formation) as moderately interpretable with medium confidence, and four horizons (Salina F Unit, Salina D Unit, Salina A2 Unit Carbonate, and Guelph Formation) as challenging to interpret with low confidence.

Two distinct methods were employed to produce smoothed surfaces: the mean smoother method and the gridding method. The mean smoother method uses an averaging filter to smooth surfaces by offsetting cells or bins, effectively leveling out extremes in well-sampled data. For example, with a data volume bin size of 25 m x 12.5 m, a 5 x 5 smoother corresponds to a 125 m x 62.5 m smoothing window. In contrast, the gridding method is applied to hard-to-pick horizons where confident interpretation is not feasible across all seismic lines. This method does not use a “filter” but instead creates a smoothed grid, such as a 75 m x 75 m grid, to generate cells of that size. The resulting surface is then resampled to match the native lateral seismic resolution.

Table 2 Levels of confidence for picking horizons

| Confidence | Explanation |
|------------|---|
| 3 | Easy interpretation - strong, continuous, and easy-to-pick reflections, consistent across the 3D volume. High confidence. |
| 2 | Moderate interpretation - weak, but continuous reflections that present a moderate challenge to pick. Medium confidence. |
| 1 | Hard interpretation - inconsistent, semi-continuous reflections with large areas of discontinuities. Low confidence. |

Table 3 Summary of horizon picking method and confidence of picks

| Horizon Name | Confidence (1-3) | Picking method | Method Reason | Smoothing/Gridding method |
|-----------------------|------------------|--|---|---|
| Precambrian | 3 | Flood pick - Seed pick on every 4th line w/ manual cleanup picks line by line | Strong reflection consistent across the area | Mean 5x5 smoother |
| Gull River | 3 | Flood pick - Seed pick on every 4th line w/ manual cleanup picks line by line. Interpolated through missing picks | Strong reflection mostly consistent across the area. Gaps were small and consistent with not fully formed troughs (i.e. local trough with a positive amplitude) | Mean 5x5 smoother |
| Coboconk | 3 | Flood pick - Seed pick on every 4th line w/ manual cleanup picks line by line | Strong reflection consistent across the area | Mean 5x5 smoother |
| Kirkfield | 2 | Grid to horizon - Inlines picked every 4th line, Cross lines picked every 10. | Consistent reflection, with some areas that may confuse the flood picks. Provided a clean pick. | Grid 75mx75m to provide a smooth grid |
| Sherman Falls | 3 | Flood pick then manual - Seed pick on every 4th line w/ manual cleanup picks line by line | Strong reflection with areas of less consistent areas. | Mean 5x5 smoother |
| Cobourg / Collingwood | 3 | Flood pick - Seed pick on every 4th line w/ manual cleanup picks line by line | Strong reflection consistent across the area | Mean 5x5 smoother |
| Georgian Bay | 2 | Grid to Horizon – Picked every 10 th inline and every 10 th cross line | Weak inconsistent trough | Grid 75mx75m to provide smooth grid |
| Queenston | 3 | Manual line by line | Consistent to inconsistent pick, flood pick failed | Mean 5x5 smoother |
| Manitoulin | 3 | Manual line by line | Consistent to inconsistent pick, flood pick had sections of difficulty | Mean 5x5 smoother |
| Cabot Head | 3 | Manual line by line | Consistent to inconsistent pick, flood pick had sections of difficulty | Mean 5x5 smoother |
| Goat Island | 3 | Manual line by line | Inconsistent pick across the 3D. Attributes of Instantaneous phase and cosine of instantaneous phase and filtered data sets were used to attempt easier picks | Mean 5x5 smoother |
| Guelph | 1 | Manual line by line, subtracted 2 ms to Goat Island and manually added in the reef. The 2 ms was taken from well synthetic data time interval. | Inconsistent pick across the 3D. Attributes of Instantaneous phase and cosine of instantaneous phase and filtered data sets were used to attempt easier picks | Mean 5x5 smoother |
| Salina_A2 Carbonate | 1 | Grid to horizon - Manual every 5 th Inline pick with some cross line picks to stabilize | Very inconsistent pick across the 3D. Attributes of Instantaneous phase and cosine of instantaneous phase and filtered data sets were used to attempt easier picks | Grid 75 mx75 m to provide a smooth grid |
| Salina_D | 1 | Manual line by line | Mostly inconsistent pick, flood pick had sections of difficulty. Attributes of Instantaneous phase and cosine of instantaneous phase and filtered data sets were used to attempt easier picks | Mean 5x5 smoother |
| Salina_F | 1 | Grid to horizon - Manual every 6 th Crossline pick with some Inline picks to stabilize | Above sonic logging level. Consistent to inconsistent pick, flood pick had sections of difficulty. Attributes of Instantaneous phase and cosine of instantaneous phase and filtered data sets were used to attempt easier picks | Grid 75mx75m to provide a smooth grid |

4 INTERPRETATION OF HORIZONS IN TIME AND STRUCTURE MAPPING

4.1 Description of horizons

After the stratigraphic horizons were picked as per the descriptions and tables above, their geometry in the time domain and amplitudes are evaluated. The traveltimes presented in the time-domain maps indicate that the lower traveltimes values correspond to shallower depths, whereas the higher traveltimes values correspond to deeper depths. Traveltimes shown are the two-way time. The amplitude maps are the amplitude of the seismic trace at the picked time horizon. Spatial variability in seismic amplitudes from each of the stratigraphic horizons are presented which are potentially related to lateral changes in rock heterogeneity (e.g. petrophysical, lithological, etc.). However, variabilities in amplitude can also result from difficulties in tracing the horizon across the seismic volume, potentially incorporating amplitude values from adjacent rock units in challenging areas. The traveltimes and amplitude maps for each of the stratigraphic horizons interpreted are summarized below and the corresponding time and amplitude maps are depicted in the Appendix A. Two of the figures are reproduced within this section, including Figure 7 (Guelph Formation) and Figure 8 (Cobourg Formation – Collingwood Member).

4.1.1 Upper Silurian Seismic Horizons

Seismic horizons interpreted within the Upper Silurian include the Salina Formation F-Unit, D-Unit and the A2 Unit.

The Salina Formation F-Unit is the shallowest horizon identified in the seismic volume and is made up of repeating deposition of carbonate, evaporites, and shales. Figure A-1 shows the time structure and seismic amplitude of the upper horizon of the Salina Formation F-Unit. The reflection event was inconsistent in some areas of the seismic volume as the fold was low at this shallow depth, causing difficulties with the automatic picking tool. The time horizon clearly displays the draping over the reefal structure in the Guelph Formation, highlighting its footprint on shallower layers with weaker seismic amplitudes to the east, particularly over the reef.

Figure A-2 shows the time structure and seismic amplitude of the Salina Formation D-Unit which is characterized as a carbonate/evaporate unit. Similar to the Salina F-Unit, the D-Unit horizon was also difficult to pick as a result of the shallow portion of the seismic volume having low seismic fold. It was manually picked every 6th crossline (75 m) and infilled with automatic picking. The horizon was then manually edited using the instantaneous phase attribute as a guide. A 75 m x 75 m smoothing operator was applied to the seismic data volume to aid in picking this horizon. The time horizon clearly depicts the footprint of the Guelph Reef feature in the east. Limited insights can be obtained from the amplitude plots; however, a seismic anomaly begins to emerge as a low amplitude, north-south oriented feature within the eastern half of the plot.

Figure A-3 shows the time structure and seismic amplitude of the Salina Formation A2 Unit carbonate. This horizon was very inconsistent within the data volume as it is a very low amplitude reflection. It was manually picked every 5th inline (125 m) before automatic picking. The amplitude map exhibits a similar north-south feature in the central region, akin to the one observed in the D-Unit, particularly prominent in the northern portion. This amplitude anomaly may be linked to compositional or lithological variations, possibly associated with deeper Silurian structures. Additionally, amplitude values on the eastern side

of the volume show a significant increase, likely due to a tuning effect as the A2 carbonate thins over the reef. The seismic tuning effect refers to the phenomenon that occurs when the thickness of a geological layer is such that the seismic reflections from the top and bottom of the layer interfere constructively or destructively. This interference can significantly affect the amplitude and shape of the reflected seismic signal.

4.1.2 Lower Silurian Seismic Horizons

The lower Silurian-aged seismic horizons interpreted include the Guelph, Goat Island, Cabot Head, and Manitoulin formations.

Figure A-4 (also reproduced as Figure 7) shows the time structure and seismic amplitude of the Guelph Formation. The shape of a reef is evident in this map, which also shows SB_BH01 located east of the highest point of the reefal feature. This horizon proved challenging to pick consistently. To assist with the picking process, 2 milliseconds (ms) were initially subtracted from the underlying Goat Island Formation, and then manually adjusted in the reef area based on the drape of the overlying layers and the synthetic tie analysis to SB_BH01, which intersected this reef. The regional thickness of the Guelph Formation is generally too thin to be reliably picked outside the reef, requiring the use of the Goat Island horizon as a guide. However, within the reef, the Guelph Formation exhibits sufficient thickness, enabling a clear identification of the top horizon where both the upper and lower wavelets can be distinctly resolved. The Guelph Formation consists of reefal to inter-reefal dolostones. In both the amplitude and time maps, the north-south feature described earlier is primarily evident in the central northern region, where the time map highlights a structural high (lower traveltimes) indicative of elevated topographic relief, bordered by relatively flatter layers (higher traveltimes).

Figure A-5 shows the time structure and seismic amplitude of the horizon corresponding to the Goat Island Formation, which is 28.98 m thicker in borehole SB_BH01 (45.12 m) when compared to SB_BH02 (16.14 m). The Goat Island horizon was a straightforward pick as a single peak, except in areas of low thickness near the reef structure where it became more difficult to interpret. An increase in amplitudes under the reef is observed, which might be due to tuning effects.

Figure A-6 shows the time structure and seismic amplitude of the Cabot Head Formation. This horizon was reasonably consistent across the seismic volume. The time structure map clearly shows the influence of the bedrock high as represented by lower traveltimes along the eastern portion of the survey.

Figure A-7 shows the time structure and seismic amplitude of the Manitoulin Formation that was picked as a peak. The area towards the east displays lower traveltimes with slight variation in amplitude. This suggests a relatively consistent layer in terms of seismic response and thickness, similar to the bedrock high highlighted above. The Manitoulin Formation represents the base of the lower Silurian where an unconformity exists to the underlying Ordovician-aged Queenston shale.

4.1.3 Upper Ordovician Seismic Horizons

The time-domain interpretation of seismic horizons within the Upper Ordovician-aged stratigraphy includes the Queenston, Georgian Bay, Cobourg, Sherman Falls, Kirkfield, Coboconk, and Gull River formations.

Time structure and seismic amplitude of the Queenston Formation shale are presented in Figure A-8. The Queenston shale horizon was easy to automatically pick throughout the volume. The eastern area

displays generally lower traveltimes, suggesting a structural high that reflects the overall WSW-dipping trend. This region is also characterized by predominantly strong negative amplitudes, particularly beneath the reef. The north-south trend observed in the shallower layers of the north-central region diminishes at this formation, as neither the amplitude nor the time maps exhibit evidence of its continuation at greater depths. This suggests that the anomaly may originate from the Lower Silurian formations, particularly the Guelph Formation, where the anomaly is most pronounced.

Figure A-9 shows the time structure and seismic amplitude of the Georgian Bay Formation. The Georgian Bay horizon was a weak and inconsistent reflection event.

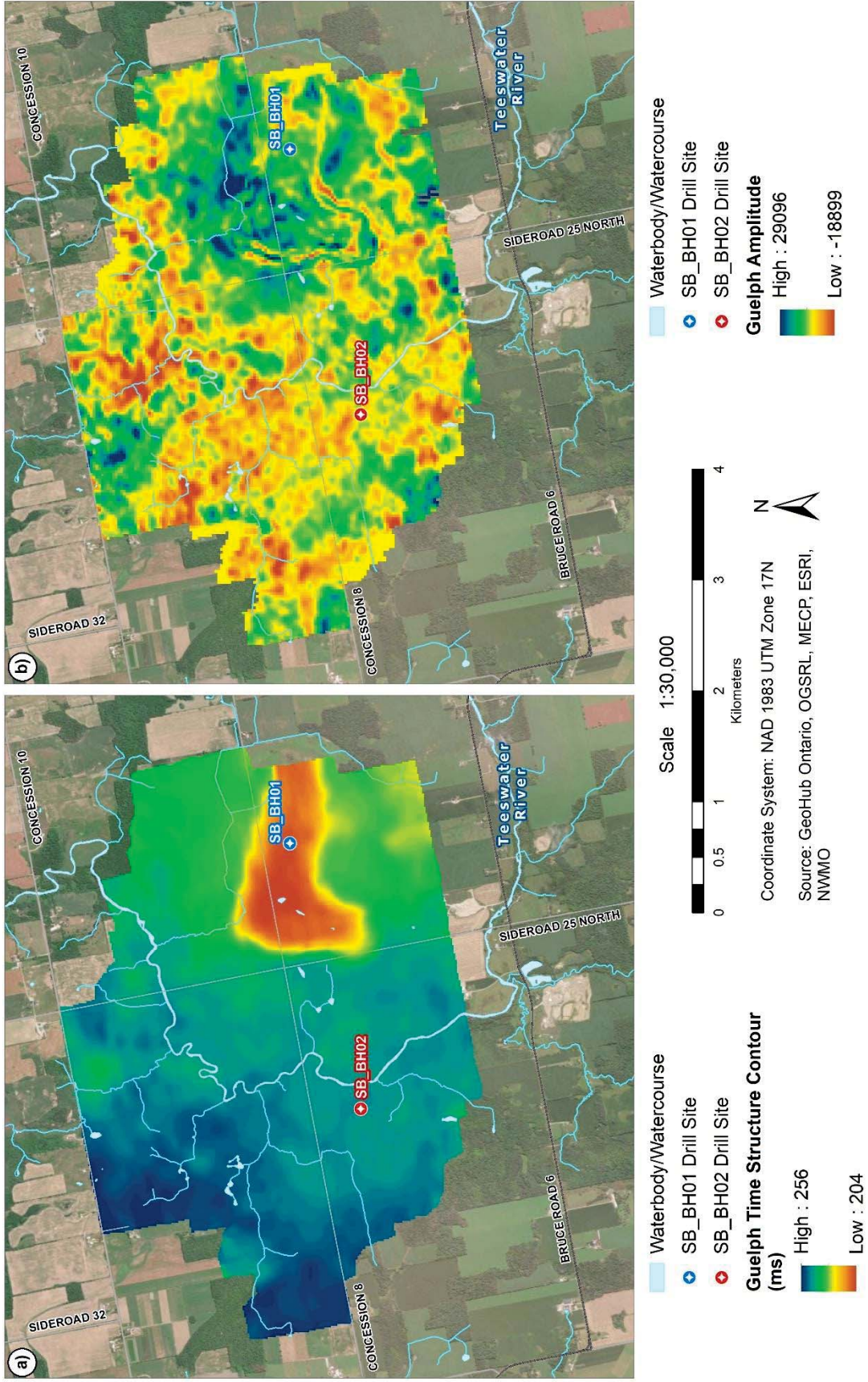


Figure 7 Guelph Formation (a) plan view of interpreted time structure; (b) seismic amplitude. (also shown as Figure A-4) in Appendix A.

Figure A-10 (also reproduced as Figure 8) shows the time structure and seismic amplitude of the Cobourg Formation - Collingwood Member. The Cobourg - Collingwood pick was a strong reflection event consistent across the entire seismic volume. This horizon shows consistent amplitude across the volume and represents the top of the Trenton Group. The red boundary around the amplitude horizon indicates that the original picks extended beyond the muted data volume, these values represent a processing artifact.

Figure A-11 shows the time structure and seismic amplitude of the Sherman Falls Formation. The Sherman Falls pick was strong and consistent throughout the data volume. Overall, both amplitude and time maps exhibit characteristics similar to the overlying formations, with a notable topographic high to the east (indicating lower traveltimes).

Figure A-12 shows the time structure and seismic amplitude of the Kirkfield Formation. The Kirkfield pick was inconsistent throughout the volume. This required a 75m X 75m smoother operator to be applied to improve image interpretability.

Figure A-13 shows the time structure and seismic amplitude of the Coboconk Formation. The Coboconk peak represents the top of the Black River Group and was a relatively consistent peak that could be automatically picked after providing seed lines every 4th crossline.

Figure A-14 shows the time structure and seismic amplitude of the Gull River Formation. The Gull River pick was relatively consistent within the data volume.

4.1.4 Precambrian Seismic Horizon

Figure A-15 shows the time structure and seismic amplitude of the Shadow Lake – Precambrian horizon pick. The Shadow Lake/Precambrian pick is a strong peak across the data volume, and it was easily interpreted.

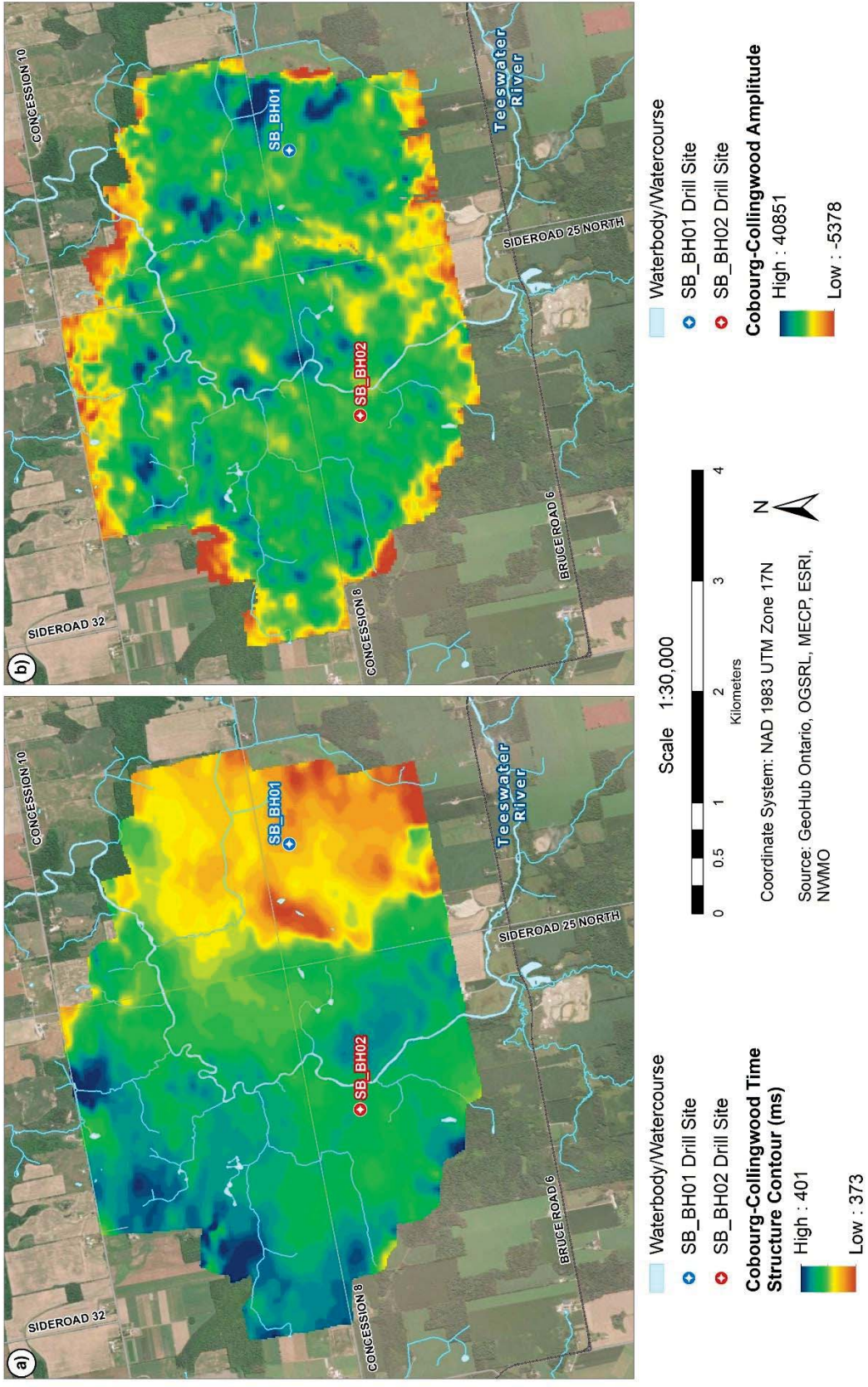


Figure 8 Cobourg Formation – Collingwood Member (a) Plan view of interpreted time structure; (b) Seismic amplitude. (also shown as Figure A-10) in Appendix A.

4.2 Reef Interpretation

An isochron map was generated to represent the time difference between the top of the Guelph Formation and the underlying Cabot Head Formation. This facilitated the identification of a reef structure in the eastern portion of the study area, the Guelph Reef, as illustrated in Figure 9. The reef was initially recognized through borehole SB_BH01 without prior seismic imaging or knowledge. Its geometry and extent were subsequently delineated through analysis of the 3D seismic volume. Borehole data indicate that the Guelph Formation at SB_BH01 is approximately 50 m thick, while the orange coloration west of SB_BH01 on the isochron map suggests even greater thicknesses in that region. The reef structure spans a surface area of approximately 200 hectares, with a maximum isochron of 30 ms, corresponding to an estimated thickness of ~65 m at its thickest point. Using the mapped outline and thickness estimates, the reef's total volume is calculated to be approximately 60 million cubic meters.

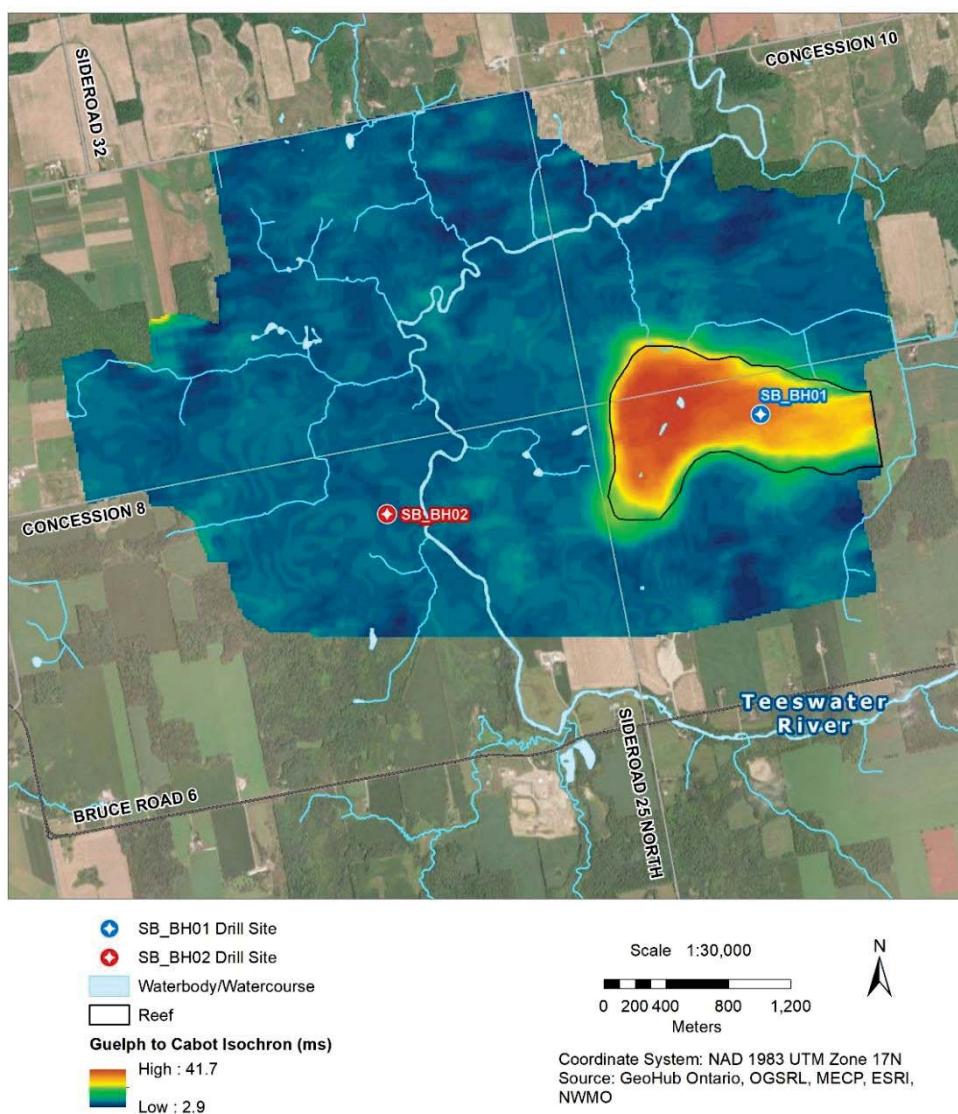


Figure 9 Guelph – Cabot Isochron depicting the reef outline.

4.3 Seismic Anomaly near Reef

Seismic anomalies were investigated line by line in both east-west and north-south orientations within the data volume and if observed they were assigned a planar location. As an example, a seismic anomaly was noted in these data along the western flank of the interpreted reef, along crossline 207 as depicted in Figure 10. At this time, it is referred to as a seismically identified linear trend of undetermined origin. Two hypotheses that could explain these features are presented within this report. However, borehole drilling may be required to confidently confirm or refute these hypotheses.

One hypothesis is that the observed seismic anomalies may represent velocity pull-ups caused by lateral velocity contrasts between the carbonate reef and the surrounding rock units (Fagin, 1991; Shragge et al., 2019). These velocity contrasts result in faster seismic wave propagation through the high-velocity carbonate reef compared to the adjacent lower-velocity rock units. This differential velocity causes underlying formations to appear uplifted on seismic sections, creating a mounded reflection pattern. This effect, highlighted by the arrows in Figure 10, is particularly evident beneath the low-frequency shale sequences of the Queenston, Georgian Bay, and Blue Mountain Formations. Another hypothesis that may contribute to this seismic anomaly is a potential reef buildup at the edge of a fault block causing the reef to form in a linear manner. Sanford et al. (1985) suggests that pinnacle reef growth in SW Ontario occurred on topographic highs created on the up-thrown side of fault blocks, which were part of a regular and extensive fault network in southern Ontario. As mentioned above, further investigations of this seismic anomaly are required to better understand its origin.

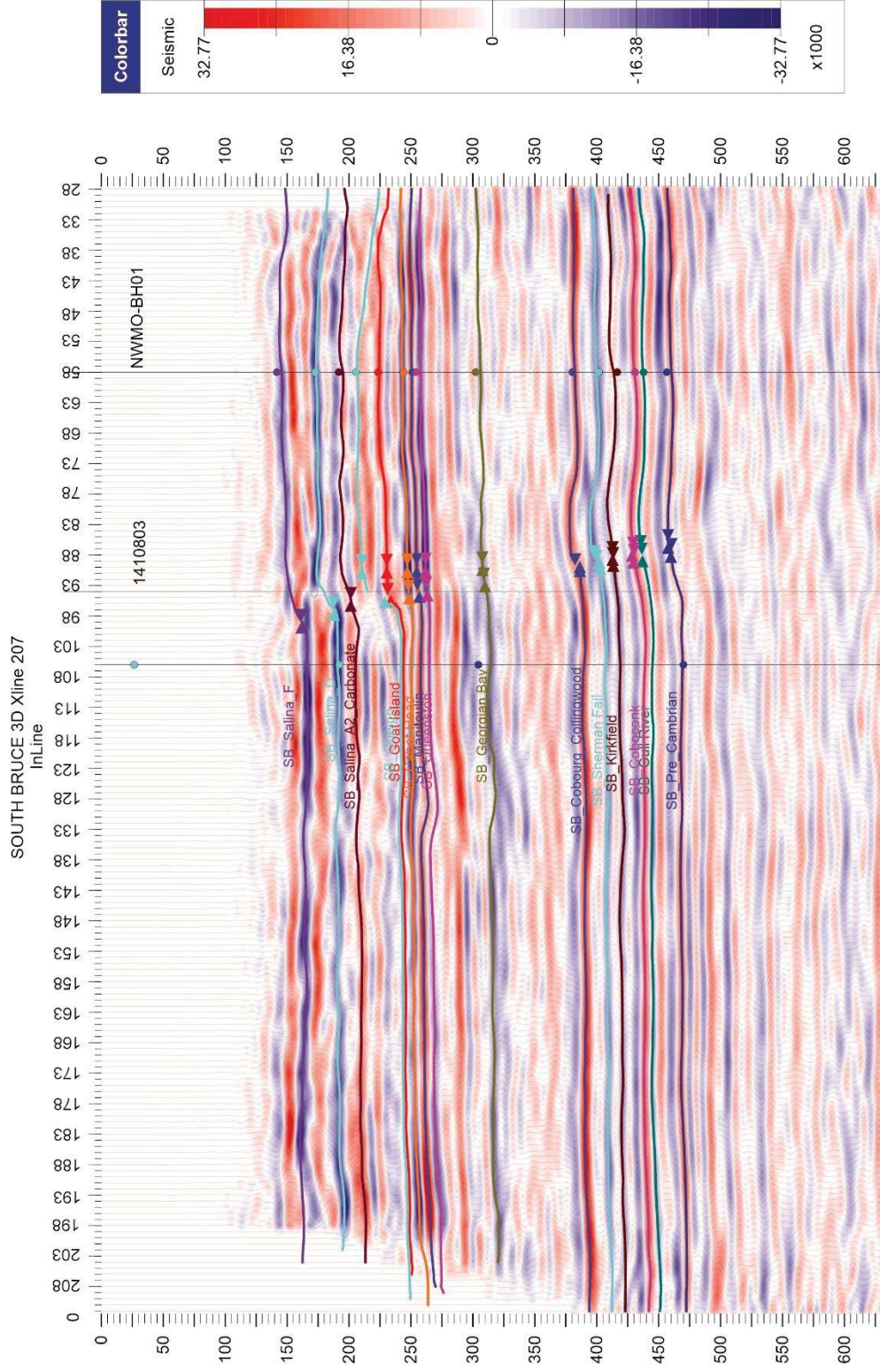


Figure 10 Cross-line 207 showing the mounded reflection pattern near the anomaly on the western flank of the Guelph Reef.

5 VELOCITY MODELING AND DEPTH CONVERSION

Velocity modeling and depth conversion was completed by Schlumberger Canada (SLB). The primary data source for the velocity model was the RMS (Root Mean Square) velocity volume. Several methods were explored to determine the best way to construct the velocity model. Initially, the RMS stacking velocity volume was converted into an average velocity cube through Dix conversion, to be used in depth converting the time surfaces that were gridded from the interpreted horizons. The Dix conversion is a mathematical approach employed in seismic data analysis to transform interval velocities obtained from seismic reflection data into root mean square (RMS) velocities and vice versa. After conversion, depth discrepancies between the picked surfaces and the formation tops were identified in both SB_BH01 and SB_BH02 with differences ranging from 38 m to 114 m as summarized in Table 4.

To improve this velocity model an updated method was adopted which involved creating a 3D velocity grid model. To define zones, structural maps (from Salina F to Precambrian) were used (Figure 11). The grid resolution is set to 50 x 50 m with the vertical resolution of an average 4.31 m. The average velocity logs (derived from sonic logs) and the average velocity cube from seismic were upscaled into the 3D grid. Well log upscaling involves converting fine detailed well log data to a coarser resolution that matches the grid of a reservoir model. Arithmetic averaging was used for this process, which is important for accurately incorporating fine-scale data into larger geological or reservoir models. Subsequently, the average velocity logs were populated using the seismic velocity cube as the trend (Figure 12). For the population of velocity and generation of the final velocity model, the moving average algorithm was used (Figure 13).

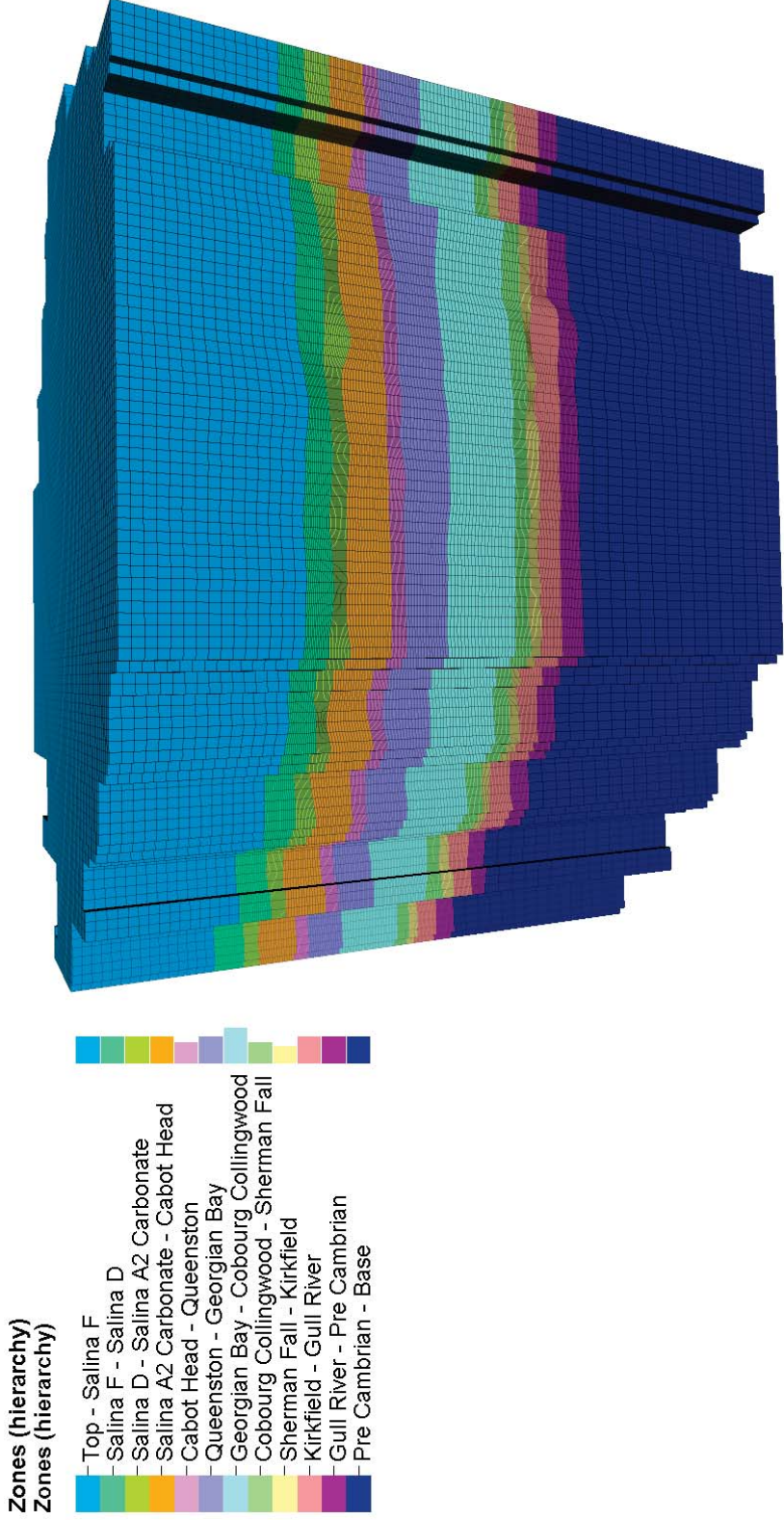


Figure 11 Zones (hierarchy) property showing the zones of the 3D gridded model

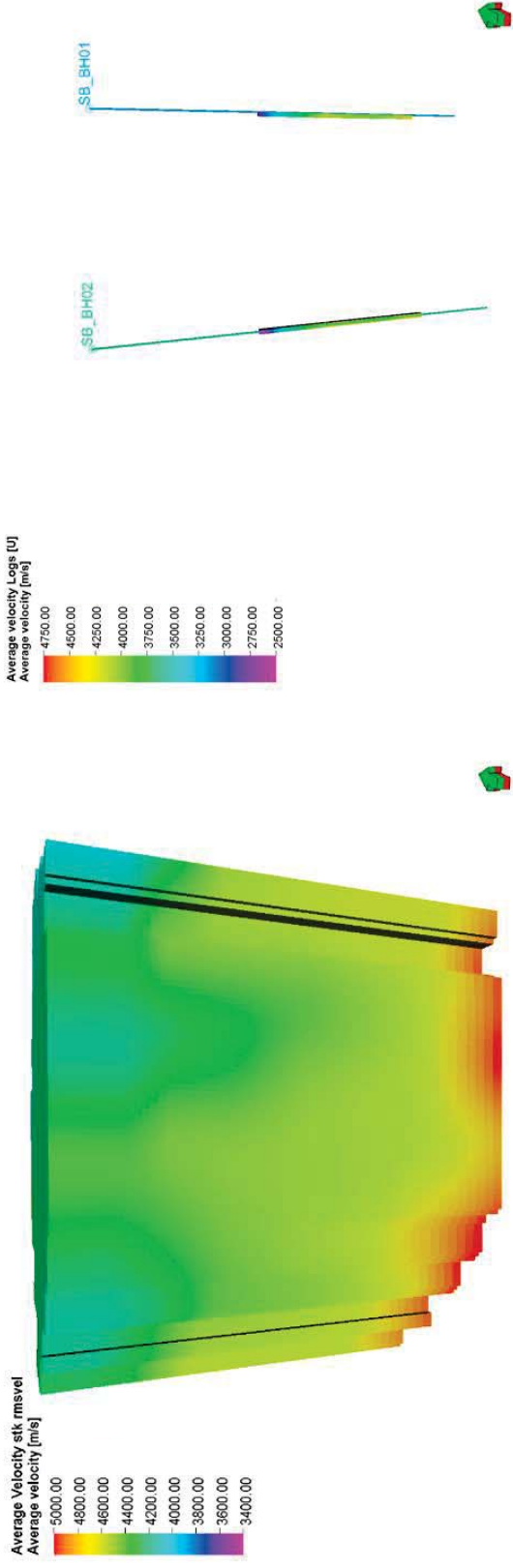


Figure 12 Upscaled average velocity (left) and upscaled average velocity logs (right)

The upscaled average velocity log was incorporated into the designated cells of the 3D grid model. The approach was further refined by employing the upscaled seismic data as a guiding framework. To effectively distribute velocity within the model domains, the moving average algorithm was implemented. The 3D model domain displayed in Figure 13 is also used to populate petrophysical properties as discussed later in this report.

Moving Average:

$$V_{avg}(i, j, k) = \frac{1}{N} \sum_{p=-h}^h \sum_{q=-h}^h \sum_{r=-h}^h V(i + p, j + q, k + r)$$

- $V(i, j, k)$ is the velocity at grid point
- N is the total number of points in the moving window, $N = (2h+1)^3$
- h is the half-window size, i.e., if the window size is 3x3x3, then $h=1$

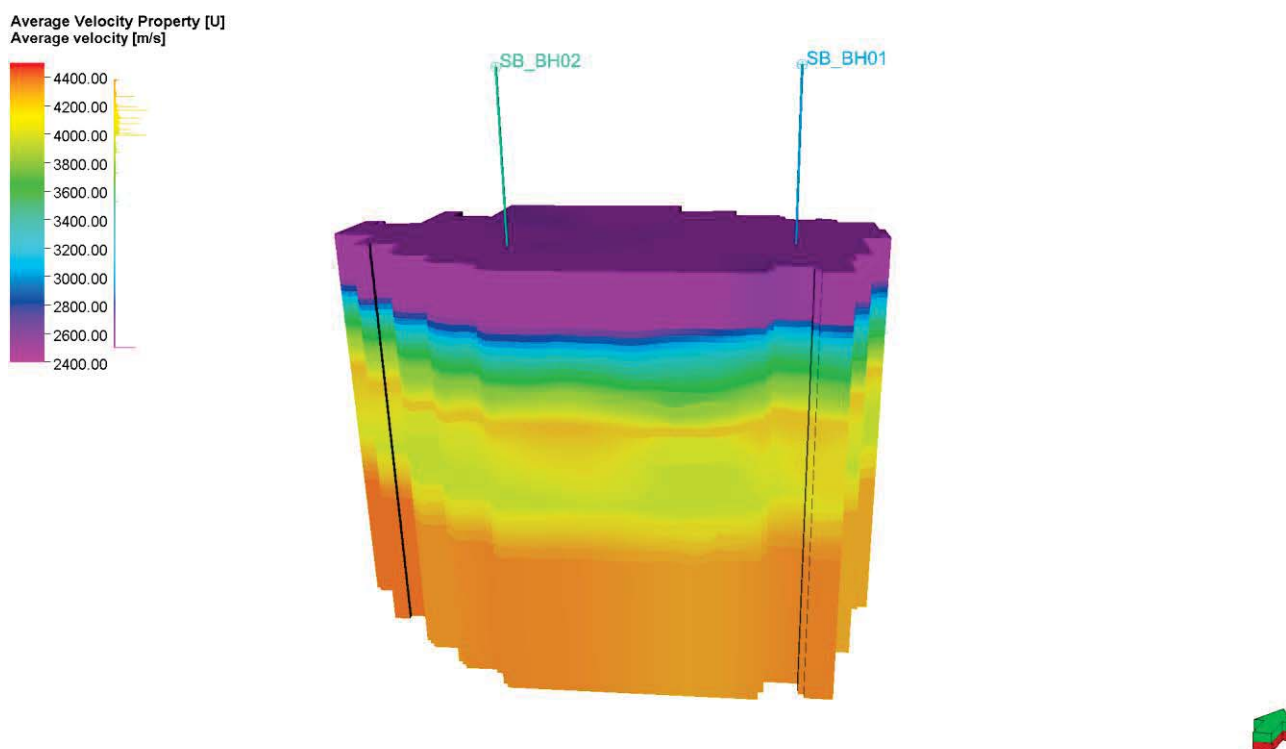


Figure 13 Final velocity model incorporating seismic and borehole data

The final (updated) average velocity model in Figure 13 served as the primary velocity input for this workflow. A layer cake model was used based on the stratigraphic seismic horizons and associated stratigraphic formation tops (well tops) identified from SB_BH01 and SB_BH02. This updated method improved the average range of mismatch between -4.45 m and 12.32 m, a result that was encouraging, prompting to proceed with the well top correction.

Table 4 and Table 5 represent a comparative analysis of velocity model results before and after incorporating the updated velocity model, before well top correction. Table 4 summarizes the initial velocity model results and difference in horizon depths at the well location compared to well tops while using the average velocity cube obtained after Dix conversion of stacking velocity. Table 5 summarizes the depth differences before well top correction using the updated velocity model. This comparison elucidates the effectiveness of the final model in refining the velocity parameter to better align with observed data. A final step involving well top corrections effectively reduces the depth differences to zero at each well location. This correction process is also applied to the underlying updated velocity model to ensure that the formation top depth (horizon) in seismic data matches the formation top depth identified in well logs.

The updated velocity model serves as a cornerstone in the process of converting seismic data from the time to the depth domain. Figure 14 provides a visual representation of the domain conversion process, demonstrating the transition from the time domain to the depth domain. The illustration comprises two distinct sections. The top section of Figure 14a illustrates stratigraphic surfaces interpreted from seismic data, superimposed with SB_BH01 and SB_BH02 showing top of formation picks from existing data (Section 2.1), and expressed in units of time along the vertical axis. The bottom section of Figure 14b showcases the same interpreted seismic stratigraphic surfaces and superimposed borehole log formation picks with the vertical axis showing depth, expressed in units of elevation (meters above sea level, mASL).

Table 4 Comparative analysis of depth-converted seismic horizons and their corresponding geological markers using the initial velocity.

| Formation | Well | X-value | Y-value | Z-value | Horizon after | Difference |
|--------------------------------|---------|----------|-----------|---------|---------------|------------|
| Salina F | SB-BH01 | 473712.1 | 4873187 | 148.32 | 81.87 | 66.46 |
| | SB-BH02 | 471318.4 | 4872548.6 | 98.94 | 30.28 | 68.66 |
| Salina D | SB-BH01 | 473712.1 | 4873187 | 82.11 | 18.6 | 63.51 |
| | SB-BH02 | 471318.4 | 4872548.6 | 27.85 | -30.55 | 58.4 |
| Salina A2 Carbonate | SB-BH01 | 473712.1 | 4873187 | 37.63 | -29.64 | 67.27 |
| | SB-BH02 | 471318.4 | 4872548.6 | -15.48 | -69.18 | 53.7 |
| Guelph | SB-BH01 | 473712.1 | 4873187 | 0.19 | -63.22 | 63.42 |
| | SB-BH02 | 471318.4 | 4872548.6 | -95.35 | -151.94 | 56.59 |
| Goat Island | SB-BH01 | 473712.1 | 4873187 | -48.51 | -106.69 | 58.18 |
| | SB-BH02 | 471318.4 | 4872548.6 | -100.37 | -157.11 | 56.74 |
| Cabot Head | SB-BH01 | 473712.1 | 4873187 | -104.49 | -147.75 | 43.26 |
| | SB-BH02 | 471318.4 | 4872548.6 | -127.79 | -174.72 | 46.93 |
| Manitoulin | SB-BH01 | 473712.1 | 4873187 | -124.32 | -163.02 | 38.7 |
| | SB-BH02 | 471318.4 | 4872548.6 | -148.61 | -193.55 | 44.94 |
| Queenston | SB-BH01 | 473712.1 | 4873187 | -132.88 | -179.92 | 47.04 |
| | SB-BH02 | 471318.4 | 4872548.6 | -157.76 | -210.31 | 52.55 |
| Georgian Bay | SB-BH01 | 473712.1 | 4873187 | -217.61 | -287.11 | 69.51 |
| | SB-BH02 | 471318.4 | 4872548.6 | -243.21 | -320.61 | 77.4 |
| Cobourg Collingwood | SB-BH01 | 473712.1 | 4873187 | -353.28 | -455.59 | 102.32 |
| | SB-BH02 | 471318.4 | 4872548.6 | -378.2 | -492.83 | 114.63 |
| Sherman Fall | SB-BH01 | 473712.1 | 4873187 | -401.1 | -494.62 | 93.53 |
| | SB-BH02 | 471318.4 | 4872548.6 | -424.88 | -533.84 | 108.96 |
| Kirkfield | SB-BH01 | 473712.1 | 4873187 | -446.17 | -523.98 | 77.81 |
| | SB-BH02 | 471318.4 | 4872548.6 | -470.54 | -561.66 | 91.12 |
| Coboconk | SB-BH01 | 473712.1 | 4873187 | -489.56 | -565.91 | 76.35 |
| | SB-BH02 | 471318.4 | 4872548.6 | -514.14 | -607.06 | 92.92 |
| Gull River | SB-BH01 | 473712.1 | 4873187 | -510.74 | -582.97 | 72.24 |
| | SB-BH02 | 471318.4 | 4872548.6 | -535.22 | -621.44 | 86.22 |
| Precambrian | SB-BH01 | 473712.1 | 4873187 | -568.84 | -636.6 | 67.77 |
| | SB-BH02 | 471318.4 | 4872548.6 | -595.44 | -680.53 | 85.09 |

Table 5 Comparative analysis of depth-converted seismic horizons and their corresponding geological markers using the updated velocity.

| Formation | Well | X-value | Y-value | Z-value | Horizon after | Difference |
|---------------------|---------|----------|-----------|---------|---------------|------------|
| Salina F | SB-BH01 | 473712.1 | 4873187 | 148.32 | 145.24 | 3.08 |
| | SB-BH02 | 471318.4 | 4872548.6 | 98.94 | 93.74 | 5.2 |
| Salina D | SB-BH01 | 473712.1 | 4873187 | 82.11 | 80.43 | 1.68 |
| | SB-BH02 | 471318.4 | 4872548.6 | 27.85 | 23.23 | 4.62 |
| Salina A2 | SB-BH01 | 473712.1 | 4873187 | 37.63 | 28.95 | 8.68 |
| Carbonate | SB-BH02 | 471318.4 | 4872548.6 | -15.48 | -11.89 | -3.59 |
| Guelph | SB-BH01 | 473712.1 | 4873187 | 0.19 | -7.47 | 7.66 |
| | SB-BH02 | 471318.4 | 4872548.6 | -95.35 | -107.67 | 12.32 |
| Goat Island | SB-BH01 | 473712.1 | 4873187 | -48.51 | -55.87 | 7.36 |
| | SB-BH02 | 471318.4 | 4872548.6 | -100.37 | -113.69 | 13.32 |
| Cabot Head | SB-BH01 | 473712.1 | 4873187 | -104.49 | -108.05 | 3.56 |
| | SB-BH02 | 471318.4 | 4872548.6 | -127.79 | -131.31 | 3.52 |
| Manitoulin | SB-BH01 | 473712.1 | 4873187 | -124.32 | -120.79 | -3.53 |
| | SB-BH02 | 471318.4 | 4872548.6 | -148.61 | -146.07 | -2.54 |
| Queenston | SB-BH01 | 473712.1 | 4873187 | -132.88 | -137 | 4.13 |
| | SB-BH02 | 471318.4 | 4872548.6 | -157.76 | -160.17 | 2.41 |
| Georgian | SB-BH01 | 473712.1 | 4873187 | -217.61 | -217.12 | -0.48 |
| Bay | SB-BH02 | 471318.4 | 4872548.6 | -243.21 | -250.78 | 7.57 |
| Cobourg | SB-BH01 | 473712.1 | 4873187 | -353.28 | -364.18 | 10.9 |
| Collingwood | SB-BH02 | 471318.4 | 4872548.6 | -378.2 | -383.86 | 5.66 |
| Sherman Fall | SB-BH01 | 473712.1 | 4873187 | -401.1 | -412.11 | 11.01 |
| | SB-BH02 | 471318.4 | 4872548.6 | -424.88 | -434.57 | 9.69 |
| Kirkfield | SB-BH01 | 473712.1 | 4873187 | -446.17 | -444.88 | -1.28 |
| | SB-BH02 | 471318.4 | 4872548.6 | -470.54 | -466.09 | -4.45 |
| Coboconk | SB-BH01 | 473712.1 | 4873187 | -489.56 | -492.61 | 3.05 |
| | SB-BH02 | 471318.4 | 4872548.6 | -514.14 | -519.84 | 5.7 |
| Gull River | SB-BH01 | 473712.1 | 4873187 | -510.74 | -513.82 | 3.08 |
| | SB-BH02 | 471318.4 | 4872548.6 | -535.22 | -538.97 | 3.75 |
| Precambrian | SB-BH01 | 473712.1 | 4873187 | -568.84 | -575.78 | 6.95 |
| | SB-BH02 | 471318.4 | 4872548.6 | -595.44 | -611.2 | 15.76 |

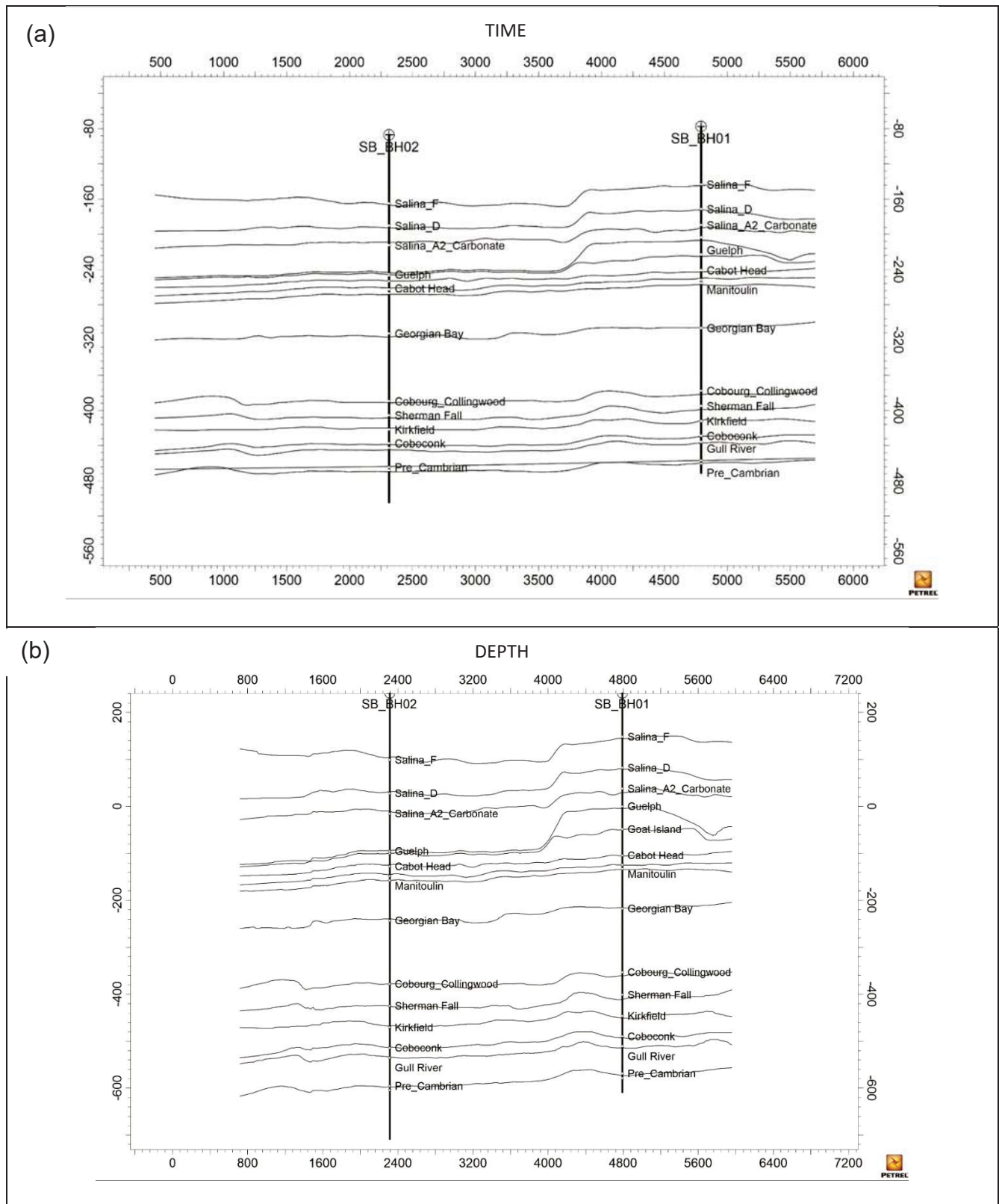


Figure 14 Cross-section of (a) the time horizons and (b) the depth horizons for the time to depth conversion.

6 SEISMIC INVERSION

6.1 AVO Inversion

This study incorporates geophysical well log data from two boreholes (SB_BH01 and SB_BH02) which are used as constraints for the inversion of acoustic impedance (AI), Vp/Vs velocity ratio, and density from the seismic volume. The geophysical well logs included gamma-gamma density, and Vp and Vs velocities derived from borehole sonic logs (Geofirma Engineering Ltd, 2024d and 2024e). Acoustic impedance and the Vp/Vs ratio logs are derived from the velocity and density logs. The original sampling rate of these well logs was 0.02 m; they are then resampled at 0.5 m creating a smoothed version. Resampling is completed to bring the well log results and the seismic volume to approximately the same resolution. The resulting resampled logs are labelled with extension SR as follows: AI_SR, VpVs_SR, and Density_SR.

The next step included wavelet extraction, a process which involves identifying and isolating the seismic wavelet from seismic data. The wavelet is the basic shape of the seismic signal, and its extraction is important for inversion and interpretation processes. Seismic trace alignment was also completed, which aligns seismic traces to a common reference, often a horizon or a reflection event. Accurate alignment is essential for stacking, correlation, and comparison of seismic data, which improves the overall quality and interpretability of seismic images. Finally, low-frequency model construction is completed to refine inputs for simultaneous inversion. In seismic inversion, a low-frequency model provides the initial subsurface properties at low frequencies, which are not well captured by seismic reflection data.

Low-frequency models are combined with higher-frequency seismic data to create a more accurate and detailed representation of the subsurface. Employing the “primary-primary” (PP) AVO technique, the study aims to characterize subsurface properties for physical properties and lithology predictions (Aki, K. and P.G. Richards, (1980), “PP” refers to the reflection of P-waves (primary waves) from a subsurface interface back to the surface as P-waves. This is contrasted with other types of reflections, such as PS (P-wave reflecting and converting to an S-wave), which involve mode conversion. Primarily, acoustic impedance, Vp/Vs velocity ratio, and density logs were used as input data for the inversion.

For the generation of synthetic seismograms, two distinct wavelets were derived from the full stack seismic data. A deterministic method was employed during the wavelet extraction. The wavelets’ time vs amplitude graphs are shown in Figure 15. Full stack wavelets are used in the synthetic generation workflow.

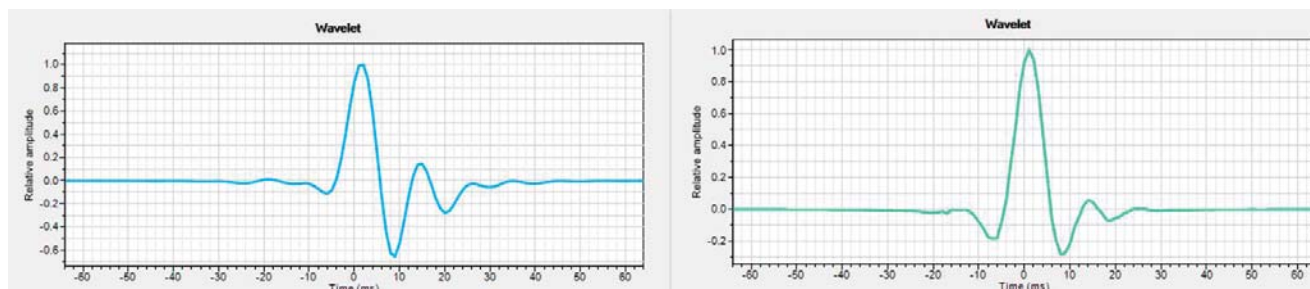


Figure 15 Wavelet generated from full stack for SB_BH01 (left) and SB_BH02 (right) for synthetic seismograms.

Ensuring an accurate time-depth relationship is essential for successful interpretation. Prior to initiating the inversion workflow, it was evident that SB_BH01 and SB_BH02 were well tied as shown by the close match between the synthetic seismic data compared to the actual seismic data as shown in Figure 16 (SB_BH01) and Figure 17 (SB_BH02). Figure 16 and Figure 17 display multiple log tracks: the initial track features the density curve (in blue) and the sonic curve (in black); the second track exhibits both the acoustic impedance (in black) and the resampled acoustic impedance (in red); the third track illustrates actual seismic data along the borehole; the fourth track showcases the synthetic data; and the fifth track presents the P-wave interval velocity. Upon finalizing the well tie, we conducted a secondary QC check by verifying the alignment of well tops and horizon interpretations in the time domain to ensure optimal tie. Figure 18 shows the seismic section as a straight line between SB_BH01 and SB_BH02 with interpreted seismic horizons along with stratigraphic well tops. Overall, there is a good agreement between the seismic and well-log-derived datasets, with varying degrees of correlation between actual and synthetic reflections. For instance, a slight misalignment is observed in the shallow section of SB_BH01, particularly around the Salina D unit.

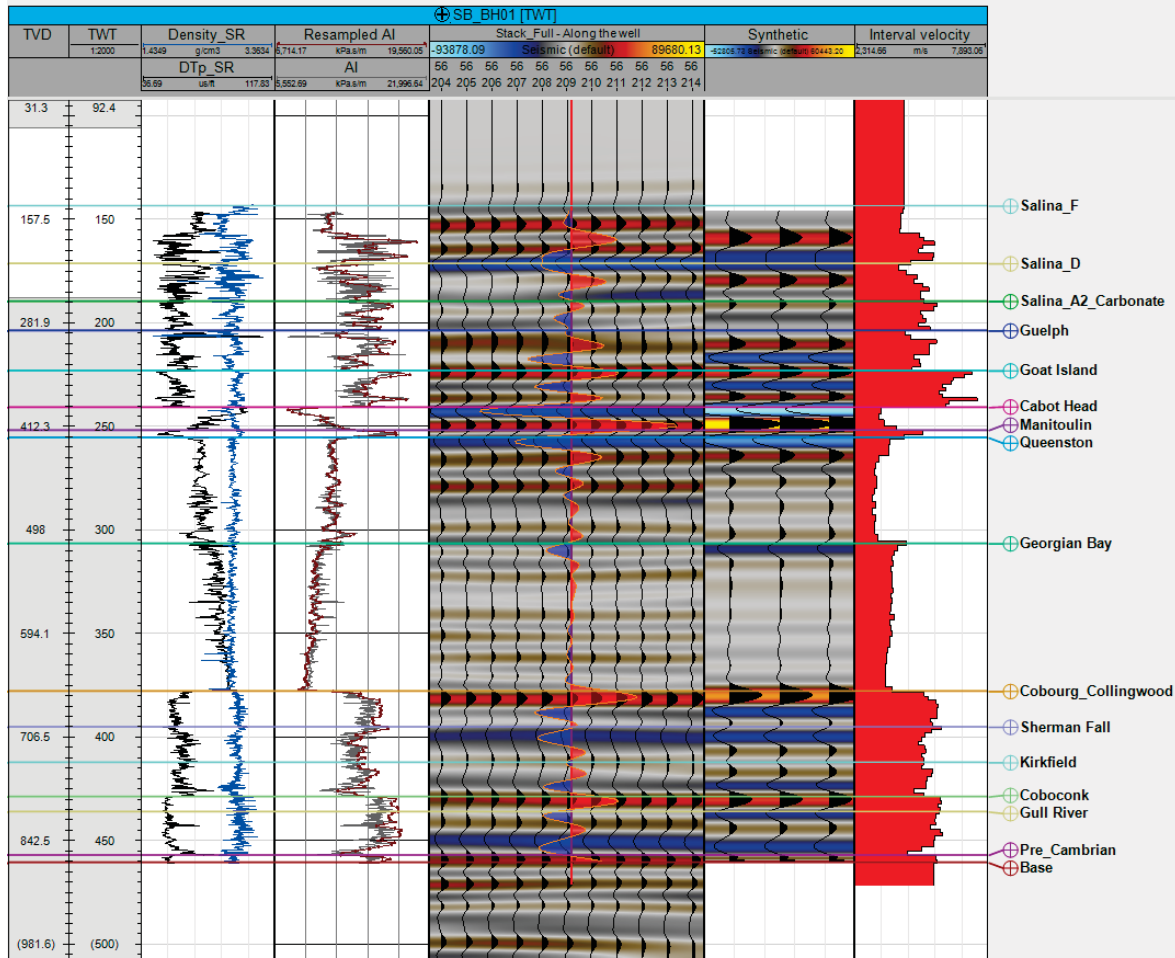


Figure 16 SB_BH01 - Borehole geophysical data (left) alongside actual and synthetic seismic data (right), with a cross-correlation of 99.7% between synthetic and actual seismic traces.

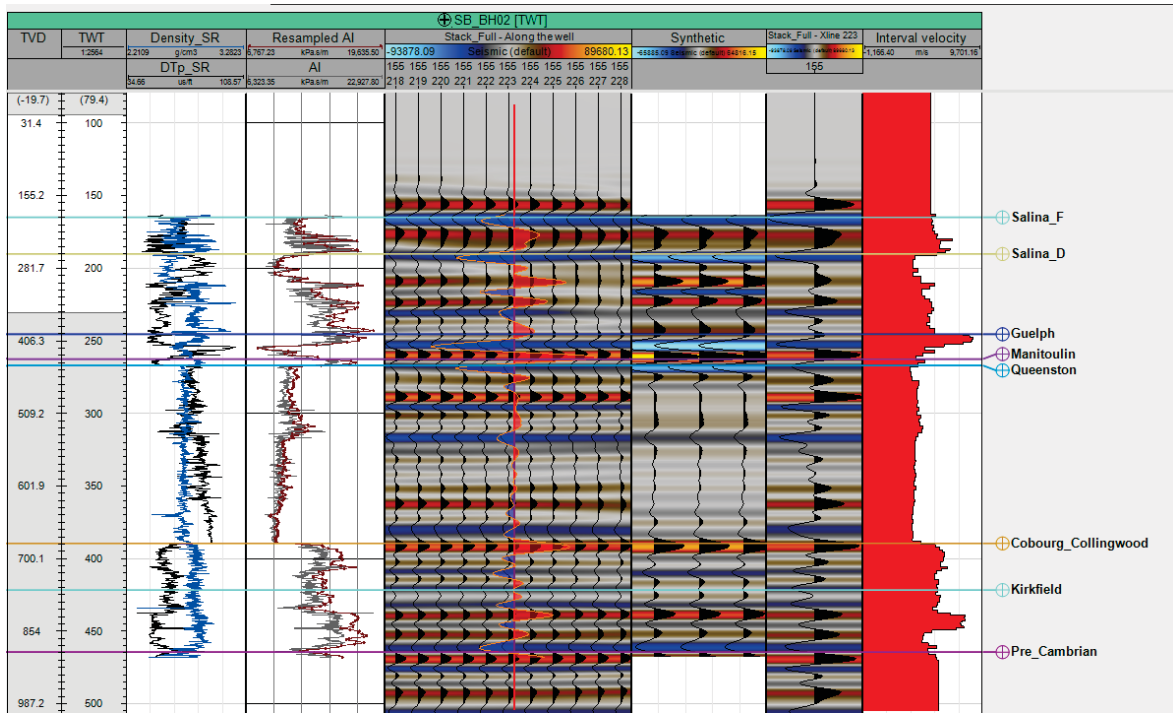


Figure 17 SB_BH02 - Borehole geophysical data (left) alongside actual and synthetic seismic data (right), with a cross-correlation of 98.2% between synthetic and actual seismic traces.

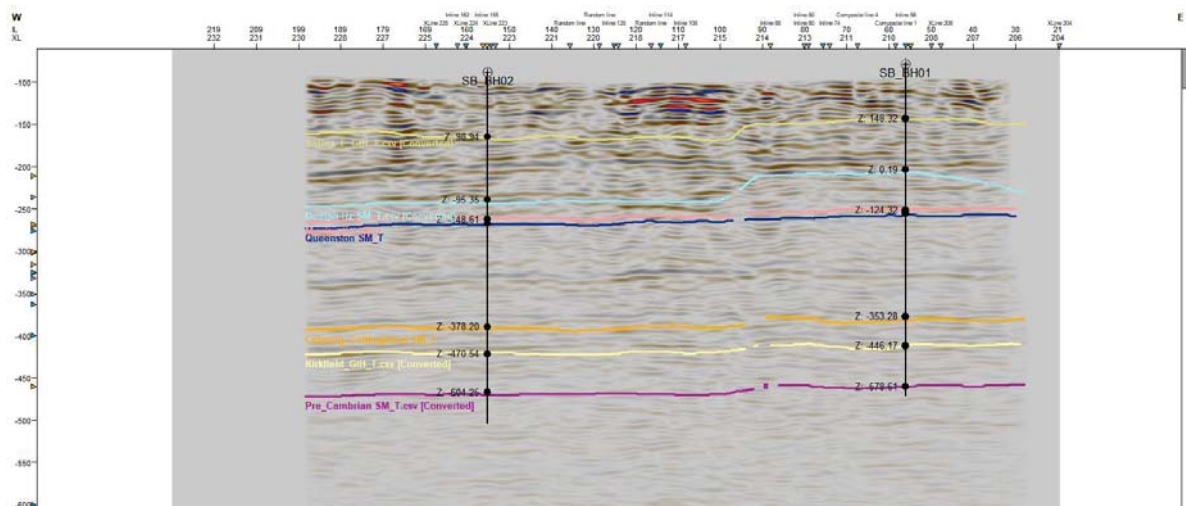


Figure 18 SB_BH01 and SB_BH02 well tops, alongside the time-domain horizons.

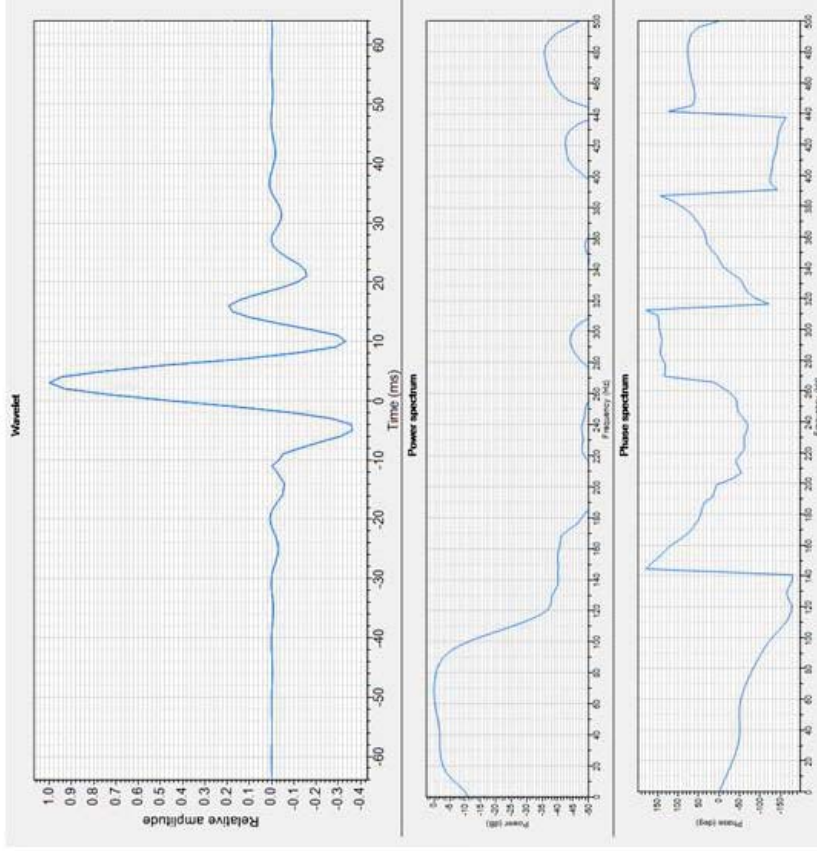
For the simultaneous seismic inversion, angle gathers 4-14, 14-21, 21-28, and 28-38 were chosen. Wavelets were extracted individually for SB_BH01 and SB_BH02. A deterministic approach was employed in the wavelet extraction process to ensure complete control and to achieve optimal predictability as shown in Figure 19. Figure 19 shows the wavelet shape and its associated power and phase spectrum for angle gather 14-21. Angle gathers 4-14, 21-28, and 28-38 are included in Appendix B. The predictability metric evaluates how well the extracted wavelet can predict the seismic data. A higher predictability ratio indicates a better match between the predicted and actual seismic traces.

In simultaneous inversion, each angle gather can accommodate only one wavelet input. As we obtained two wavelets per angle gather from SB_BH01 and SB_BH02, averaging these wavelets allowed us to utilize a single input for the process (Figure 20).

During the last stage of wavelet extraction, a Hanning filter was utilized to remove high-frequency noise from the average wavelets. The filter was configured with a low cutoff of 0 Hz and a high cutoff of 125 Hz.

SB BH01: 14-21

Predictability: 60.917%



SB BH02: 14-21

Predictability: 60.295%

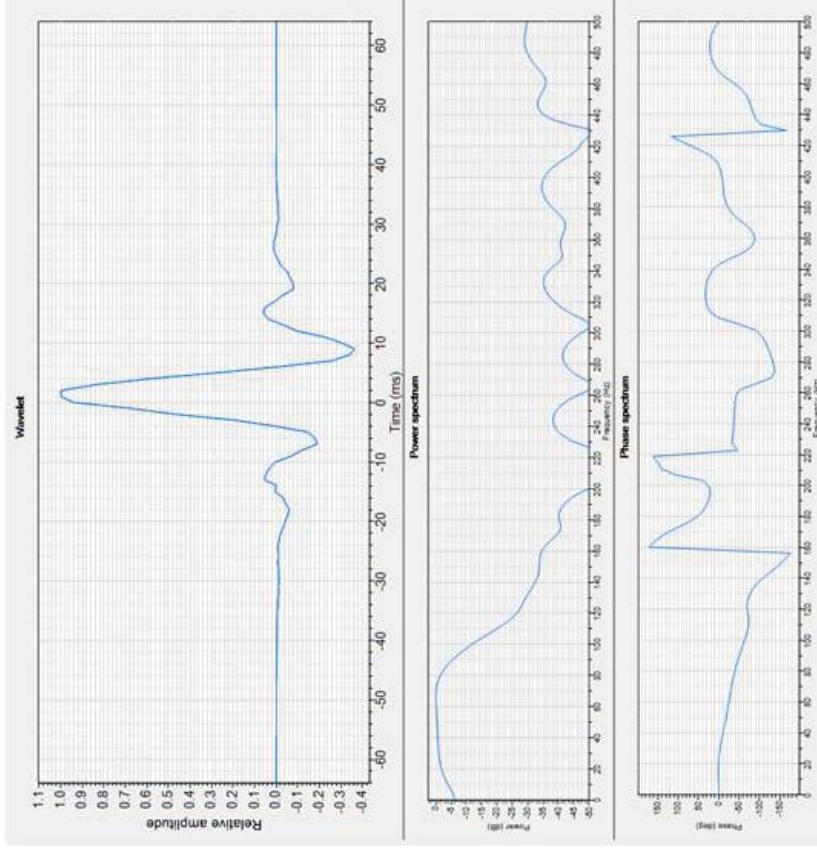


Figure 19. Wavelets extracted from angle gathers (14–21 degrees) for SB_BH01 (left) and SB_BH02 (right), illustrating the wavelet shape, power spectrum, phase spectrum, and predictability ratios.

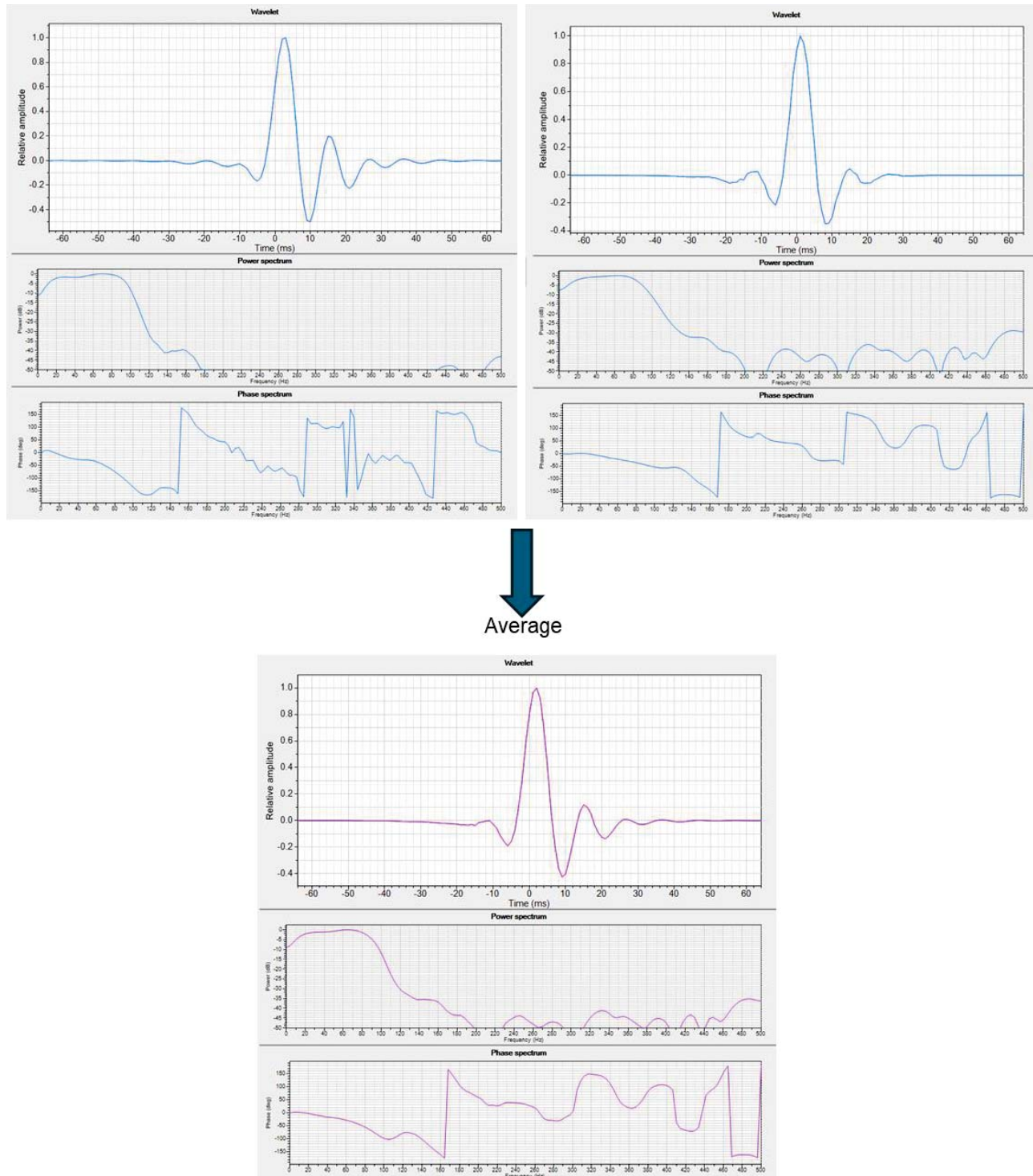


Figure 20 Wavelets extracted from SB_BH01 and SB_BH02 for the 14–21° angle gather, averaged to produce a single wavelet input for simultaneous inversion.

6.2 Initial Low Frequency Model

A low-frequency model (LFM) is a representation of the subsurface properties, such as acoustic impedance or velocity, that primarily contains low-frequency components (typically below 10-15 Hz). This model is essential because seismic data often lack low-frequency information due to the band-limited nature of seismic sources and the attenuation of low frequencies as waves propagate through the Earth. The low-frequency model provides a smooth, large-scale background trend of the subsurface properties, which is then combined with higher-frequency information derived from seismic data to create a more detailed and accurate subsurface model. The inclusion of the low-frequency model helps to constrain the inversion process, leading to more realistic and geologically plausible results.

For the construction of the LFM, acoustic impedance, V_p/V_s ratio, and density logs from SB_BH01 and SB_BH02 were used, along with the interpreted seismic horizons.

For quality control (QC) of the LFM results, we generated three cross-sections intersecting the position of the existing boreholes. These included acoustic impedance LFM (Figure 21), V_p/V_s LFM (Figure 22), and density LFM (Figure 23). The borehole logs are reviewed in comparison with the resulting LFM properties. For the comparison of results, a high-cut filter with an 8-Hz cutoff was applied to the well-log properties. The workflow successfully generates a low-frequency model (LFM) that shows a strong correlation with borehole data, which is essential for seismic inversion. The application of an 8-Hz high cut filter helps to match the frequency content of the seismic data with the well log, further enhancing the reliability of the model. This strong correlation ensures that the LFM provides a robust foundation for accurate subsurface characterization through seismic inversion.

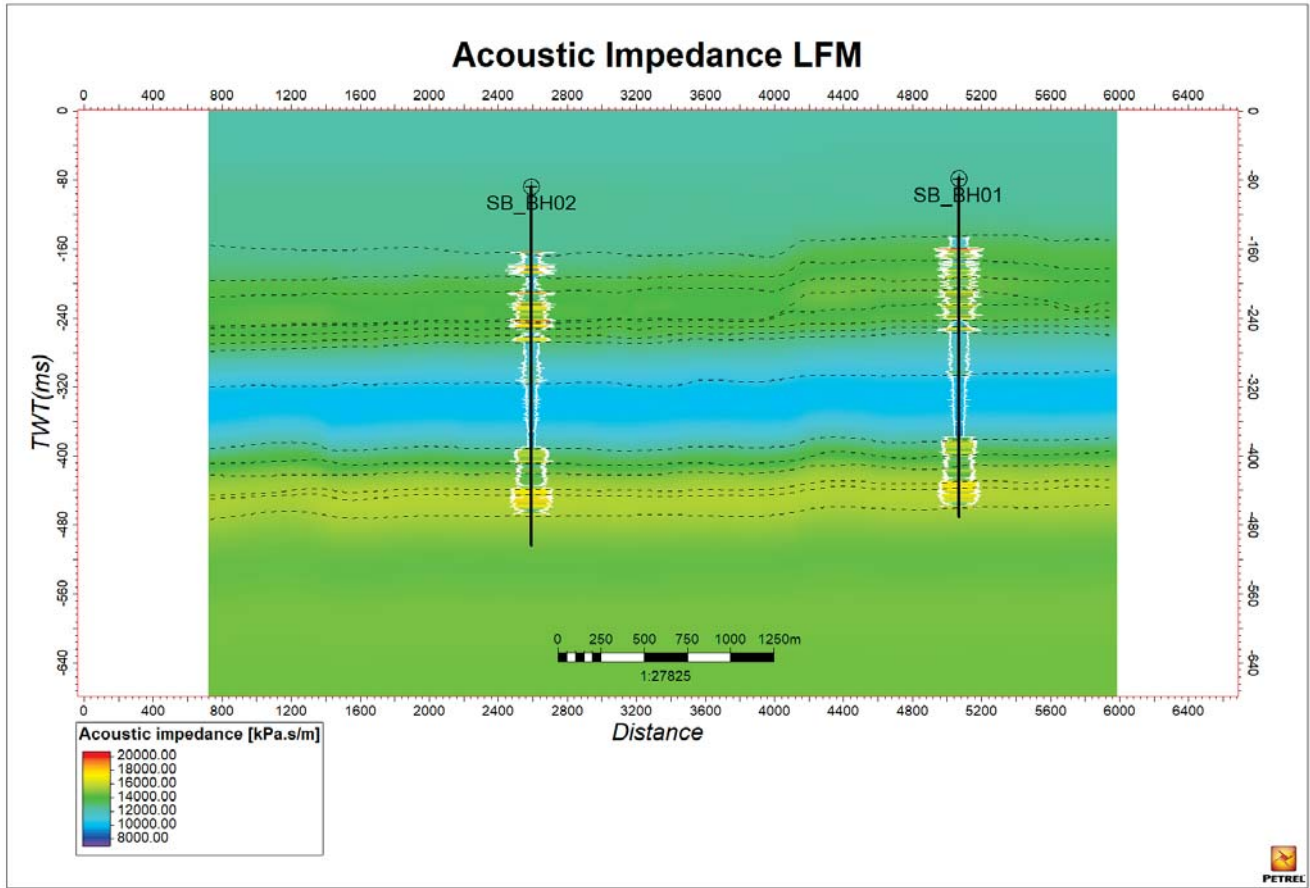


Figure 21 Acoustic impedance LFM cross-section.

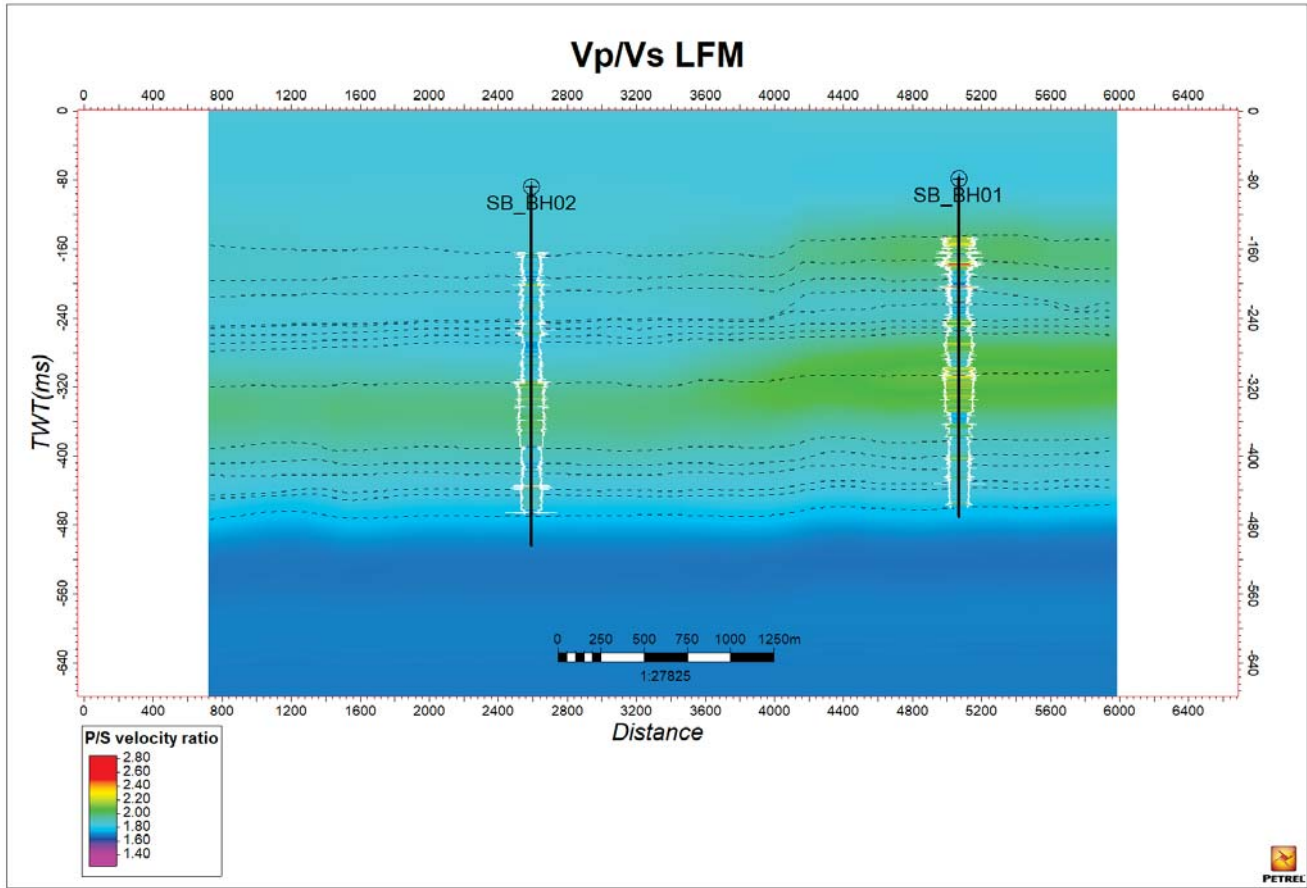


Figure 22 Vp/Vs LFM cross-section along SB_BH01 and SB_BH02.

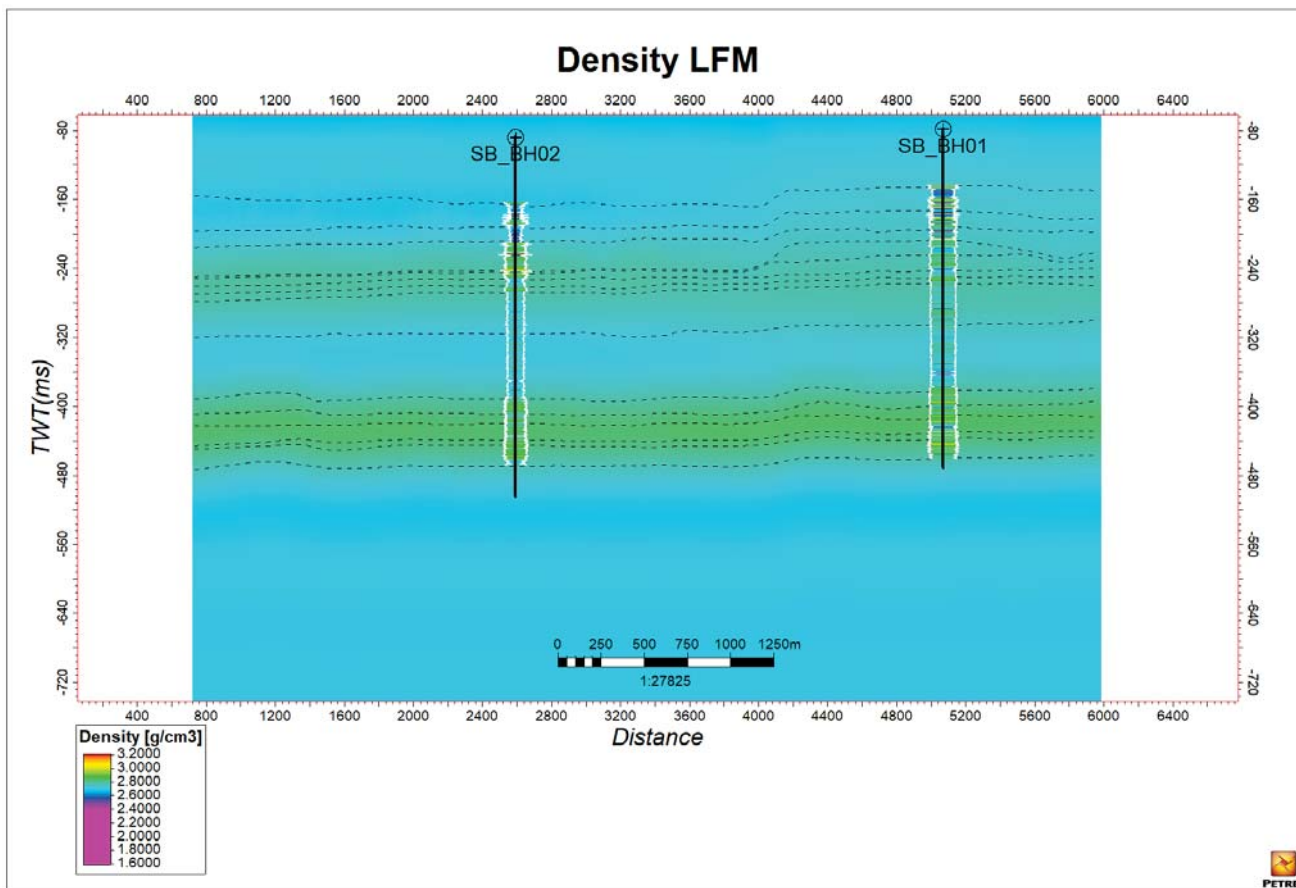
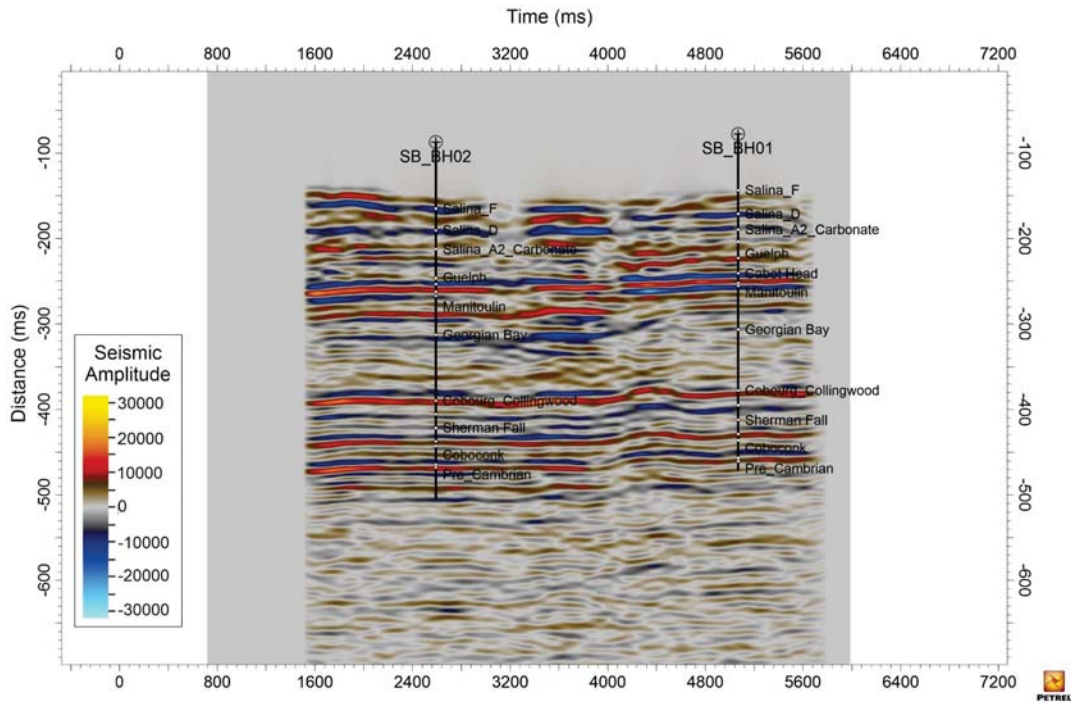


Figure 23 Density LFM cross-section along SB_BH01 and SB_BH02

For AVO inversion, an angle gather is a collection of seismic traces that have been sorted based on the angle of incidence of the seismic waves at the reflection point. This sorting allows to analyze how the amplitude of the reflected seismic signal changes with the angle of incidence. By examining these variations, it is possible to infer changes in the subsurface properties, such as lithology, porosity, and fluid content. Angle gathers are crucial for AVO inversion because they provide the necessary data to model and interpret these amplitude changes, leading to more accurate subsurface characterizations. For this study, trace-aligned angle gathers (4-14°, 14-21°, 21-28°, 28-38°) were used. Displayed below are random intersection lines through these angle gathers with both wells. Figure 24a shows one of the four angle gather stacks utilized in this study (4-14), while Figure 24b exhibits another (14-21).

(a)



(b)

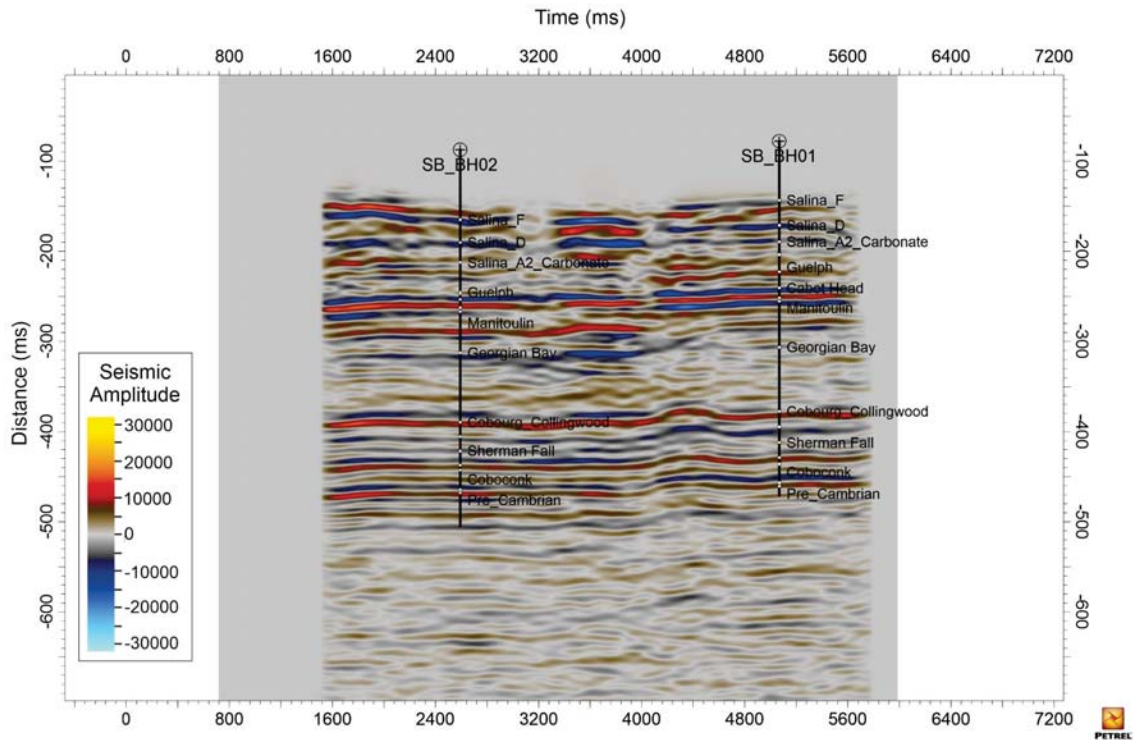


Figure 24 Two of the four angle gather stacks utilized in the inversion study. (a) Angle gather 4-14; (b) Angle gather 14-21.

6.3 Simultaneous Inversion

Simultaneous inversion is a seismic inversion technique that integrates multiple types of seismic data or attributes simultaneously. Instead of inverting each data type separately and then combining the results, simultaneous inversion jointly inverts data sets such as P-wave (compressional wave) information, AVO attributes, and other relevant seismic attributes.

By using this approach, simultaneous inversion leverages the complementary information contained in the different data sets, leading to more accurate and reliable estimates of subsurface properties like acoustic impedance, shear impedance, and density. This integrated method improves the resolution and robustness of the inversion results.

Input data:

- Angle gathers (4-14°, 14-21°, 21-28°, 28-38°)
- Average wavelets
- Low frequency models (Ai, Vp/Vs ratio, Density)

Inversion parameters:

Reflection Threshold: This is the minimum amplitude of seismic reflections considered in the inversion process. It helps in filtering out noise and focusing on significant reflections for accurate modeling. The reflection threshold used for this study was 0.00015.

Tie to LFM (Low-Frequency Model): The process of aligning the inversion results with a pre-established low-frequency model to ensure consistency and improve the accuracy of the subsurface properties. The parameters used are AI: 0.08, Vp/Vs ratio: 0.05, Density: 0.05. A higher value will allow more variation in the inversion result away from the input low-frequency model. A lower value will tie the inversion result closer to the input low-frequency model. A start parameter of 0.14 (14%) is the default. The usual parameter range being 0.01 to 0.20. The tie value must always be larger than that of the horizontal continuity.

Horizontal Continuity: This parameter enforces the smoothness and consistency of the inverted properties across horizontal layers, ensuring that geological features are accurately represented and continuous. The parameters for horizontal continuity used in the study include AI: 0.07, Vp/Vs ratio: 0.04 and Density: 0.04. A low value will enforce higher horizontal continuity while higher value will enforce less horizontal continuity. A start value of 0.12 (12%) is the default. The usual parameter range being 0.01 to 0.20. The value of the horizontal continuity must always be smaller than the value of 'Tie to LFM'.

Time range: The specific interval of seismic data, defined by start and end times, that is used in the inversion process. This range determines which portion of the seismic record is analyzed and modeled. For the study, an interval of 100ms to 600ms was used.

Initially, an interval velocity cube was going to be used as guidance to the inversion process, however, due to velocity artifacts at the edges, velocity guidance was not used in the inversion study.

6.4 AVO Inversion Results

For quality control, the well logs were juxtaposed against the logs drawn from the inversion cubes on a log scale. This aids in evaluating the results on a bitmap scale. To harmonize the frequency range between the well log and inversion curves, a frequency filter was applied to the well log curve.

Figure 25 (SB_BH01) and Figure 26 (SB_BH02) present Inversion QC plots. The well log tracks are categorized into three groups: AI, Vp/Vs ratio, and Density. Each group comprises four well log tracks. The first and third tracks exhibit bitmap seismic inversion results, the second track illustrates the well log bitmap track, and the fourth one displays the log curves.

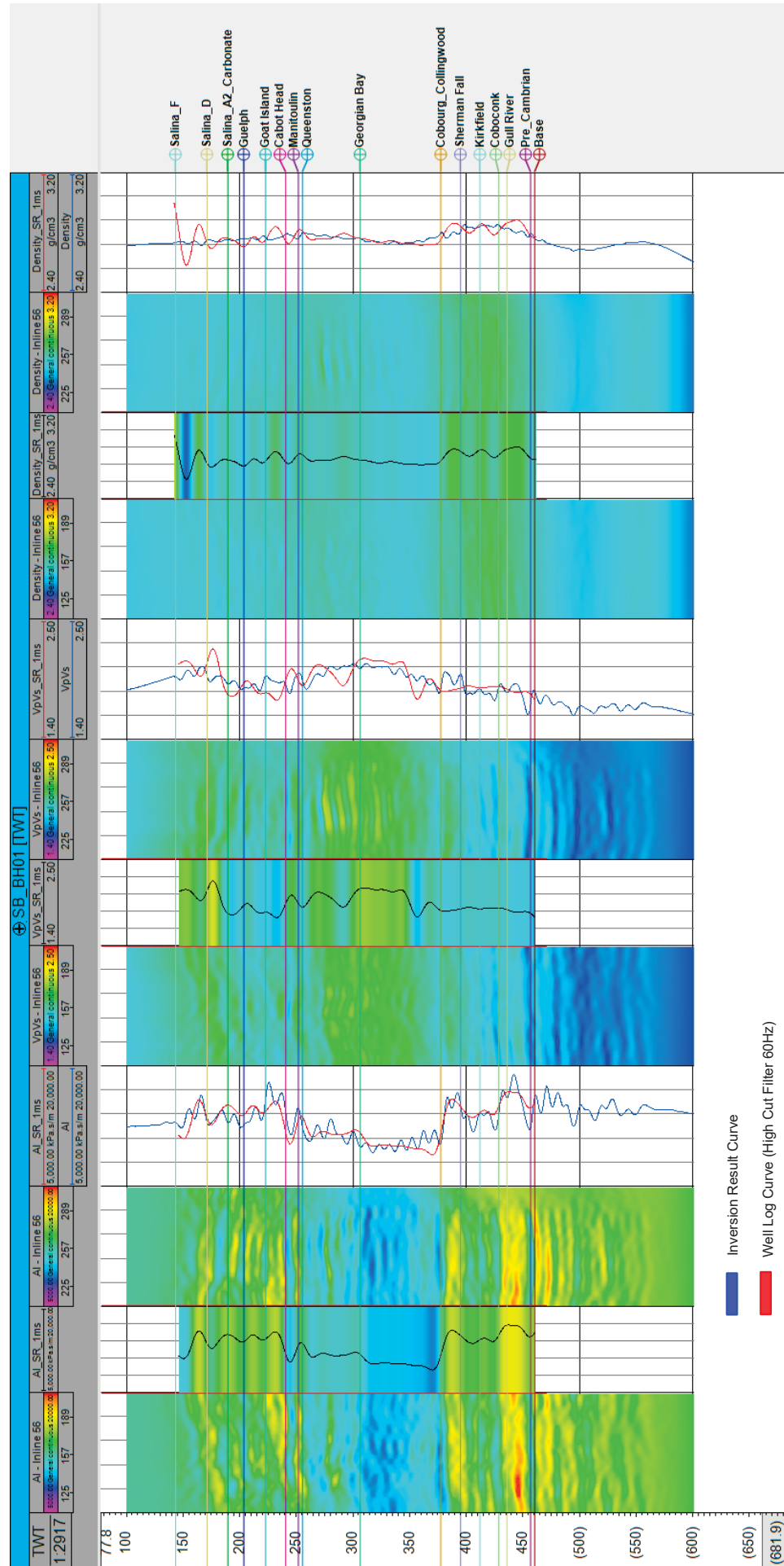


Figure 25 SB_BH01 Inversion Results

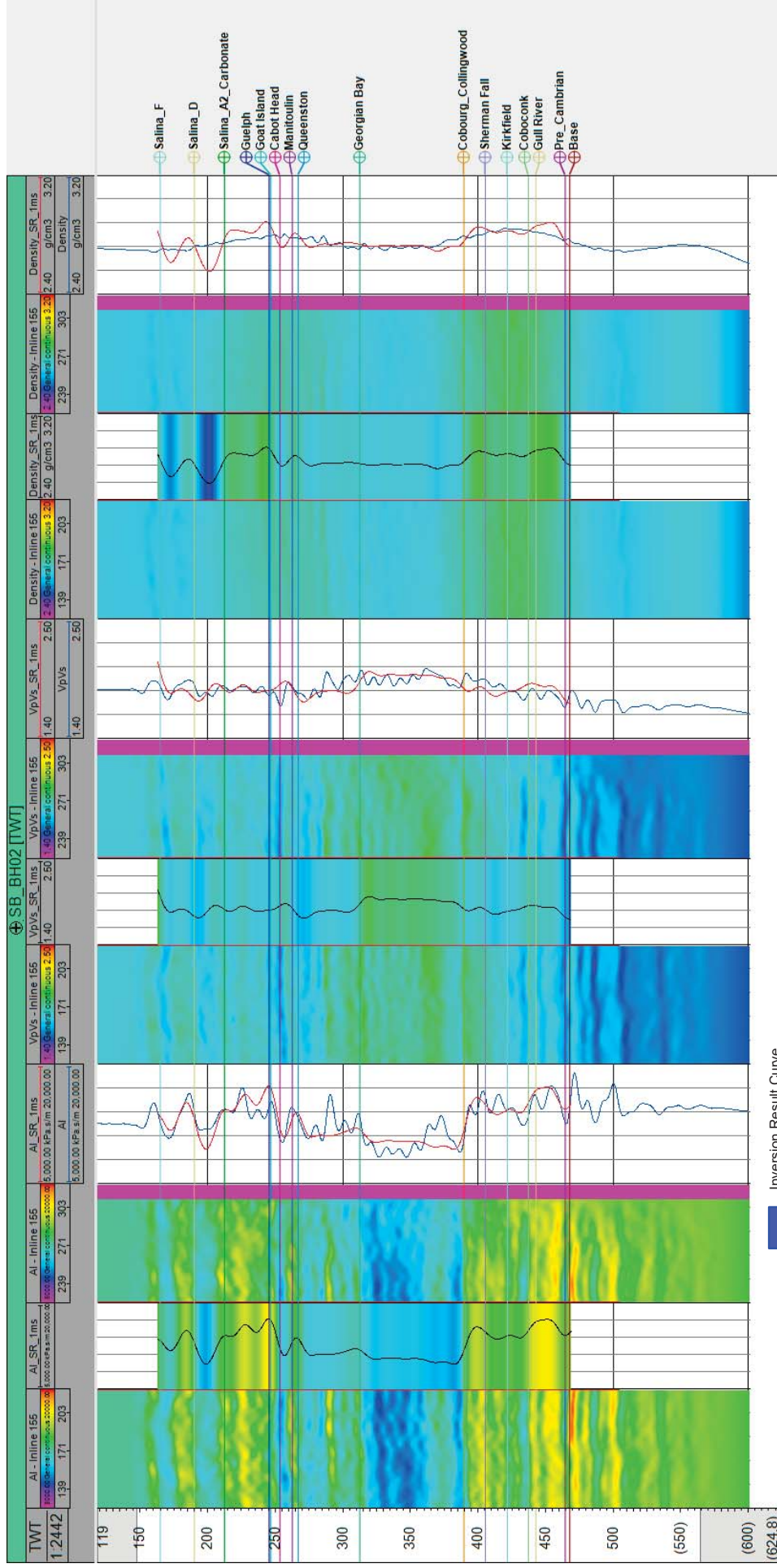


Figure 26 SB_BH02 Inversion Results

6.5 AVO Inversion Data Quality

The AI inversion results align well with the well logs in many sections, particularly in the middle part of the section (225 - 400 ms). There is a reasonable alignment between the well logs and inversion results, though some deviations can be observed, especially in more complex zones.

The Vp/Vs ratio inversion shows a good match with the well logs across most of the section. The alignment is particularly strong in the middle layers. The inversion results show good alignment with the well logs, indicating a reliable inversion for this property.

The density inversion results align well with the well logs, especially in the middle sections. Similar to the AI inversion, there are some discrepancies in the shallow section. These could be due to challenges in resolving density contrasts from seismic data. Particularly due to the large angle range, i.e., wide-angle arrivals, that are required for determining density from PP seismic datasets.

Overall, the inversion results closely match well log data. Some minor discrepancies were observed due to lower signal-to-noise ratio in the seismic data, but the general trend and major features were well captured. It is however noteworthy to state that limitations in the well count in the field could affect significant capture of lateral changes.

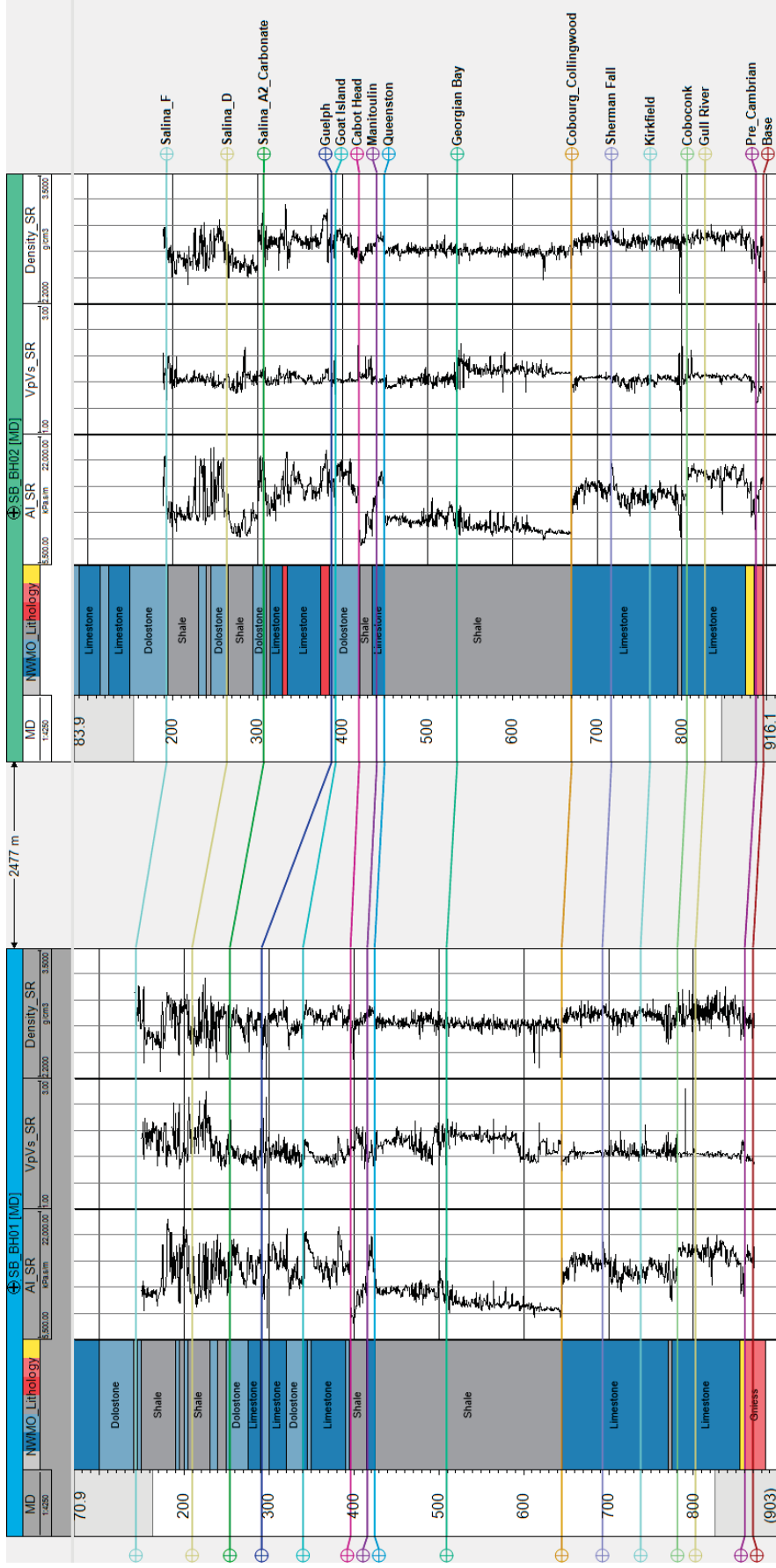
The outputs from the inversion study include the acoustic Impedance (TWT), Vp/Vs (TWT), Density (TWT) and Inversion Residuals Angle gathers (residual seismic data modeled from the input reference $residual = seismic - synthetic$) 4-14°, 14-21°, 21-28°, 28-38° cubes. These were then converted into depth cubes using the updated average velocity model.

6.6 Lithology Prediction

The process of lithology analysis and prediction is a rock physics-based workflow that combines well logs, seismic inversion, geological modeling, and interpretation. It offers an estimation of the most likely lithology as well as an assessment of the uncertainty linked to the prediction.

A simplified lithology log was provided for each borehole that assigned a dominant lithology for each 5-metre moving window using the core logging data (Geofirma). The preliminary lithology log comprised seven types: unconsolidated, limestone, dolostone, shale, anhydrite, gneiss, and sandstone.

However, the study was limited to primarily three dominant lithologies, including limestone, dolostone, and shale. This limitation arises because the seismic amplitudes showed a lack of sensitivity towards the other rock types. The anhydrite and sandstone intervals identified in the simplified lithology were left blank for the input and resulted in being assigned as limestone during the machine language routine using Petrel. All units in the lithology prediction below the top of Precambrian were assigned as gneiss manually. The geophysical logs used for lithology analysis included AI_SR, VpVs_SR, and Density_SR. Figure 27 illustrates the display of AI, Vp/Vs ratio, and density logs alongside the facies log in the first track.



| Lithology | Swatch |
|-----------|----------|-----------|----------|-----------|----------|-----------|----------|-----------|----------|-----------|----------|
| Dolostone | [Swatch] | Limestone | [Swatch] | Shale | [Swatch] | Sandstone | [Swatch] | Anhydrite | [Swatch] | Gneiss | [Swatch] |

Figure 27 The lithology logs of SB_BH01 and SB_BH02

Within given facies, log responses can vary due to factors like fluid content, saturation, mineral makeup, temperature, and others, highlighting the intrinsic differences in rock characteristics. A primary aim at this stage is to understand the relationship between continuous log curves and discrete lithology logs.

Machine Learning was employed to predict the lithology based on training data provided (i.e., AI, Vp/Vs ratio, and density logs). The machine learning engine is Petrel - Ikon Science - QI ML Training and Prediction. The machine learning function utilizes the FastTree method, a gradient boosting algorithm. It constructs each regression tree incrementally, using a predefined loss function to evaluate the error at each step and adjust it in the subsequent step. This allows for the prediction of lithology cube using similar correlation for the input seismic volumes of AI, Vp/Vs ratio, and density.

Lithology classification below the Precambrian is not included in the machine learning algorithm and manually set to Gneiss. The results of the prediction are illustrated in Figure 28. Limestone is depicted in brown, dolostone in green, and shale in light blue. Note that seismic data is less sensitive to variations between limestone and dolostone, making it challenging to distinguish between them accurately. Consequently, the confidence level in distinguishing between limestone and dolostone is lower than in differentiating them from shale. This is particularly pronounced in the upper portion of the volume, where dolostone formations are prevalent.

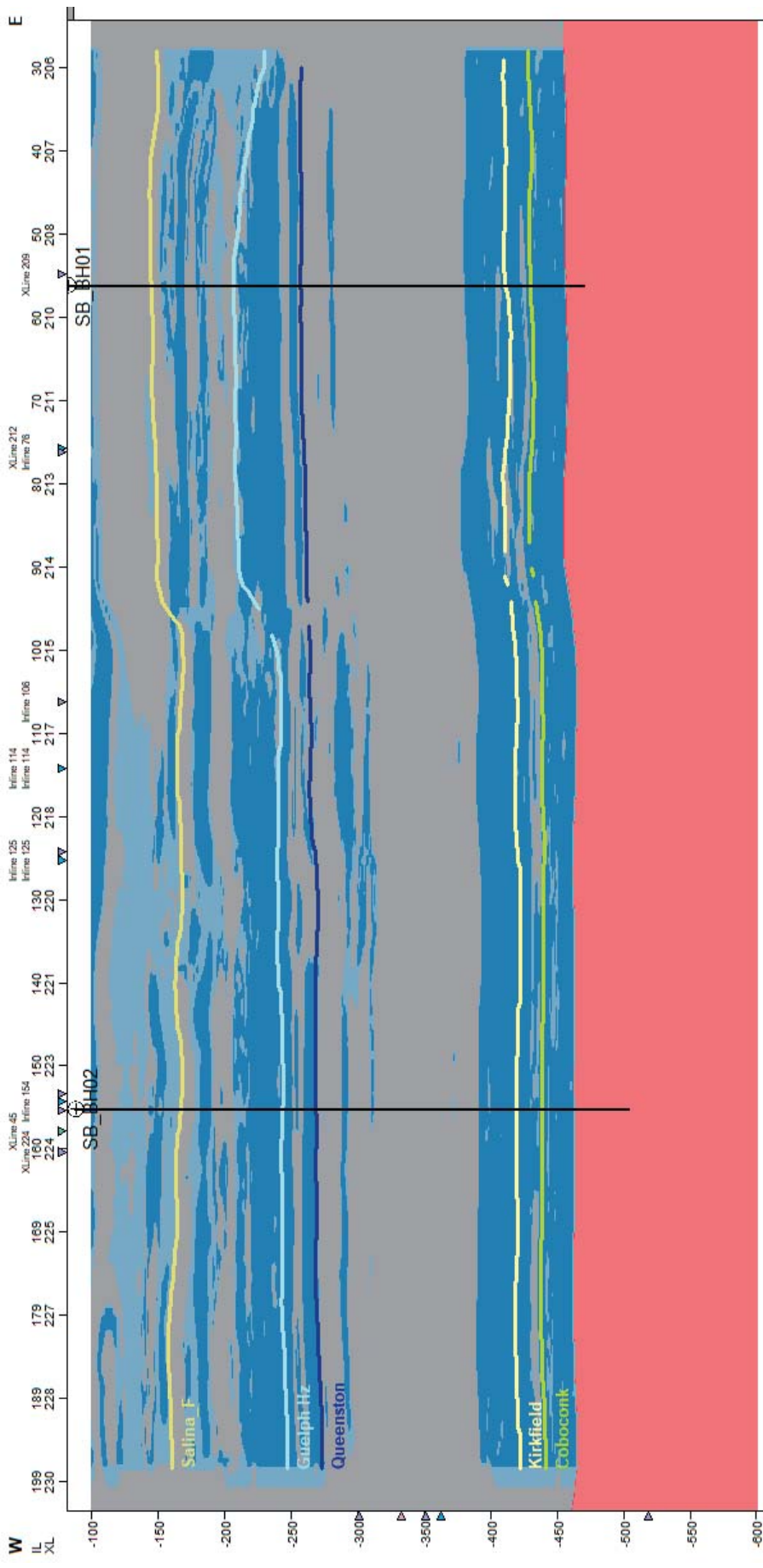


Figure 28 Lithology Prediction Intersection

7 CONCLUSIONS

This 3D seismic reflection study focuses on an area of approximately 18 km² located northwest of the community of Teeswater, Ontario, known as the South Bruce site. The study provides high confidence seismic interpretation and inversion of physical properties within the bounds of the seismic volume. Two deep bedrock boreholes, recently drilled and tested by Geofirma as part of the NWMO program, were critical to help guide the interpretation on different locations of the seismic data volume. One borehole was drilled within a reefal structure providing localized data, and one borehole provided data representative of more regional conditions. Data collected from these boreholes supported the interpretation of fifteen horizons (bedrock formation tops) in the seismic data, with varying levels of confidence, to provide a complete profile across the entire seismic volume. The reefal structure was interpreted in the eastern portion of the study near one of the recently drilled boreholes. The size of the reef was estimated to be ~300 acres in aerial extent and about 2.1 Bcf in volume. A seismic anomaly is observed in the data along the western side of the reef that requires further investigation to better understand its geological significance.

AVO inversion results closely matched the borehole geophysical data from the two nearby deep bedrock boreholes (SB_BH01 and SB_BH02). While some minor discrepancies were observed due to seismic quality, the general trend and major features were well captured and interpreted with confidence. Therefore, the AVO inversion results are considered good, however with only two boreholes to correlate with identifying lateral variations is difficult. This work is considered to be a good initial model that will benefit from additional data collected from drilling additional wells strategically placed in areas of uncertainty (i.e. seismic anomalies) which advance the confidence in lithological / structural interpretations and rock property estimation.

8 REFERENCES

K. Aki & P. G. Richards, (1980). *Quantitative Seismology, Theory and Methods*. Volume I: 557 pp., 169 illustrations. Volume II: 373 pp., 116 illustrations. San Francisco: Freeman.

Armstrong, D.K. and T.R. Carter, (2010). *The Subsurface Paleozoic Stratigraphy of Southern Ontario*. Ontario Geological Survey – Special Volume 7; 301p.

Carter, T.R., Logan, C.E., Clark, J.K., Russell, H.A.J., Priebe, E.H., and Sun, S., (2022). A three-dimensional bedrock hydrostratigraphic model of southern Ontario; Geological Survey of Canada, Open File 8927, 1 .zip file. <https://doi.org/10.4095/331098>.

Fagin, S. W. (1991). *Seismic modeling of geologic structures: Applications to exploration problems*. Society of Exploration Geophysicists. Case History 8, 197-208. Gao, C (2011). Buried bedrock valleys and glacial and subglacial meltwater erosion in southern Ontario, Canada – *Can. J. Earth Sci.*, Vol. 48, p.801-818.

Gao, C., Shirota, J., Kelly, R.I., Brunton, F.R., and Van Haaften, S., (2006). Bedrock topography and overburden thickness mapping, southern Ontario. Ontario Geological Survey, Miscellaneous Release—Data 207.

Geofirma Engineering Ltd., (2024a). 3D Seismic Data Acquisition and Processing Report, South Bruce, Ontario. Revision 0, in progress.

Geofirma Engineering Ltd., (2024b). Data Report for 2D Seismic Paleochannel Characterization, South Bruce, Ontario. Revision 1, in progress.

Geofirma Engineering Ltd., (2024c). WP03: Data Report: Geological and Geotechnical Core Logging, Photography, and Sampling for SB_BH01. January 12.

Geofirma Engineering Ltd., (2024d). WP05: Data Report for Geophysical Well Logging and Interpretation for SB_BH01, January 12.

Geofirma Engineering Ltd., (2024e). WP05: Data Report for Geophysical Well Logging and Interpretation for SB_BH02, February 7.

Geofirma Engineering Ltd., (2022). Data Report: Geological and Geotechnical Core Logging, Photography, and Sampling for SB_BH02. November 9.

Sanford, B.V., F.J. Thompson, F.J. and G.H. McFall, (1985). Plate Tectonics, A Possible Controlling Mechanism in the Development of Hydrocarbon Traps in Southwestern Ontario. *Bulletin of Canadian Petroleum Geology* 33, 52-71.

Shragge, J. et al., (2019). The Western Australia Modeling project — Part 2: Seismic validation. *Interpretation*, 7, T793–T807.

APPENDIX A

**Time Structure and Seismic Amplitude Figures
for Key Interpreted Horizons**

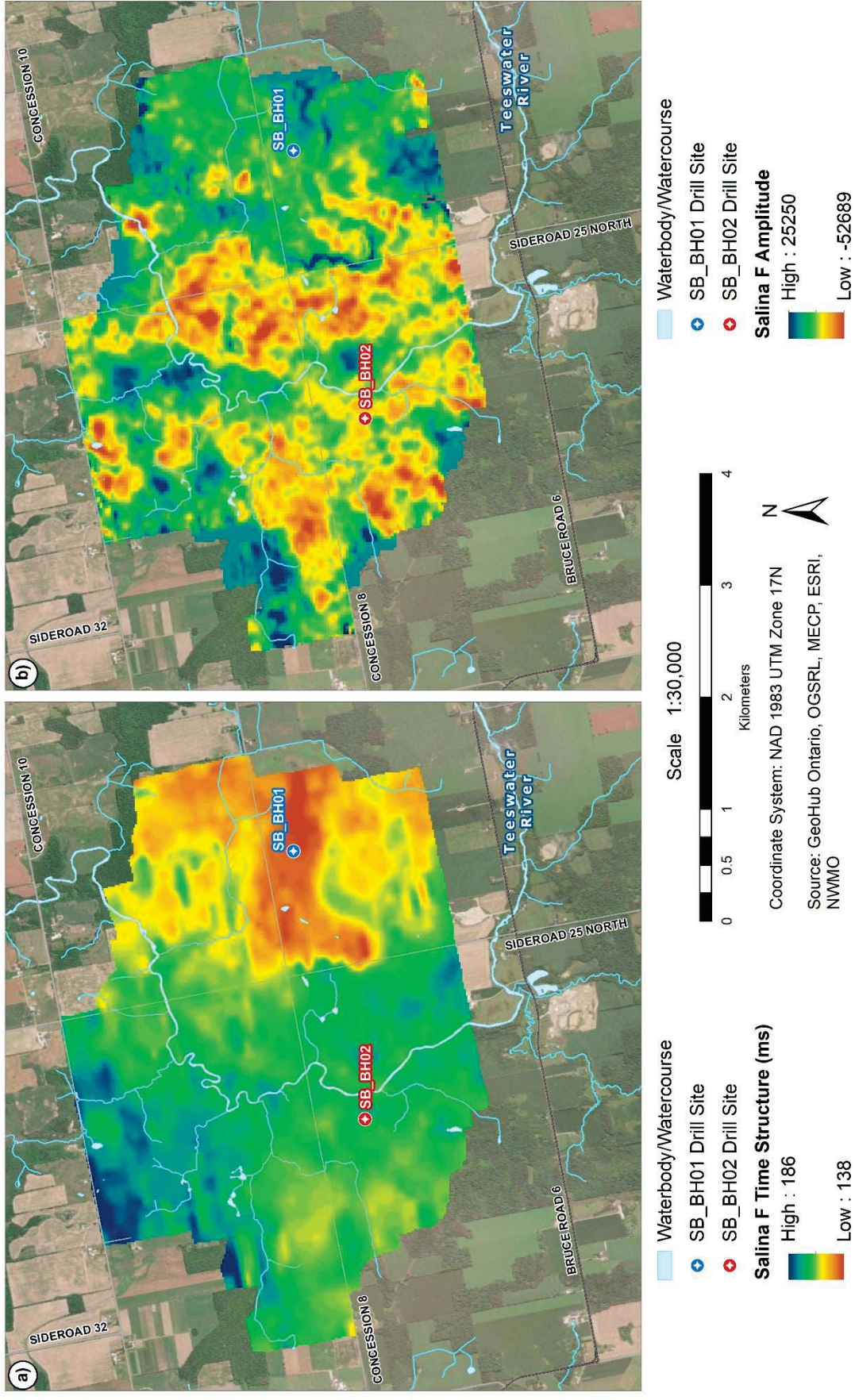


Figure A-1 Salina Formation – F Unit shale (a) plan view of interpreted time structure; (b) seismic amplitude.

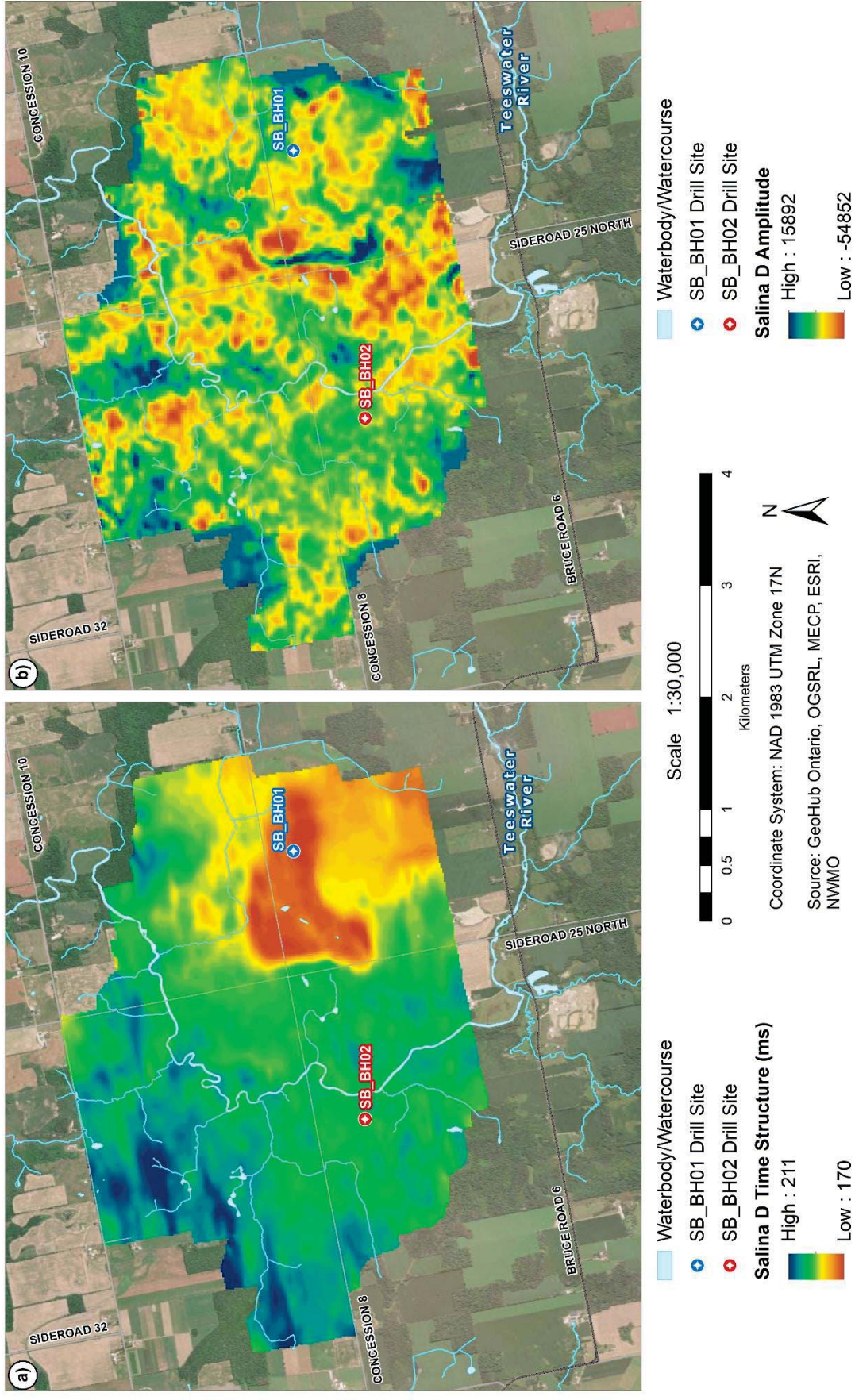


Figure A-2 Salina Formation – D Unit (a) plan view of interpreted time structure; (b) seismic amplitude.

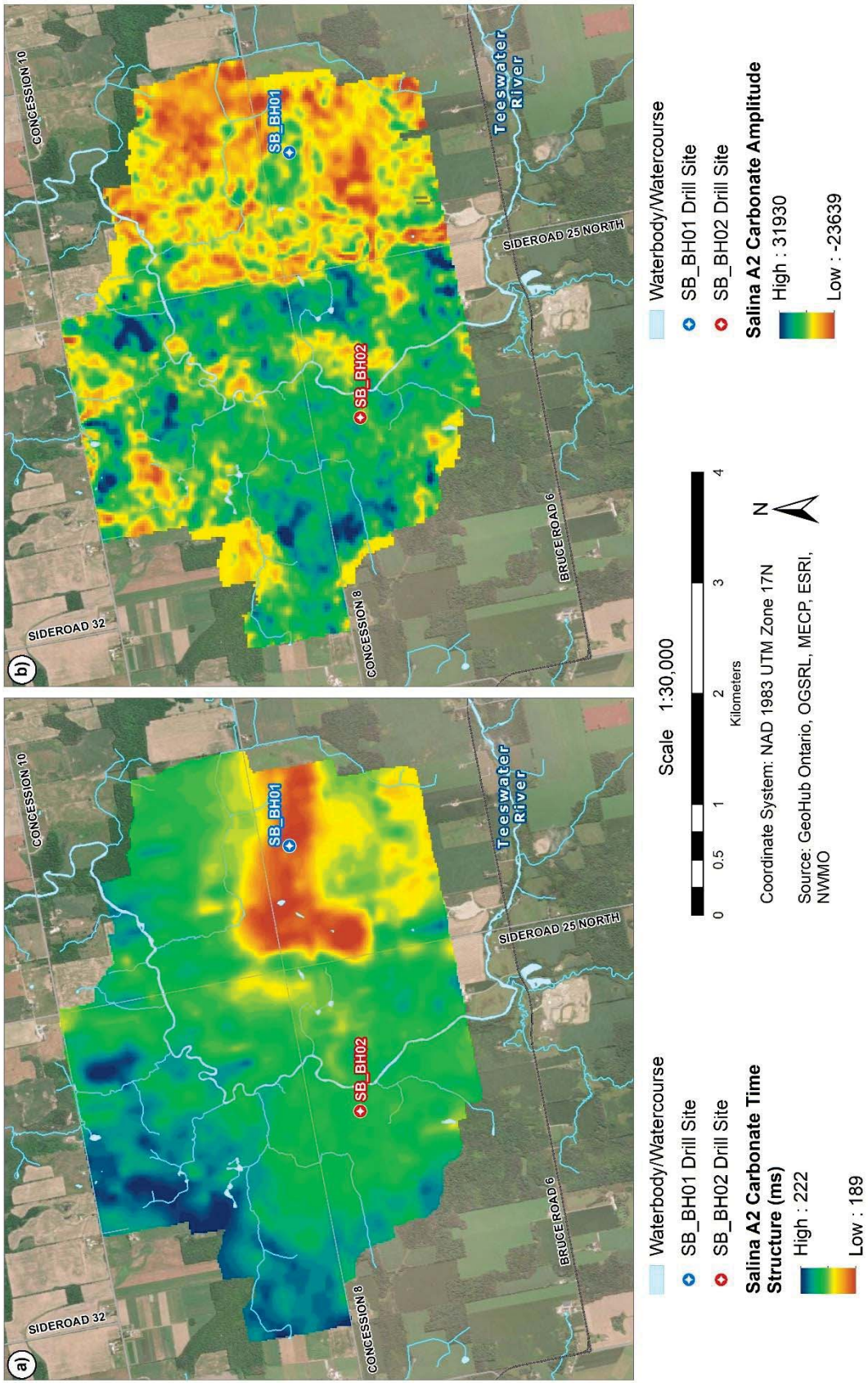


Figure A-3 Salina Formation – A2 Unit carbonate (a) plan view of interpreted time structure; (b) seismic amplitude.

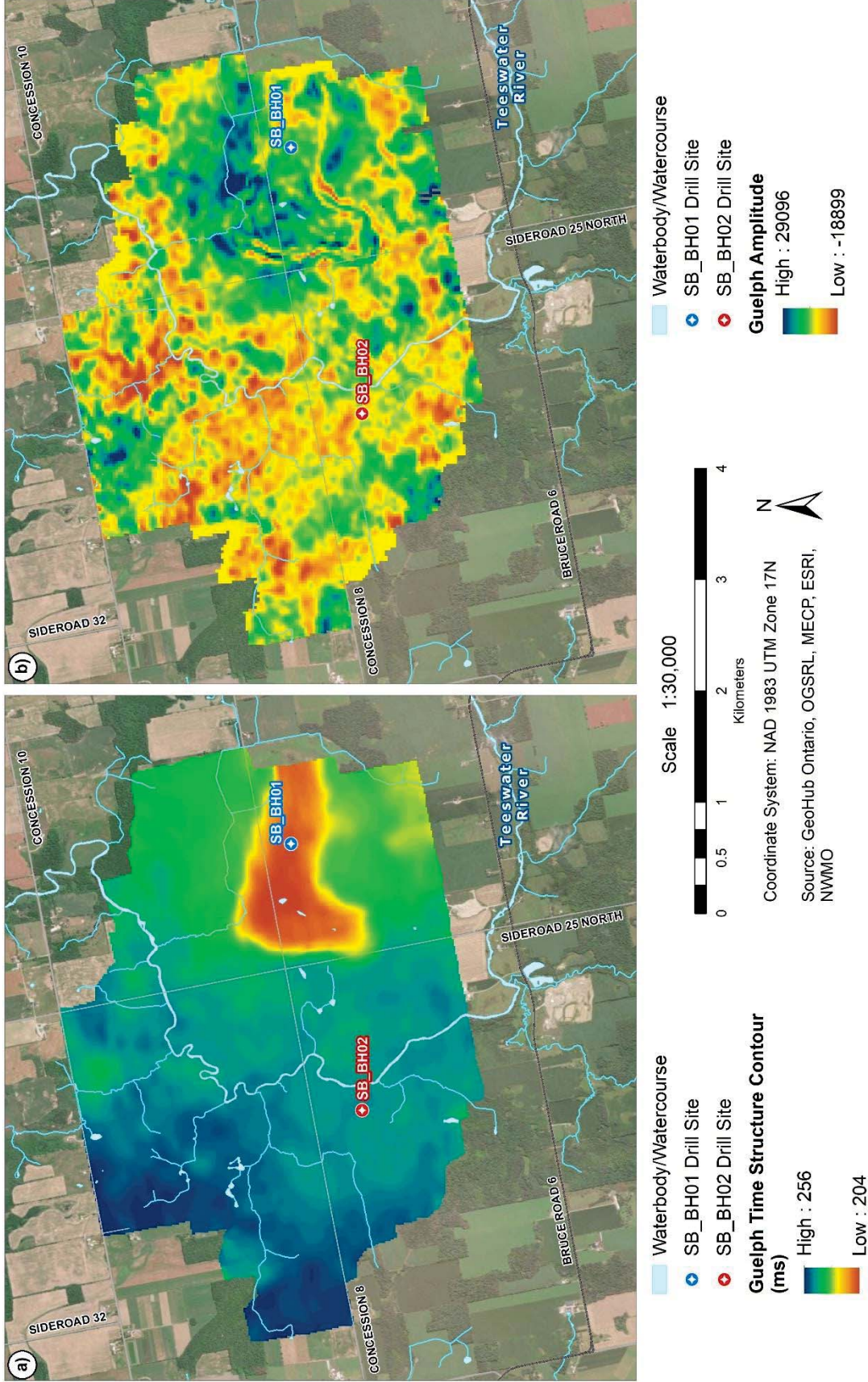


Figure A-4 Guelph Formation (a) plan view of interpreted time structure; (b) seismic amplitude.

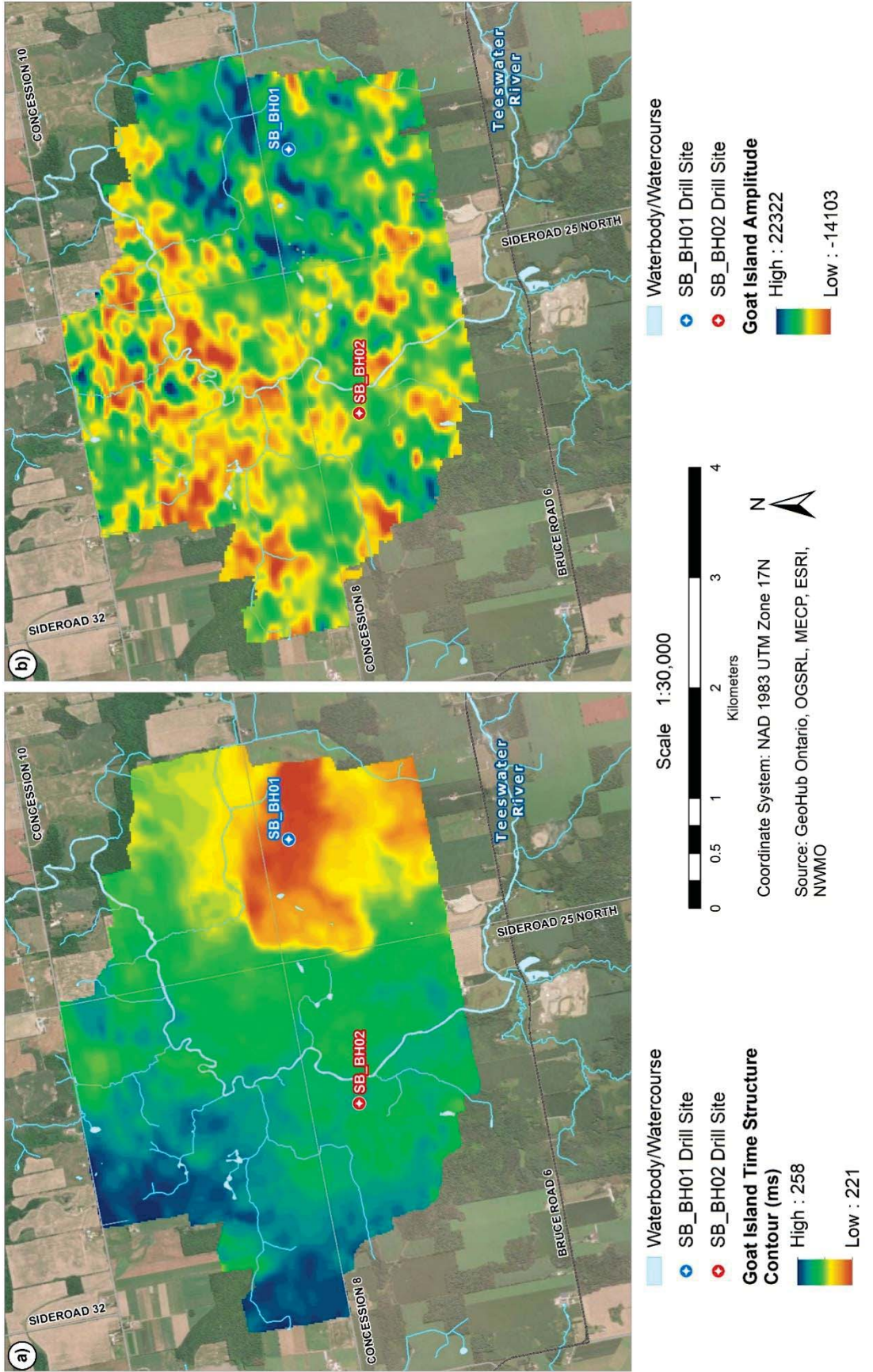


Figure A-5 Goat Island Formation (a) plan view of interpreted time structure; (b) seismic amplitude.

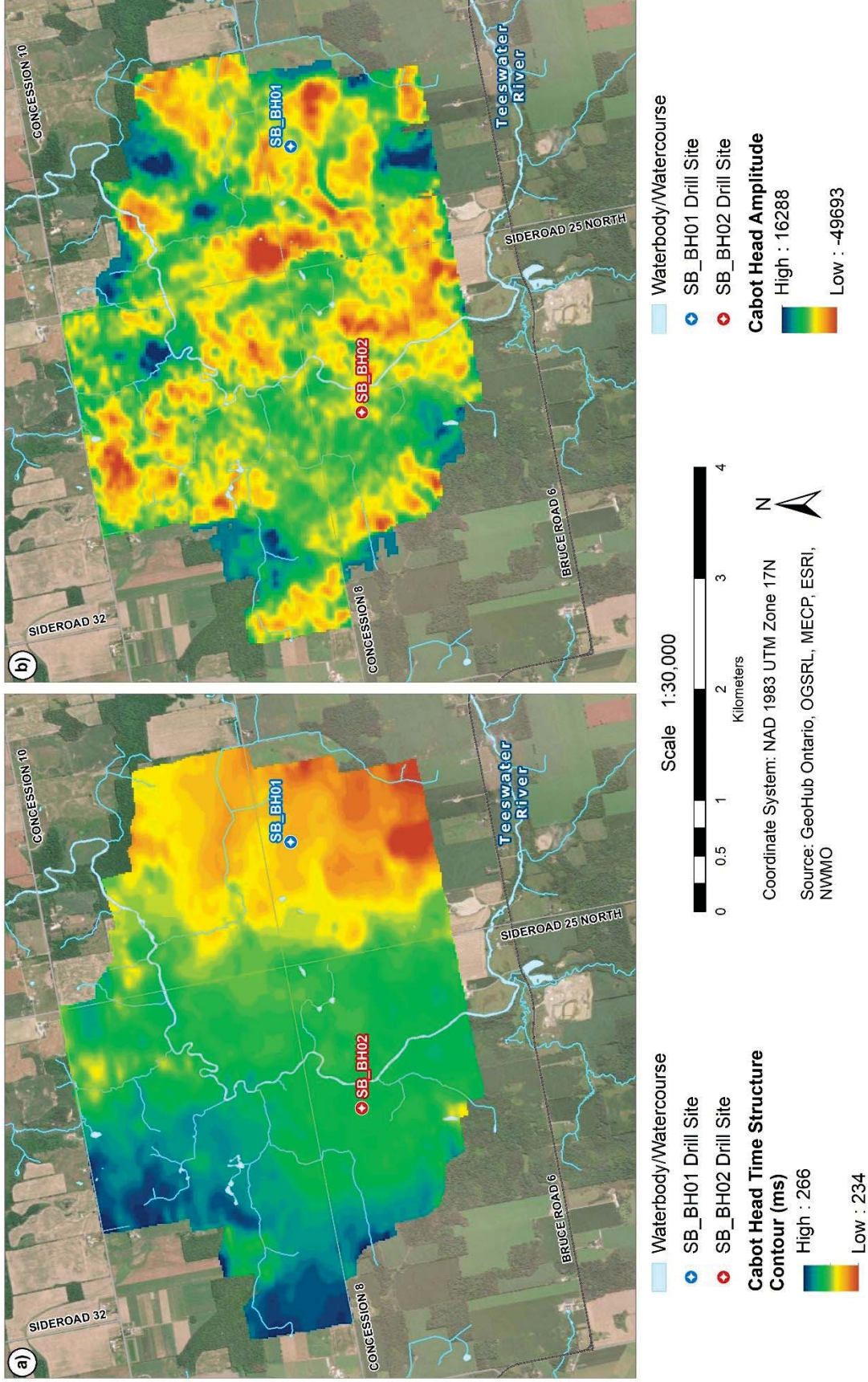


Figure A-6 Cabot Head Formation (a) plan view of interpreted time structure; (b) seismic amplitude.

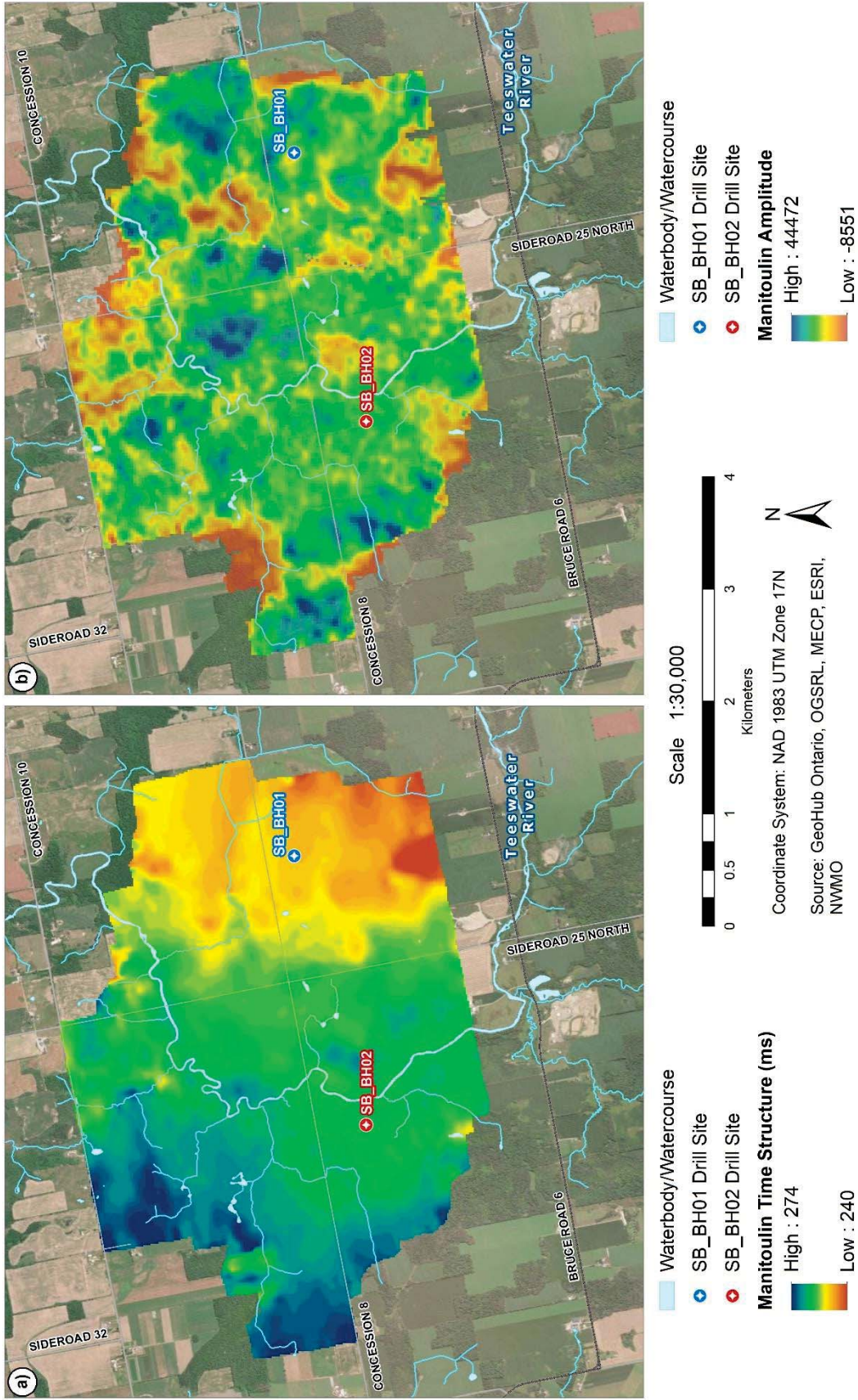


Figure A-7 Manitoulin Formation (a) plan view of interpreted time structure; (b) seismic amplitude.

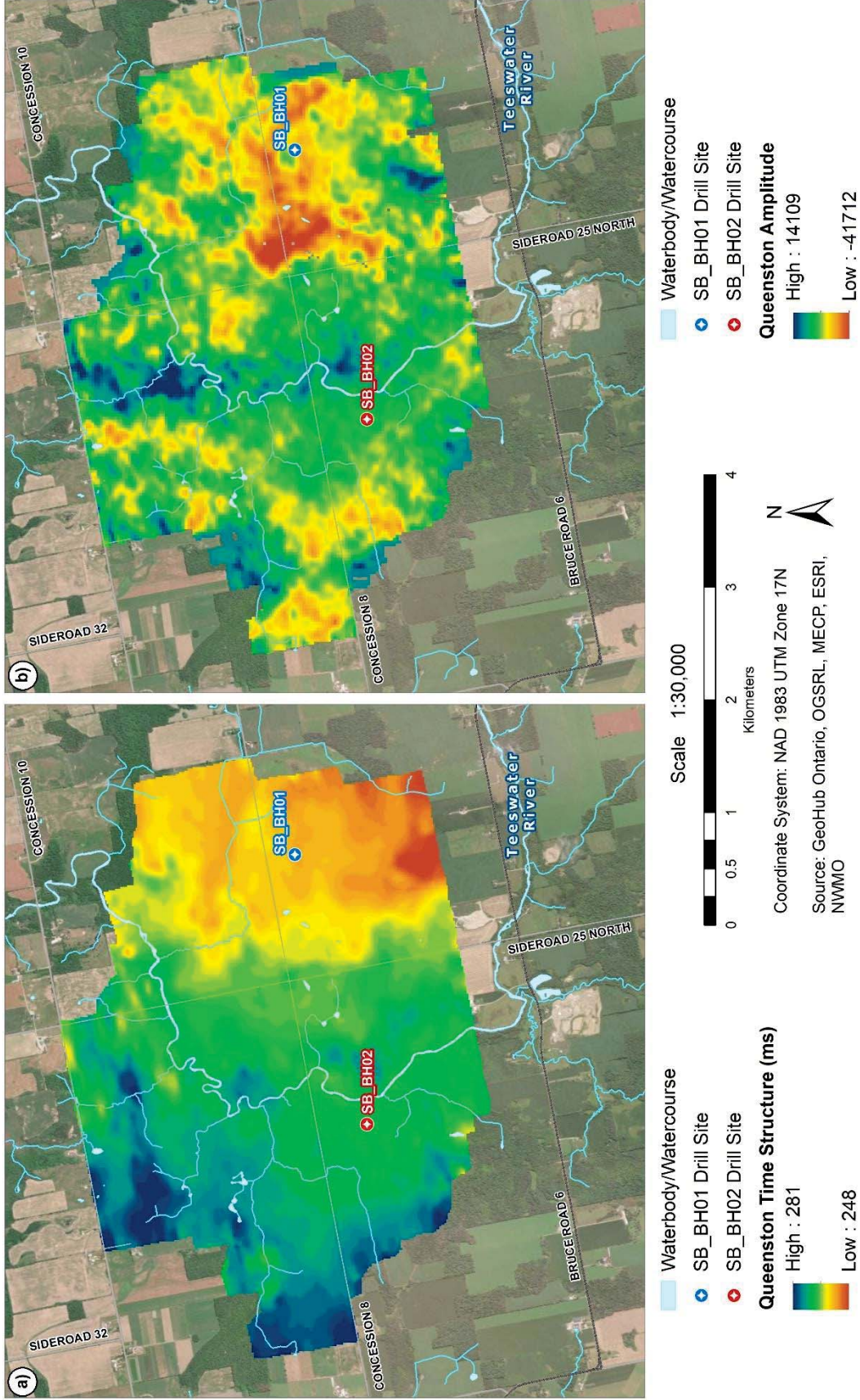


Figure A-8 Queenston Formation (a) plan view of interpreted time structure; (b) seismic amplitude.

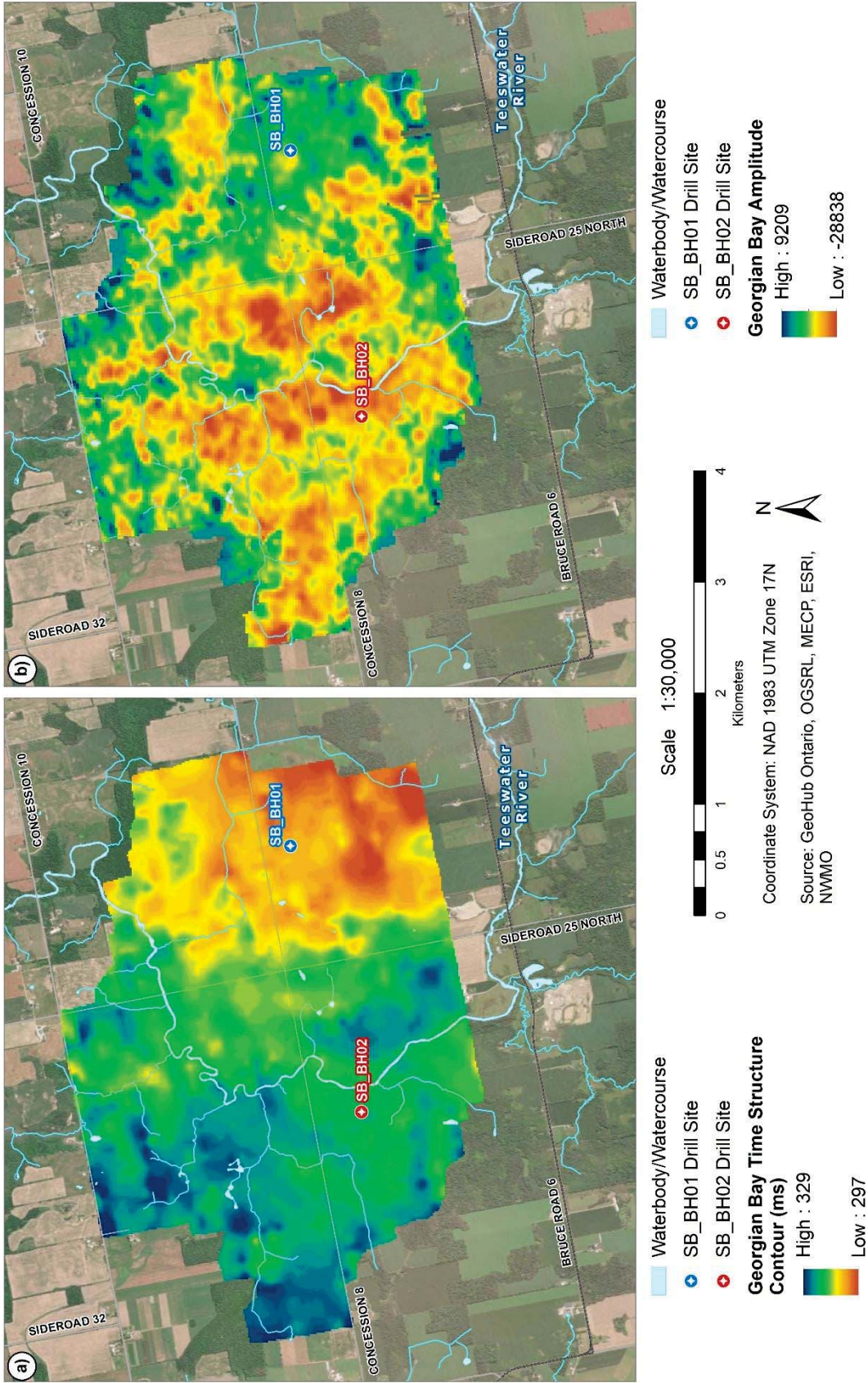


Figure A-9 Georgian Bay Formation (a) plan view of interpreted time structure; (b) seismic amplitude.

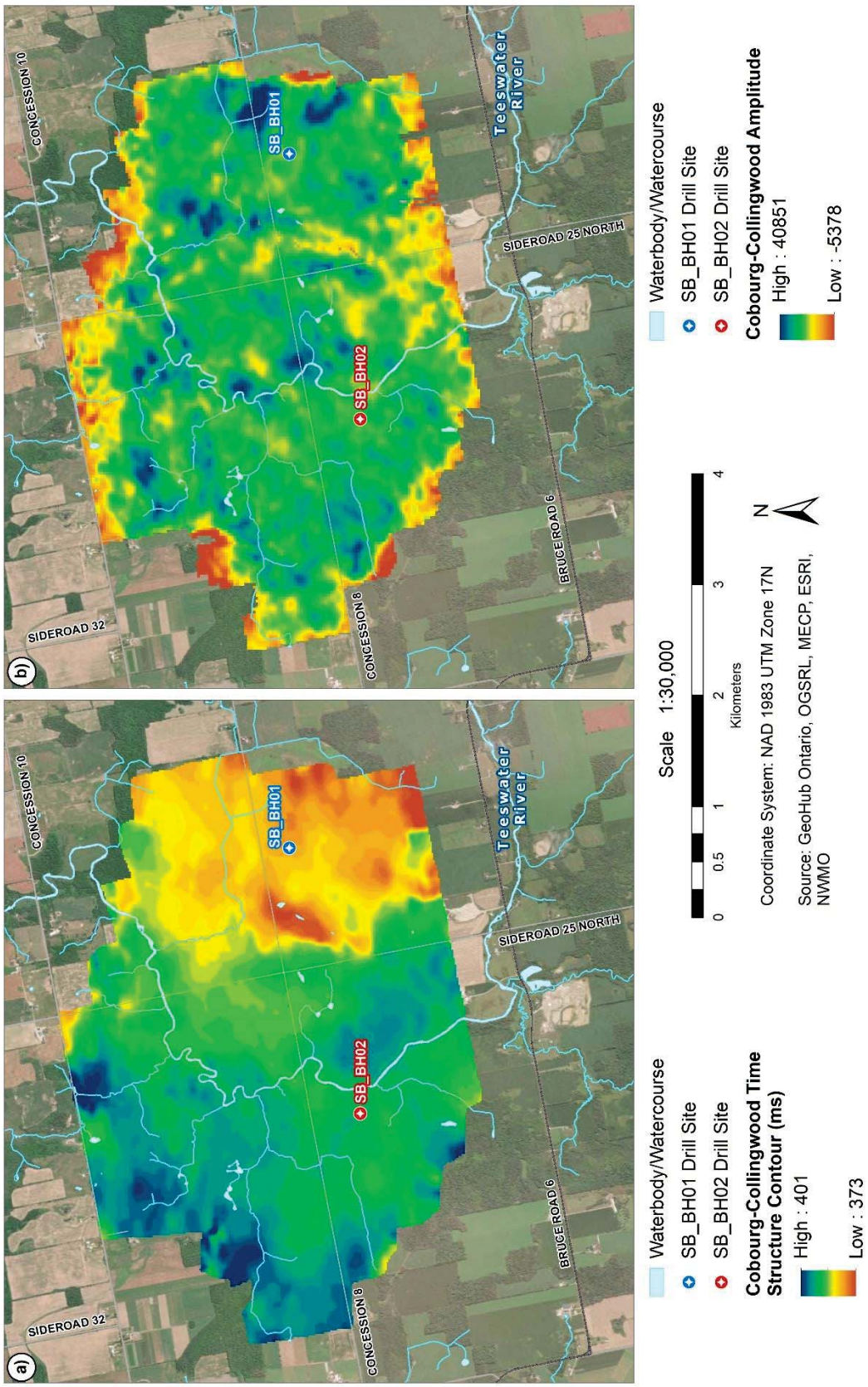


Figure A-10 Cobourg Formation – Collingwood Member (a) plan view of interpreted time structure; (b) seismic amplitude.

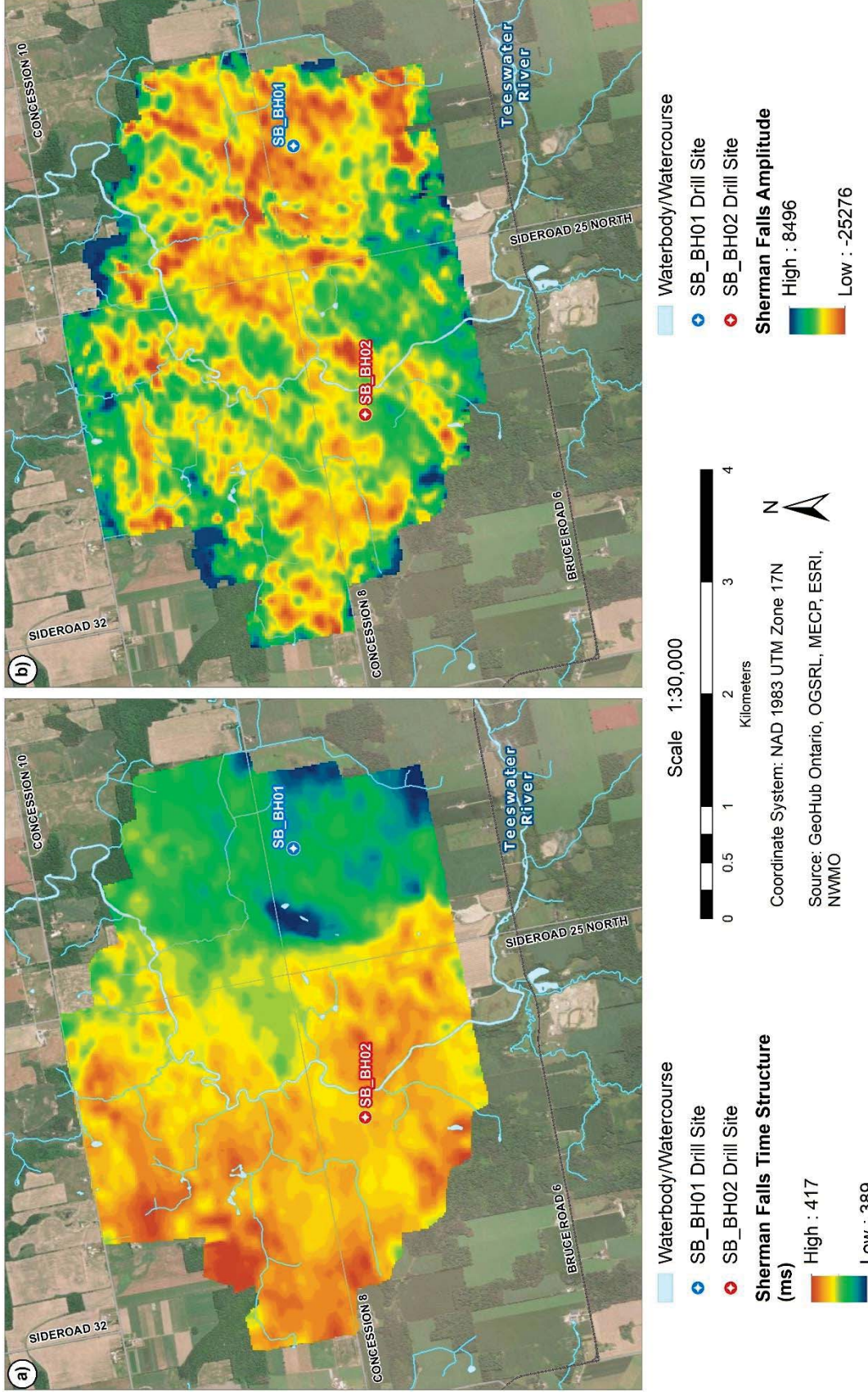


Figure A-11 Sherman Falls Formation (a) plan view of interpreted time structure; (b) seismic amplitude.

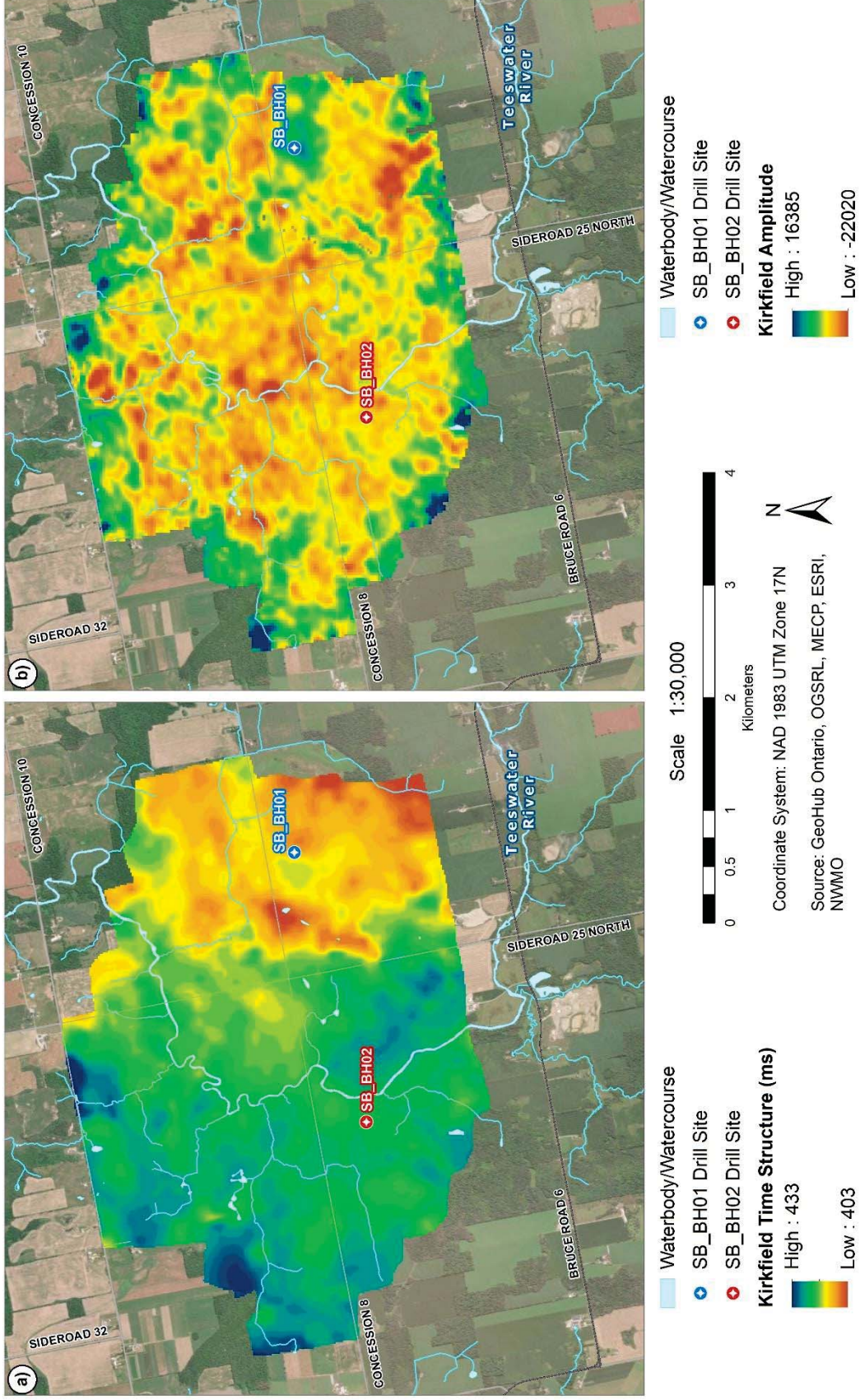


Figure A-12 Kirkfield Formation (a) plan view of interpreted time structure; (b) seismic amplitude.

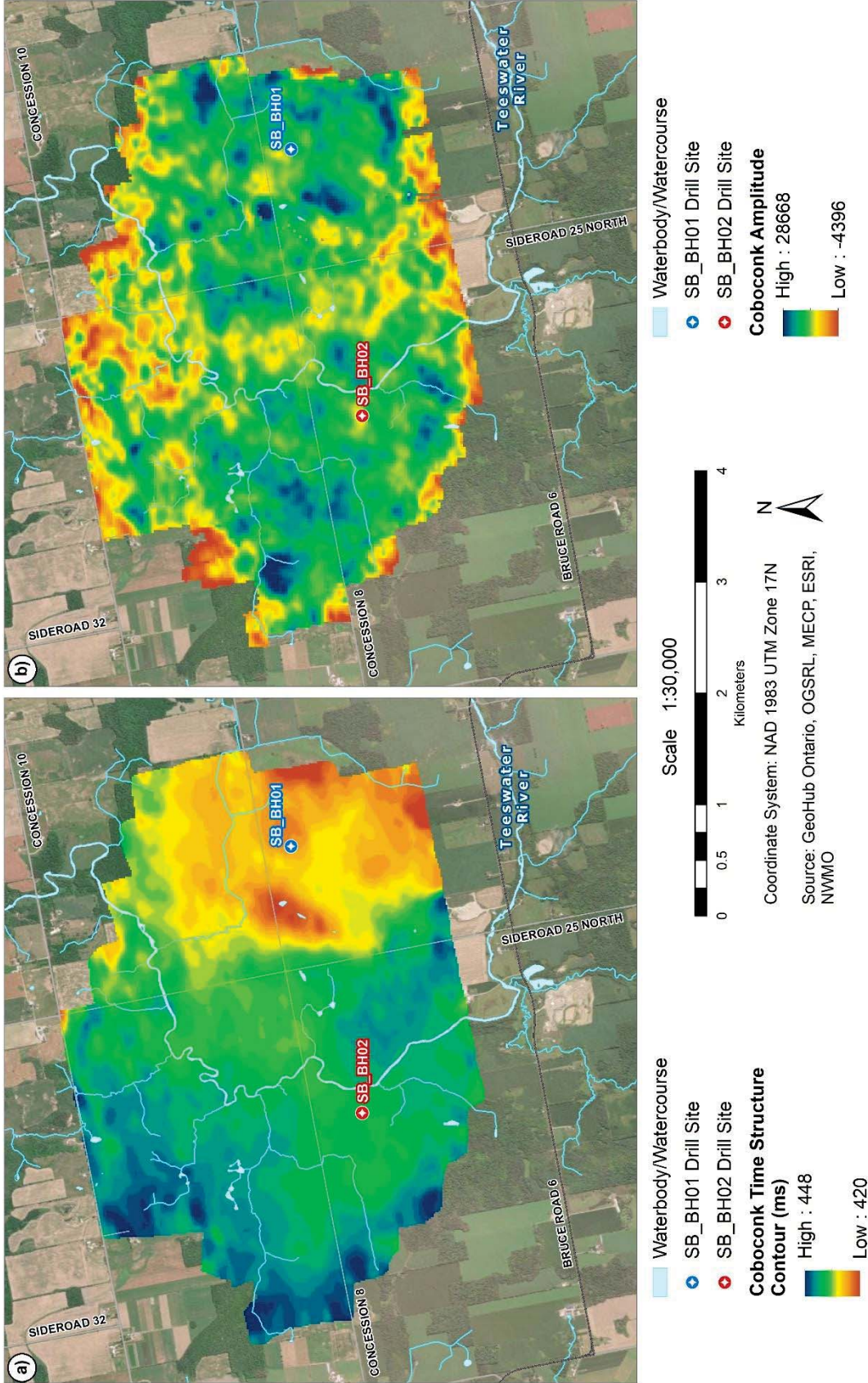


Figure A-13 Coboconk Formation (a) plan view of interpreted time structure; (b) seismic amplitude.

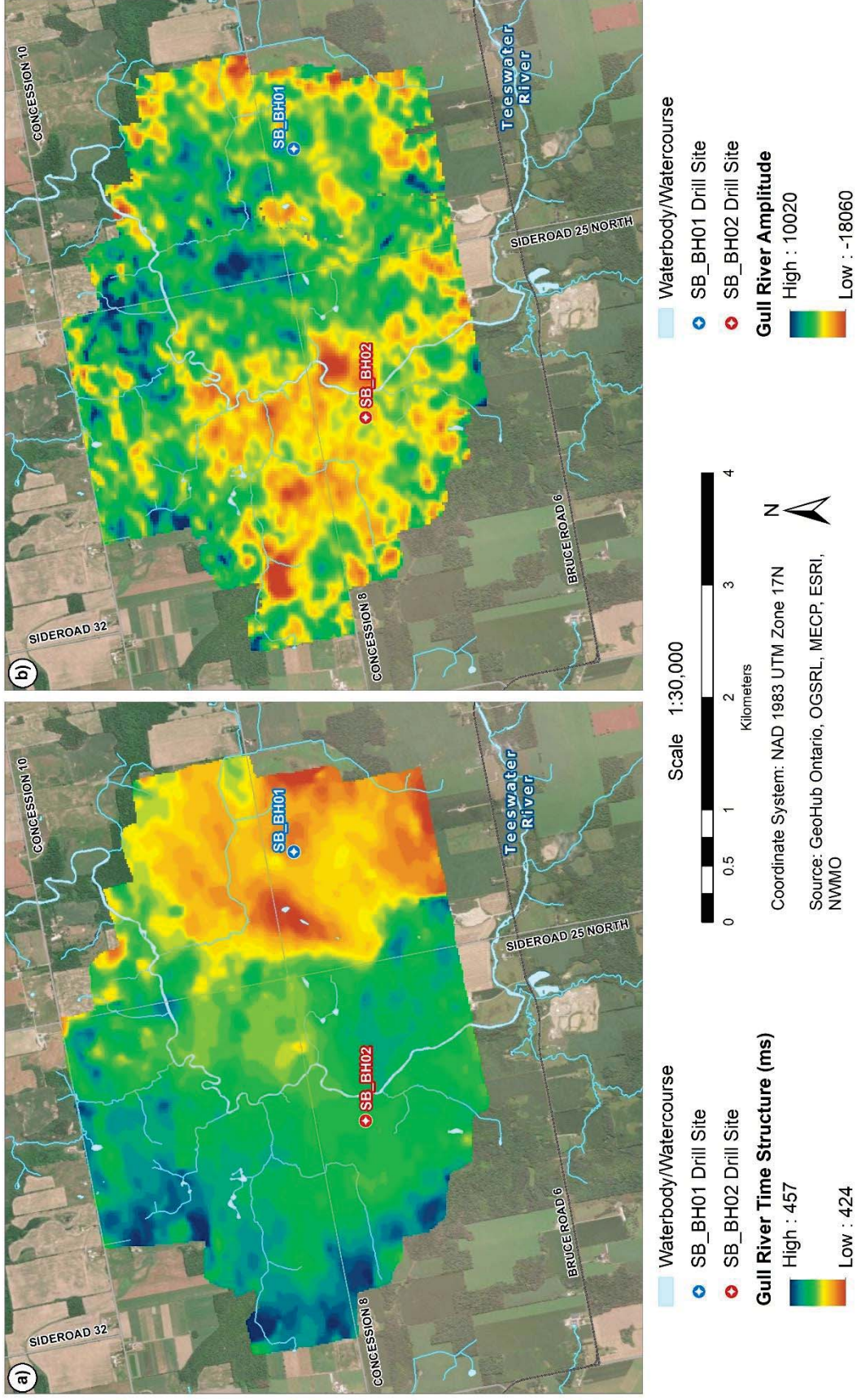


Figure A-14 Gull River Formation (a) plan view of interpreted time structure; (b) seismic amplitude.

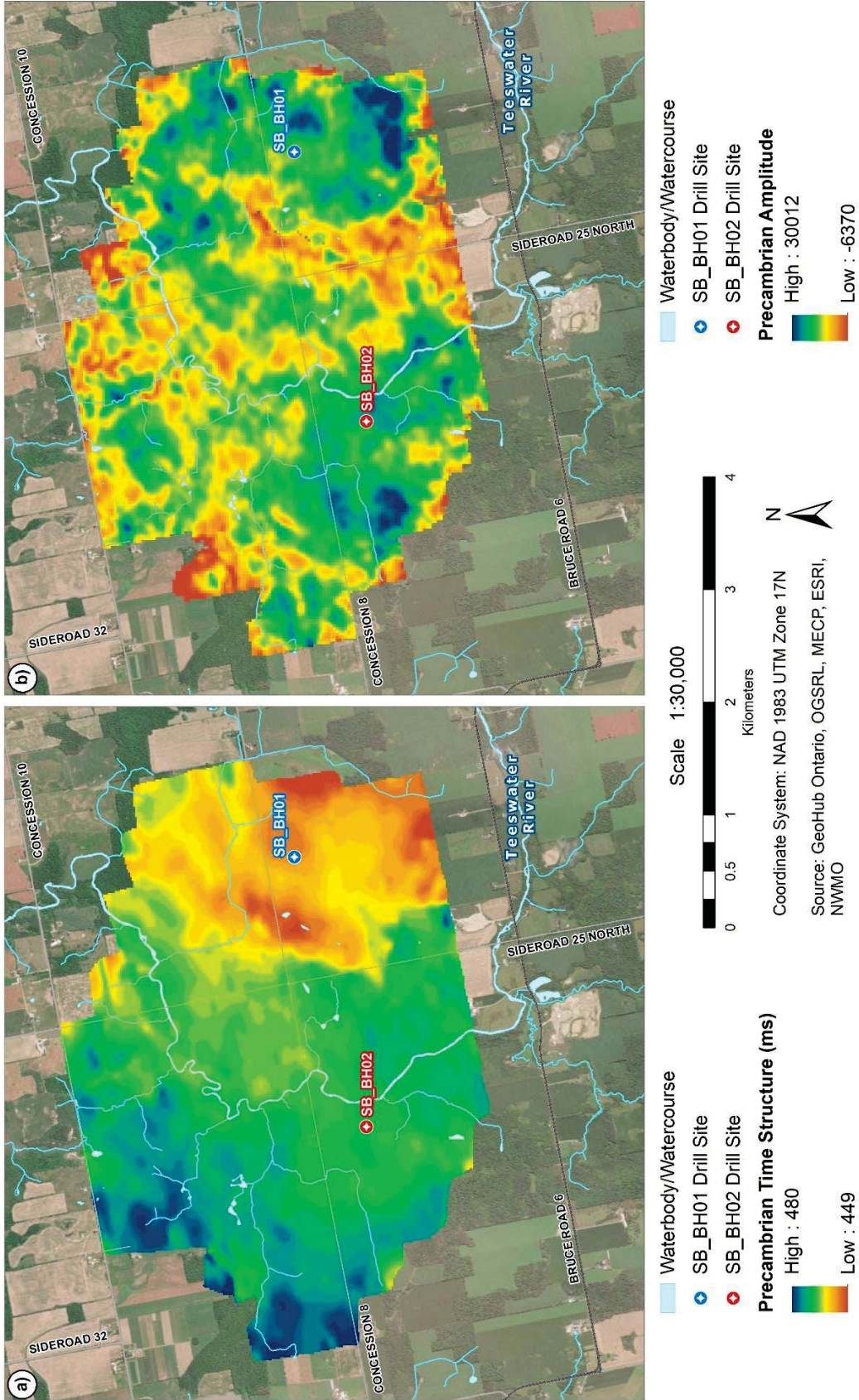


Figure A-15 Precambrian (a) plan view of interpreted time structure; (b) seismic amplitude.

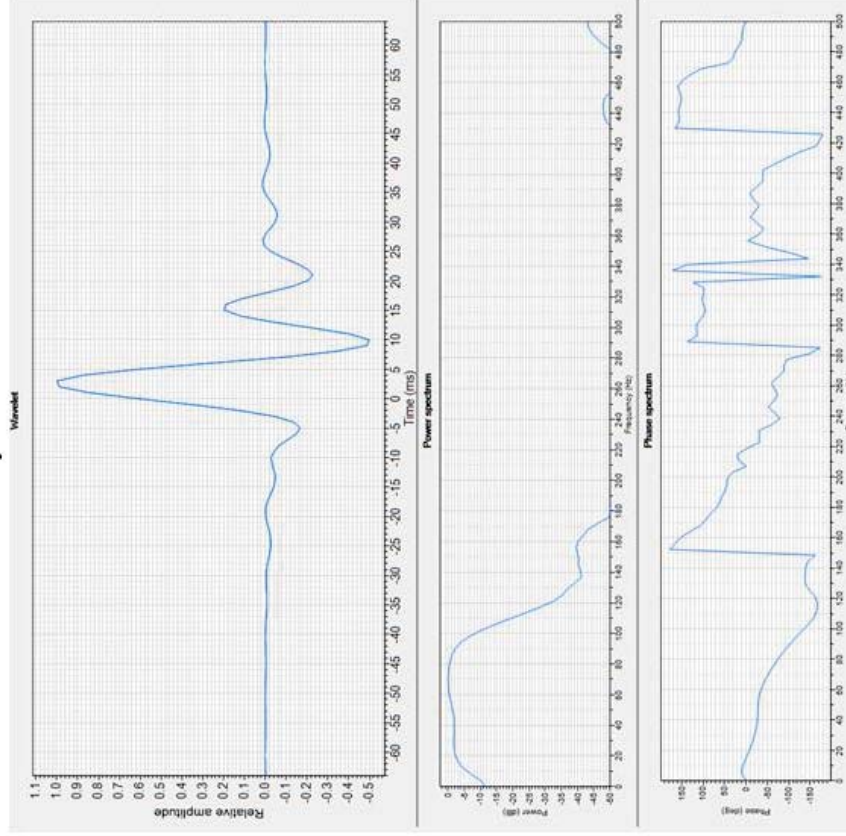
**21-210-1 Data Interpretation and Inversion Report
South Bruce 3D Seismic Reflection Study**

Appendix B

Seismic Wavelets Extracted from Select Angle Gathers

SB-BH01: 4-14

Predictability: 60.544%



SB-BH02: 4-14

Predictability: 57.715

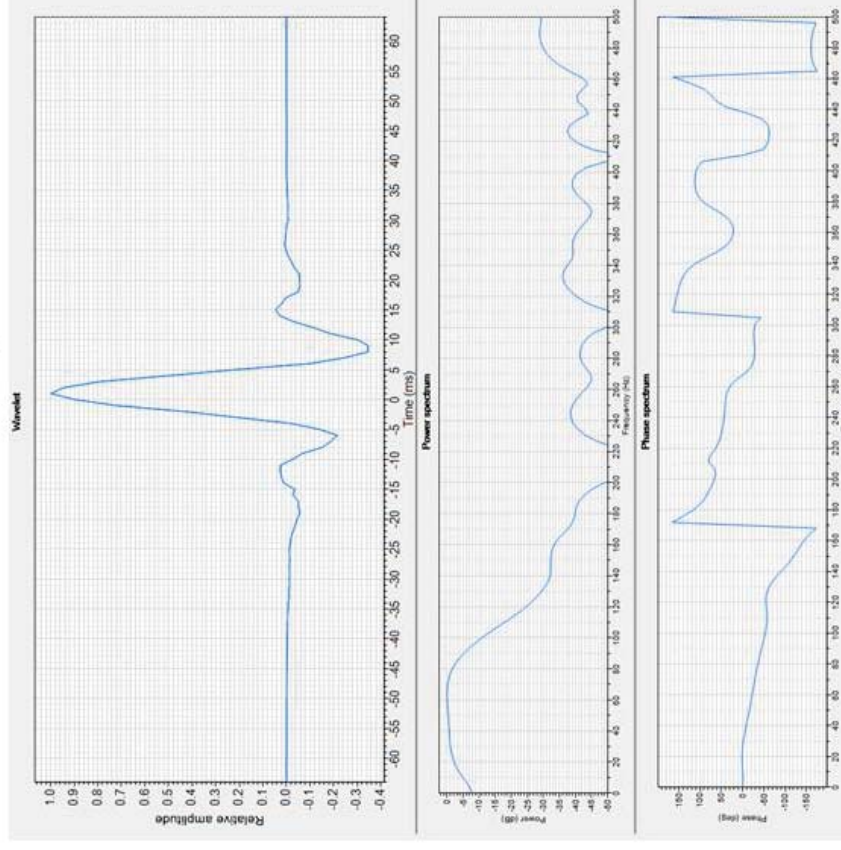
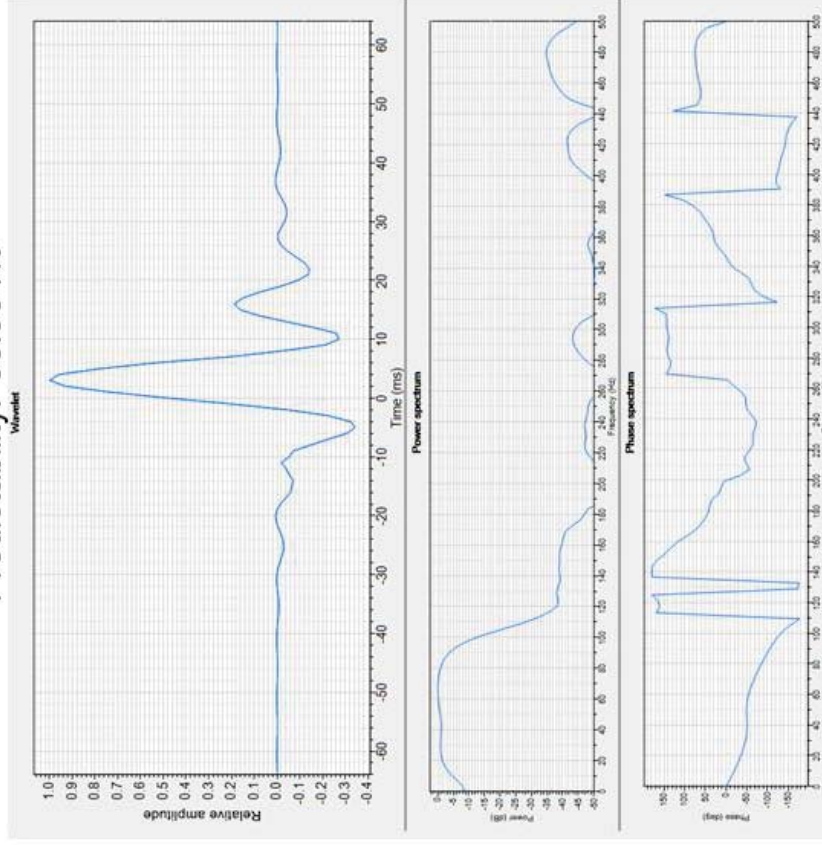


Figure B-1 Wavelets extracted from angle gathers (4–14 degrees) for SB_BH01 (left) and SB_BH02 (right), illustrating the wavelet shape, power spectrum, phase spectrum, and predictability ratios.SB_BH01SB_BH02.

SB-BH01: 21-38

Predictability: 56.954%



SB-BH02: 21-38

Predictability: 61.699%

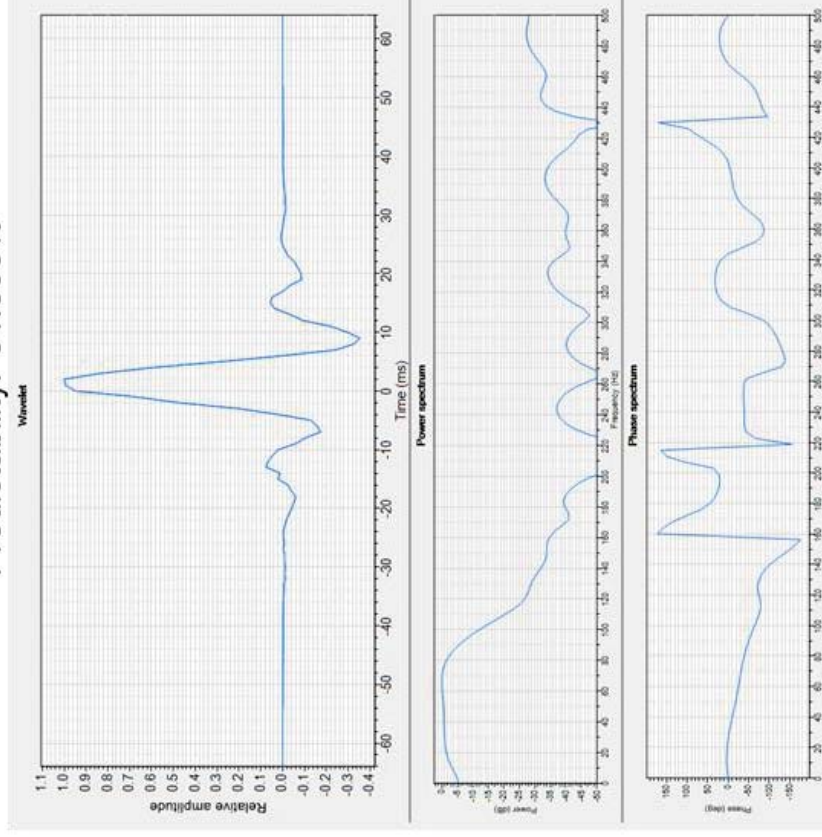
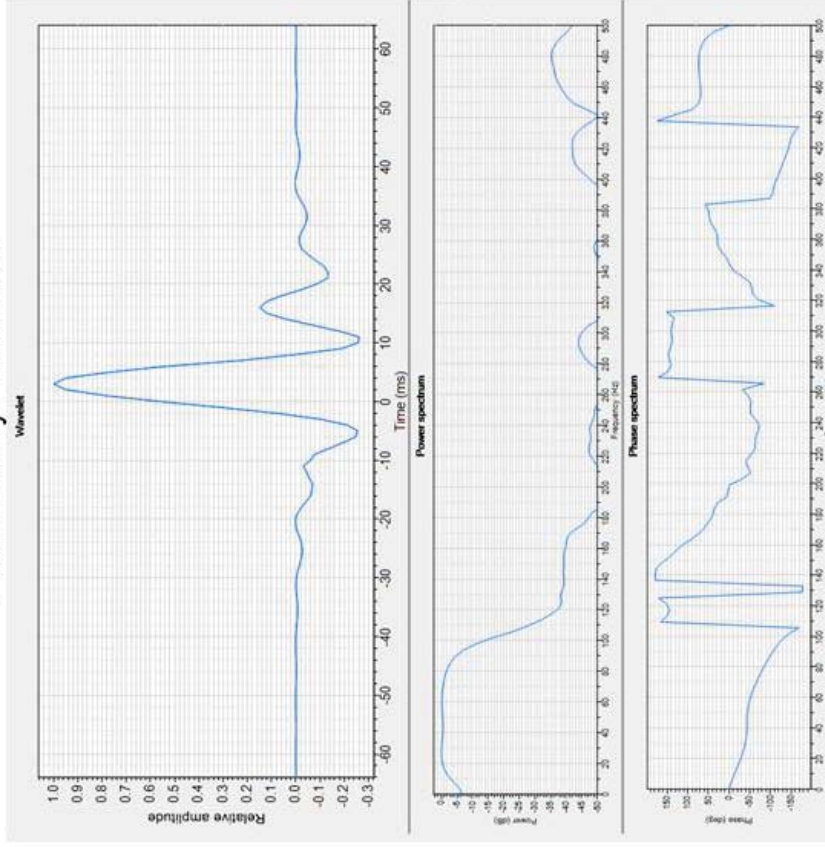


Figure B-2 Wavelets extracted from angle gathers (21–28 degrees) for SB_BH01 (left) and SB_BH02 (right), illustrating the wavelet shape, power spectrum, phase spectrum, and predictability ratios.SB_BH01SB_BH02

SB-BH01: 28-38

Predictability: 56.191%



SB-BH02: 28-38

Predictability: 63.084%

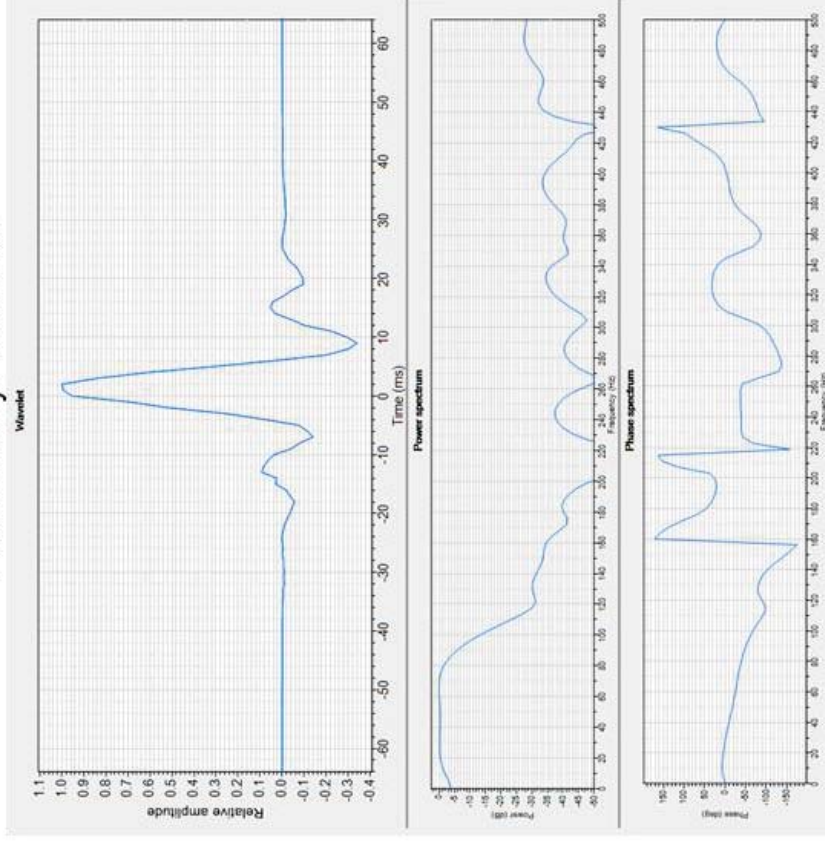


Figure B-3 Wavelets extracted from angle gathers (28–38 degrees) for SB_BH01 (left) and SB_BH02 (right), illustrating the wavelet shape, power spectrum, phase spectrum, and predictability ratios.SB_BH01SB_BH02